FEMTOSECOND ENCODER-DECODERS AND ULTRAFAST NONLINEAR THRESHOLDERS AND THEIR INTEGRATION IN A FEMTOSECOND CODE DIVISION MULTIPLE ACCESS COMMUNICATION SYSTEM TEST-BED

A Thesis

Submitted to the Faculty

of

Purdue University

By

Harshad P. Sardesai

In Partial Fulfillment of the

Requirements for the Degree

of

Doctor of Philosophy

December 1997

ACKNOWLEDGMENTS

I would like to first thank my parents for supporting me in all my decisions throughout my academic career and for always encouraging me to give my best effort. I would also like to thank my sister and brother-in-law for providing me with a home away from home and for their unconditional support. My sincere gratitude goes to Prof. Andrew Weiner for his superb direction and expert advice through all phases of this research. I would like to thank him for letting me learn from him about the exciting field of ultrafast optics and fiber communications, for financially supporting me through graduate school at Purdue, and for giving me the opportunities to succeed professionally. I would also like to thank Profs. Nolte, Elliott, and Chen for being on my committee and for offering valuable suggestions. All my colleagues in the laboratory deserve thanks for extending help whenever I asked for it. I would like to specifically thank Cheng-Chun Chang for the many discussions on optical CDMA and for making the final collaborative effort a thoroughly enjoyable one.

My previous major professor during my Master's degree program at the University of Texas at Arlington Dr. Bill Nunnally deserves special recognition for mentoring me when I was fresh out of undergraduate school, and for teaching me not to give up when things went wrong. I would like to also thank Maithili Daphtary for very enjoyable memories at Arlington, and for being a good friend after I came to Purdue.

I would like to thank several friends at Purdue for keeping me in good cheer especially when all else looked gloomy. At the risk of leaving out some, I would like to mention a few. Jamshed Patel is acknowledged for his friendship and support, and Rohit Gupta and Naresh Menon are acknowledged for their friendship and fun times. Todd Roswarski is acknowledged for first patiently listening to me complain about research, and then reminding me to hang in there. Ascen Saenz is acknowledged for her friendship

and for letting me have a social life outside science and engineering. Tom Frese and Charu Aneja are acknowledged for allowing me to hang out with them whenever I wanted, and Ken Groom is acknowledged for being a friend and neighbor for several years. Finally I would like to thank Aarati Nerurkar for asking me to finish graduate school and start living in the real world.

TABLE OF CONTENTS

LIST OF TABLES

LIST OF FIGURES

ABSTRACT

Sardesai, Harshad P. Ph.D., Purdue University, December, 1997. Femtosecond encoder-decoders and ultrafast nonlinear thresholders and their integration in a femtosecond code division multiple access communication system test-bed. Major Professor: Andrew M. Weiner.

Femtosecond code division multiple-access (CDMA) communication systems are an attractive choice for local area network applications due to their unique attributes of optical processing, asynchronous transmission, and the capability of multiple-access. In its simplest form an optical CDMA system can be described as follows. In the transmitter femtosecond pulses generated by a laser source are spectrally encoded into picosecond duration pseudonoise bursts and transmitted over a dispersion compensated fiber channel. Each user in the CDMA system is assigned a unique phase code by which it encodes all its data bits, and assigning different minimally interfering code-sequences to different users accommodates multiple users. The different users can be connected in a simple broadcast and select type architecture where all transmitters are connected to all receivers by a passive star coupler. In the receiver the decoder has knowledge of the phase code of only one particular transmitter. Hence only the encoded data bits that are intended for a particular receiver get properly decoded back into femtosecond pulses, and the encoded data bits of all other users remain as improperly decoded pseudonoise signals. A nonlinear optical thresholder that discriminates on the basis of intensity then detects the properly decoded femtosecond signal pulses and rejects the improperly decoded multi-access interference. This thesis addresses the design and construction of two of the optical CDMA component technologies, namely, femtosecond encoder-decoders, and ultrafast nonlinear thresholders. Both experimental and numerical results will be presented. These sub-systems were successfully integrated to construct an optical

CDMA test-bed. The optical CDMA test-bed will be discussed and results demonstrating CDMA transmission over 2.5km of optical fiber will be presented.

1. INTRODUCTION

1.1 Optical Communication Networks

Information transmission at optical frequencies over fiber-optic cables is a fairly well established technique. Fiber-optic communication systems offer the advantages of low loss, high bandwidth, high data transmission rates, and low operating costs [1], and are thus particularly suited for long distance data communication networks which have transmission spans from few hundred to few thousand kilometers. In addition to long distance communications, local area network's (LAN's) that typically have spans of ten kilometers or less are a new area of application for optical communications. Traditionally, a communication channel between two end-users has been partly optical and partly electronic. If one user wanted to send information to another user several 100 kilometers apart, the communication channel between the two could be conceptually divided into the following two portions. A long distance portion that is typically optical and a local access portion that is typically electronic. In the future, the optical portion of the communication system is envisioned to grow at the expense of the electronic portion. This is primarily due to the increasing usage of personal computing in businesses and homes, and the related explosive growth of the Internet and World Wide Web [2]. This addition of new users who require communication channels to transmit and receive data for a variety of services ranging from scientific usage to entertainment requires a high speed, high capacity, and multi-user-access communication network. Conventional electronic data communication networks, which have limited transmission bandwidth, would be incapable of supporting these new users and services, thus necessitating the use of fiber optics for local-access.

In additional to the above-mentioned scenario, several other applications of local area fiber-optic networks are possible. For instance, a high-speed fiber-optic network, spanning a total distance of a few kilometers and accommodating few hundred users could connect a cluster of computers on a university campus. An industrial park containing several companies could be similarly connected to a high-speed fiber-optic gateway by a high-speed fiber-optic LAN. Typically, users connected to a fiber-optic LAN can be assumed to have the following characteristics. They would transmit information asynchronously, require easy access and egress from the network, and would not be connected all at the same time (bursty users). Hence a scheme is needed that satisfies all these characteristics, and also provides high speed, high capacity communications.

There are two approaches used for building novel fiber–optic local area networks. The first approach involves making improvements in the network architecture, i.e., determining the optimum configuration of connecting different users to each other. The second approach makes improvements in the actual physical communication system, i.e., determining the optimum mechanism by which information can be generated, transmitted and received. In general, to provide the most optimal form of communication, improvements on both fronts are necessary. Note that the two approaches are also not strictly independent, and the degree of dependence between the two is decided by the choice of a particular architecture or system. In the systems approach, the communication system can be further divided into four levels, classified in decreasing order as system, sub-system, component and material. We can loosely define the four different levels in the following manner. Materials are required to make components that are then configured to build sub-systems, which are then configured to build systems. There is a much higher degree of correlation between different levels, with improvements at the lower levels generally driving development at higher levels. Fig. 1.1 shows schematic of a generic network for both long distance and local area communications.

To define the scope of this thesis we will limit ourselves to the systems approach, assuming that improvements in the architecture (if required) can be made without any major changes in the system. For simplicity we will assume that users are connected by a

broadcast and select type architecture (to be described in the next section). Within the systems approach, this thesis will primarily concentrate at the sub-system level with some emphasis on system integration. Finally, as will be described in the next sections, four different sub-systems make up the system under consideration. The author had primary responsibility for two of the four sub-systems. Hence this thesis will concentrate on two sub-systems, with the other two sub-systems only briefly described for completeness. A full definition of the problem statement of this thesis is provided at the end of this chapter.

1.2 Ultrashort CDMA Communication Systems

There are three commonly used multiple access schemes which allow multiple users to access a communication network; wavelength division multiplexing (WDM), time division multiplexing (TDM) and code division multiple access (CDMA). The first two are particularly suited for long distance communication applications, while the third is an attractive choice for local area networks. In WDM systems the optical transmission bandwidth (which is about 50 nm at 1.55μm transmission wavelength) is divided amongst different users by assigning each user a particular wavelength (frequency) within the bandwidth. In TDM systems each user is given a different time slot and higher data transmission rates are obtained by going to shorter time slots transmitted at higher repetition rates. For long distance communication systems, dispersion and loss in the transmission channel are two main constraints that determine propagation distance, system speed, and capacity. Due to advances in erbium doped fiber amplifier (EDFA) technology which mitigate effects of loss, and advances in transmission fiber manufacturing technology which mitigate effects of dispersion, WDM and TDM systems have shown impressive performance results. A 55 channel WDM system operating at a total data rate of 1.1 Tb/s over 150 km of standard optical fiber has been demonstrated [3]. 1 Tb/s WDM systems have also been demonstrated for 55 km transmission over standard fiber by using polarization multiplexing of 25 channels each operating at 20

Gb/s [4], and for 40 km transmission over dispersion shifted fiber using 10 channels each operating at 100 Gb/s [5]. Other WDM transmission experiments over longer propagation distances include a demonstration of 100 Gb/s data transmission using 20 WDM channels over 9100 km [6], and a 24 channel WDM system operating at a total data rate of 128 Gb/s over 7828 km of optical fiber [7]. In TDM systems, single channel systems operating at 400 Gb/s over 40 km of standard fiber have been demonstrated [8], and 1 Tb/s transmission over 40 km of dispersion shifted fiber using 10 TDM channels each at 100 Gb/s has been reported [5].

Although WDM and TDM systems appear to be well suited for long distance communications, they would have certain limitations for use in local area network (LAN) applications. Typically a local area network would connect a large number of users transmitting over short propagation distances, and users are more likely to be bursty and asynchronous. In WDM systems the total number of simultaneous users are limited by the availability of tunable narrow band sources and receivers. Although some experimental demonstrations have been performed using 55 channel WDM systems [1], it would be difficult to extend that number to several hundred. Some architectural improvements like wavelength routing networks [9] that increase user access by allowing wavelength reuse have been demonstrated, but with the addition of considerable network complexity. In addition to the limitation placed by availability of sources, increasing the number of channels (users) in WDM systems also increases inter-channel interference due to four wave mixing and other nonlinear processes. TDM systems require high-speed optoelectronic devices and time synchronism mechanisms in the network that can limit overall data transmission rates and add to network complexity.

In contrast to WDM and TDM systems, optical Code Division Multiple Access (CDMA) communication systems have the potential to accommodate several hundred users [10-17] and are thus an attractive choice for LAN applications. Each data bit in an optical CDMA system is coded with a code that is unique to a particular user, and multiple users accommodated by assigning different minimally interfering codes to different user pairs. Several different minimally correlated code-sequences exist in traditional digital communication systems that can be easily implemented in the optical

domain. Optical CDMA thus has the potential to accommodate several hundred users, the main constraint being the fidelity of the encoding-decoding operation for a user pair, and the consequent successful detection in the presence of interference from other users. Optical CDMA also has the advantage of using optical processing to perform certain network applications like addressing and routing making it suitable for very high-speed network operation. The asynchronous nature of data transmission considerably simplifies network management and control. Optical CDMA due to its advantages of optical processing, asynchronous transmission, and the capability of multiple-access appears to be well suited for local area network applications.

Several different optical CDMA schemes have been proposed [10-18], based on different choices of sources, coding schemes and detection. One scheme proposed the use of fiber-optic delay line encoder-decoders to code short mode-locked laser pulses, and optical monostable switch thresholders for detection [12]. Another scheme used electrical coders followed by electro-optic conversion, optical multiplexing and electronic detection [13]. Yet another scheme proposed interferometric coherence coding of noncoherent broadband sources followed by matched decoding [14]. Other optical CDMA systems have also been proposed which used fiber-optic lattices made up of a large number of interferometric stages for pulse coding [15], multi-fiber tapped delay lines for generation and detection of optical code patterns [16], pulse encoding-decoding using fiber ladder networks [17], and spectral encoding of LED light sources [18]. Our optical CDMA scheme shown in Fig. 1.2 is based on the principle of spectral encoding and decoding of ultrashort light pulses [10,11]. In the transmitter, femtosecond laser pulses are spectrally encoded and then propagated over a dispersion compensated fiber link. In the receiver, a matched spectral decoder and a nonlinear fiber thresholder detect the received data. Each user is assigned a unique phase code by which it encodes all its data bits, and this phase code is orthogonal to the phase code assigned to every other user in the system. The phase code is in the form of a pseudorandom M-sequence that spectrally encodes femtosecond pulses into picosecond duration pseudonoise signals. Different users can be connected in a simple broadcast and select type architecture where all transmitters are connected to all receivers by a passive star coupler. Each receiver

thus receives encoded data bits transmitted by every transmitter in the network, but the decoder in any one receiver has knowledge of the phase code of only one transmitter. Hence only the encoded data bits of one transmitter that are intended for a particular receiver get properly decoded back to a femtosecond pulse, and the encoded data bits transmitted by all other transmitters remain as improperly decoded pseudonoise signals. A nonlinear fiber-optic thresholder then performs the task of distinguishing between the correctly decoded femtosecond signal, and the incorrectly decoded picosecond interference. In this CDMA scheme, each transmitter can operate at moderate data rates of ~ 1 Gb/s, but having several hundred users high overall data transmission rates can be achieved. The propagation distance is limited mainly by the effectiveness of the dispersion management scheme used. The propagation distance in our CDMA test-bed is currently 2.5km, but by using programmable cubic phase correction we demonstrate almost dispersion free transmission for sub 500 fs pulses, thus opening the possibility of even longer propagation distance of tens of kilometers.

1.3 Key Technologies For Ultrashort Pulse CDMA Systems

The optical CDMA link integrates together four novel subsystems, 1)-femtosecond lasers, 2) femtosecond encoders-decoders, 3) femtosecond-dispersion compensation, and 4) ultrafast nonlinear thresholders. A proper choice of all of the above sub-systems is necessary for optimal system operation and this section will briefly introduce each of the sub-systems. More details will be provided in subsequent chapters.

1.3.1 Femtosecond lasers

Optical CDMA requires femtosecond laser pulses as they provide the wide bandwidth necessary for the encoding-decoding operation. The lower limit on the shortest femtosecond pulse that can be used is placed by the effectiveness of the

dispersion compensation scheme over the transmission distance. The upper limit on the longest femtosecond pulse that can be used is placed by the minimum bandwidth required to code the ultrashort pulses, especially with multiple users, and the short pulsewidth required for effective high contrast thresholding. Due to these conflicting requirements for optimal operation of dispersion compensation and encoding-decoding, a pulsewidth of several hundred femtoseconds appears to be the best compromise. In addition to pulsewidth, the average source power is another important criteria for selecting the laser source since it determines the total nonlinearity in the communication system, which greatly affects system performance. Issues such as source stability, jitter, drift, pump power requirements, compatibility with other sub-systems are other important technological considerations. Hence femtosecond laser sources is one key technology area which requires a judicious choice since it affects all other sub-systems and also the overall system performance. Although several different techniques exist for femtosecond pulse generation in the 1.55μm communication band, passively mode-locked fiber lasers [19-21] were used primarily because of their advantages of stable operation, ease of construction, and compatibility with all-fiber communication systems.

1.3.2 Femtosecond encoder-decoders

The optical CDMA scheme is based on encoding and subsequent decoding of ultrashort light pulses. This encoding-decoding operation can be done either in the time domain or in the frequency domain. Time domain encoding-decoding using fiber-optic delay lines [12], fiber-optic ladder networks [13], fiber interferometers [14,15], and acoustically tunable optical filters [22] has been demonstrated. Since femtosecond pulses have wide spectral widths, frequency domain encoding-decoding can be accomplished quite easily. Pulse-shapers [23-26] consisting of a pair of diffraction gratings placed at the focal planes of a pair of unit magnification plano-convex spherical lenses are ideal candidates for frequency domain encoding-decoding. They have the advantages of high-resolution pulse shaping and the flexibility to apply programmable arbitrary phase codes

of different code length [24]. Pulse shaping of picosecond pulses has been demonstrated before at visible wavelength [25]. Encoding and decoding of femtosecond pulses has also demonstrated before at visible wavelength [26], using two conjugate phase masks placed successively in the same free-space pulse-shaper. Although the construction and operation of the pulse-shapers used in optical CDMA was quite similar to the ones demonstrated before there were however several other challenges. First to demonstrate encoding-decoding using two separate pulse shapers. Second to determine the effect of the fiber channel (that separates the encoder-decoders) on the encoding-decoding operation, and third to fiber-pigtail the pulse shapers to make them compatible with the rest of the fiber-optic system. Fiber-pigtailing increases the ease with which we can either connect the pulse-shapers in the whole system, or disconnect them for individual measurements. It also has the advantage that the pulse-shapers have to be aligned only once during the initial construction phase. Related to the construction of encoder-decoders, was the choice of phase codes for encoding-decoding. While several different phase codes could be used in theory [12-14], M-sequence were the phase codes on choice. They are easy to generate, implement, and have the property that two sequences shifted by one bit are orthogonal to each other. For all of the above reasons, the encoder-decoders were built using programmable pulse-shapers and M-sequence coding.

1.3.3 Femtosecond dispersion compensation

The wavelength dependence of the refractive index of the optical fiber is called dispersion. In optical communication systems, most effects of dispersion manifest as quadratic dispersion which causes the different frequency components of a pulse to propagate at different velocities leading mainly to pulse broadening at the receiver. For large enough pulse spreading, the tails of the broadened pulse may overlap with the next bit period causing erroneous detection. Hence dispersion in the fiber channel sets a limit for the transmission distance. For femtosecond pulses, higher order dispersive effects (like cubic dispersion) that cause asymmetric pulse broadening also become quite

important. Hence optical systems using femtosecond pulse propagation require the simultaneous compensation of both the quadratic dispersion and most of cubic dispersion of the input pulse. In femtosecond optical CDMA dispersion compensation is necessary for two reasons. First, since the CDMA scheme needs linear pulse transmission due to the phase sensitive encoding-decoding operation, we cannot use soliton propagation. Soliton are pulses with a special secant-hyperbolic shape and a certain energy-pulsewidth balance. They propagate through optical fibers without changing shape resulting in almost dispersion free propagation. Since optical CDMA encodes the input femtosecond pulses in noise-like signals, neither the shape nor the energy-pulsewidth balance is maintained for soliton propagation. Second, if dispersion compensation were not used, the properly decoded pulses in the receiver after propagating through few kilometer of optical fiber would be too wide for successful nonlinear thresholder operation. Several schemes exist for dispersion compensation of ultrashort pulses [27-30]. These include the use of chirped reflection gratings, bulk grating pulse-shapers, and optical phase conjugation. Our dispersion compensation scheme involves the use of dispersion compensating fiber (DCF) [30] to compensate the quadratic dispersion and most of the cubic dispersion of standard single mode fiber (SMF) [31,32]. This dispersion compensation is possible because the DCF fiber has an opposite sign of dispersion and dispersion slope compared to the SMF fiber. Such an SMF-DCF fiber link also has much lower third order dispersion than conventional dispersion shifted fiber. Another advantage of a compensation scheme using SMF-DCF fibers is the fact that most of the transmission fiber in currently installed fiber communication systems is standard SMF. Hence an SMF-DCF compensation scheme would lend itself more easily to a practical implementation. It is important to note that since femtosecond pulse have large spectral widths, dispersion compensation over the entire spectra width is quite difficult to achieve. Further, once the second order dispersion is quite well compensated, the effects of third order dispersion become more dominant. By applying a cubic phase to the pixels of the programmable liquid crystal (LCM) in the encoder, we can almost completely remove the residual third order dispersion of the SMF-DCF link resulting in almost dispersion free transmission of femtosecond pulses over the 2.5km fiber link. This flexible and

programmable way of trimming residual third order dispersion could increase the transmission distance and also allow for some tolerance should dispersive transmitters and receivers get connected to the transmission channel.

1.3.4 Ultrafast nonlinear thresholders

Optical CDMA receivers need a thresholding device to distinguish between properly decoded femtosecond pulses and the equally energetic improperly decoded picosecond interference signals. Note that both the signal and interference are of too short a duration to be detected by ordinary photodiodes. Hence a nonlinear device which responds to peak power and pulse width is desired. It is normally accepted that most material media would exhibit a nonlinear response for a strong enough excitation. Nonlinear effects occurring in semiconductors, bulk or guided wave dielectric material, or optical fibers [33-35] could be exploited for thresholding purposes. In optical fibers, although the magnitude of the nonlinearity is small as compared to other dielectric media, the nonlinear effects can be observed at relatively low input power levels because of two important characteristics of optical fibers: small spot size and low loss. These characteristics combined with the excellent confinement properties of optical fibers give high values of optical intensities inside the fiber. The guided wave property of optical fibers also allows the nonlinearity to accumulate over long propagation distances. Hence optical fibers make excellent nonlinear devices and have been widely used for switching and extinction ratio improvement applications [36-40]. The ultrafast thresholders were constructed using optical fibers having different dispersion properties and therefore different nonlinear effects [39,40]. We used two nonlinear effects, namely, nonlinear self-phase modulation [41,42] and nonlinear Raman effects manifested as the soliton self frequency shift [43,44]. In both these effects when a high intensity femtosecond pulse is propagated in an optical fiber, the output pulse exhibits frequency shifts (away from its mean input frequency), the exact nature of the shift depending on the particular nonlinear process. The lower peak power longer duration interference signals do not exhibit any

changes to their frequency spectrum. By using a spectral filter after the fiber, these frequency shifts were filtered out resulting in high contrast thresholding.

1.4 Problem Definition

The problems that this thesis addresses are outlined below. First at the sub-system level this thesis addresses the design and implementation of the fiber-optic encoder-decoder, and the nonlinear fiber-optic thresholder. Second, at the system level this thesis addresses the construction of an optical CDMA testbed to demonstrate single user operation, and also the implementation of erbium doped fiber amplifiers which are required primarily to compensate for the insertion loss of the various sub-systems. Formally the problems are defined below.

1) To design and implement a fiber-optic coder that can code femtosecond laser pulses, to implement an encoder-decoder pair for M-sequence encoding-decoding, and to theoretically model the encoding-decoding operation using numerical simulation. Note that although two separate encoder-decoders are required for the optical CDMA system, the construction of the decoder simply follows that of the encoder.
2) To design and implement a fiber-optic thresholder that can distinguish between femtosecond pulses and equal energy picosecond pseudonoise signals. To numerically simulate thresholder behavior to understand the effects of pulse parameters and fiber characteristics on thresholder operation.
3) To construct an optical CDMA test-bed that integrates the above two sub-systems with femtosecond laser sources and dispersion compensated link to demonstrate single user operation. To construct erbium doped fiber amplifiers as required for overcoming insertion losses of various sub-systems.

Note that a colleague carried out the design and implementation of the other two sub-systems (femtosecond lasers and dispersion compensated link). Hence there is some overlap of research goals in (3).

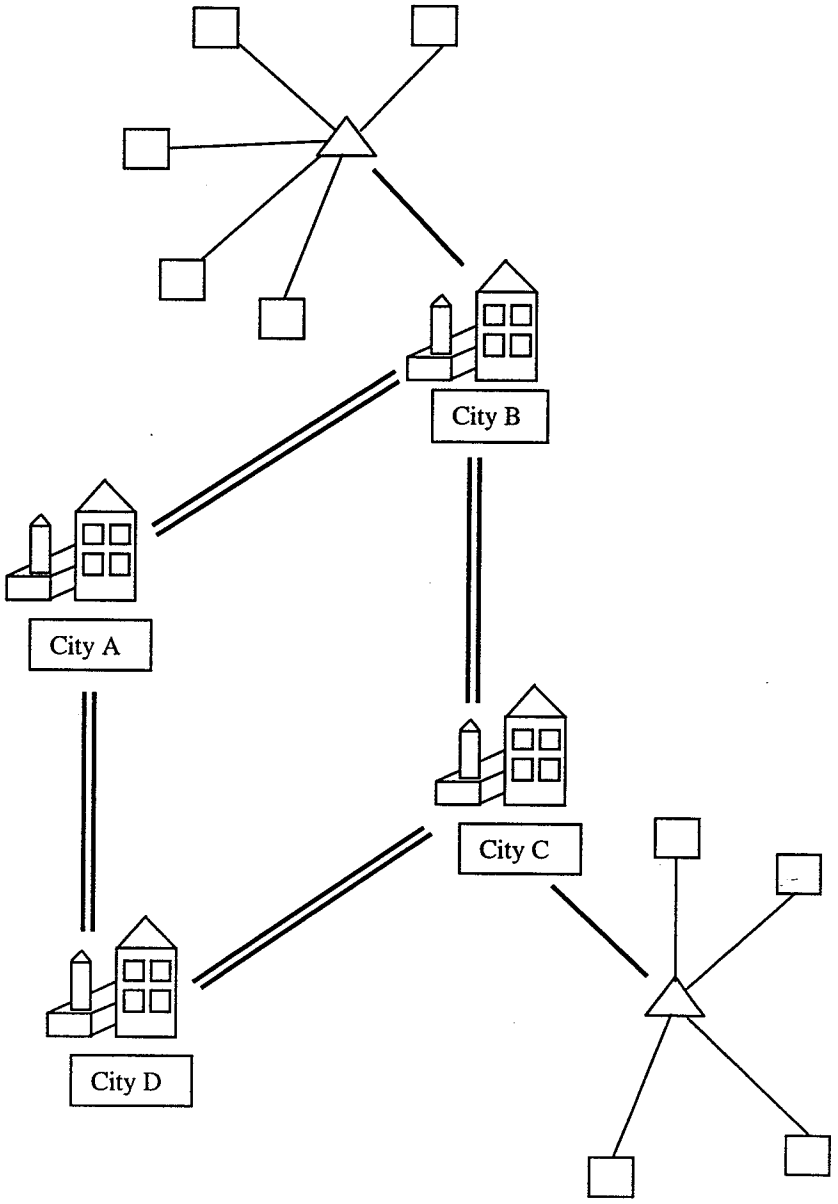

Fig.1.1. Schematic of a generic optical network for long-distance and local area communications.

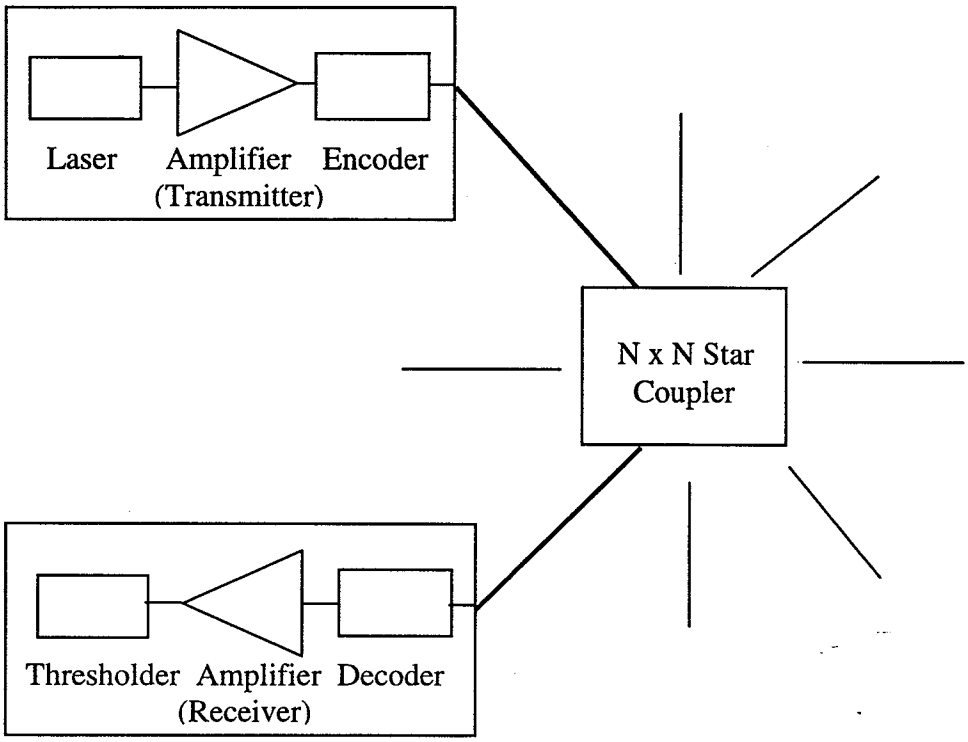

Fig. 1.2. Schematic of the femtosecond optical CDMA scheme.

2. FEMTOSECOND ENCODERS-DECODERS

The optical CDMA scheme is based on encoding and decoding of femtosecond light pulses. Hence encoders-decoders play a pivotal role in the success of the overall CDMA communication system. This chapter will discuss the construction of a femtosecond encoder (pulse-shaper) that can encode femtosecond pulses into arbitrary pulse shapes, and present the experimental results. The construction of the decoder exactly follows that of the encoder and will not be separately discussed, but experimental results for the encoding-decoding operation will be presented. Both the encoding and the encoding-decoding process were modeled using numerical simulations. This was necessary to understand the operation of the pulse-shaper and determine its limitations. The numerical analysis scheme will be discussed, and numerical results for a single pulse-shaper (encoder) and two pulse-shaper (encoder-decoder) arrangements will be presented.

2.1 Background And Literature Survey

Several different encoding-decoding schemes have been proposed for optical CDMA systems. In general, the operation of encoding-decoding can be performed either in the time domain or in the frequency domain. Time domain encoding-decoding using fiber-optic delay lines [12], fiber-optic ladder networks [16], fiber interferometers [14,15], and acoustically tunable optical filter [22] has been demonstrated before. In the fiber-optic delay lines approach [12], an input pulse from the transmitter was encoded to

form a train of N secondary pulses which were then propagated over a fiber-optic link and detected by a matched decoder in the receiver. In its most basic form the (de)coder consisted of a 1 x N tree coupler followed by N parallel fibers of different length, and another N x 1 coupler. The decoder in this scheme used incoherent optical processing, i.e.; the pulses arriving at the input of the decoder were summed on a power (incoherent) basis to form the output. The autocorrelation produced by a matched encoder-decoder pair consisted of 2N-1 pulses; the middle one of which had the highest intensity and was used for discrimination. By using tapped delay lines, where the taps on the delay line equaled the code sequence for a particular destination, either Gold codes or prime sequence codes could be used for encoding the data. Although this encoding-decoding technique was easy to implement it had two main drawbacks. First, the fraction of energy lost in one coder to generate N secondary pulses was 1/N; hence an encoder-decoder pair had an energy loss of $1/N^2$. Second, the several secondary autocorrelation pulses produced for matched encoding-decoding in the receiver constituted a loss of energy that could not be utilized for discriminating between an intended user and an interfering user.

The fiber-optic ladder encoding scheme [16] addressed some of the disadvantages associated with the fiber-optic delay line scheme. In this scheme, the encoder consisted of two parallel fibers coupled to each other at N different locations by simple 3 dB couplers forming a train of 2^N pulses in each possible output fiber (of the two ports of the final 3dB coupler). For a fiber-optic network consisting of a single transmission fiber, such an encoder would have only a 3dB energy loss representing a big improvement over the fiber-optic delay line-encoding scheme. To get around the problem of the energy loss to secondary autocorrelation pulses in the decoder, a coherent decoding scheme was proposed. In the coherent decoding scheme, the two parallel fibers that formed the encoder were both used to transmit the encoded pulse, and the decoder had a matched fiber-optic ladder consisting of two fibers. With the encoder-decoder connected back to back, and with proper phase and polarization control, near-ideal coherent superposition could be observed in the decoder with most of the energy concentrated in a single decoded pulse. Although this scheme represents an interesting choice for encoding-

decoding of data in optical CDMA, a system implementation of it would have several disadvantages. First, the effects of nonlinearity, dispersion, and the non-polarization preserving property of optical fibers would make it difficult to maintain phase and polarization control between pulse trains propagating over long transmission distances. Second, several couplers would be required to encode data with long destination addresses (as would be required for multi-user operation), and small environmental changes could destroy the phase balance. Finally, a practical implementation of the coherent decoding scheme using fiber-optic ladders would require two-transmission fibers (in each direction) adding an additional cost component.

In the interferometric encoding-decoding scheme [14,15], each encoder (or decoder) consisted of a fiber-optic Mach-Zender interferometer. In its most general form, one arm of the interferometer contained a simple time-delay element while the other arm contained a dispersive element characterized by an impulse response function. Each encoder-decoder pair was assigned a matched time-delay and impulse response function that was different from that assigned to every other encoder-decoder pair in the communication system. The output of such an encoder-decoder pair was detected using balanced photodetection between the two outputs of the decoder Mach-Zender interferometer. In its simplest form called coherence multiplexing, the impulse response function in each coder was made equal to a delta function, and only the delays of the encoder and decoder were matched. When the coder has a non-trivial impulse response function (called coherence coding), the output of encoder-decoder pair was proportional to the source coherence function convolved with the cross-correlation of the impulse responses of the encoder and decoder respectively. This approach required a matching of the optical phase and the impulse response of the encoder and decoder. Although this technique had the advantage of offering more secure communication, it required very accurate control of the birefringence in the inteferometer, and also required the interferometer to be insensitive to environmental changes.

A scheme for shaping ultrashort pulses using integrated acoustically tunable optical filters (ATOF) was demonstrated which could be potentially used in encoding-decoding of pulses for optical CDMA [22]. In the demonstrated integrated ATOF

structure [22,45], the optical pulse was coupled into a waveguide along one axis of a birefringent crystal. A radio frequency (rf) surface acoustic wave wrote a grating in the crystal causing a particular input frequency component to get diffracted or filtered out. This filtering operation was accompanied by phase-matched polarization conversion, and by placing the ATOF between two polarizers, either a notch filter or a bandpass filter was obtained. By applying multiple drive frequencies, different input frequency components of an ultrashort pulse were filtered independently creating an output spectrum having several notches, or in essence a shaped output optical pulse. This pulse-shaping operation can be used as an encoding-decoding scheme for optical CDMA. Its main advantages are its compact integrated form, and a mature fabrication technology that would make it easy to construct matched encoders-decoders. Its main disadvantages are its polarization sensitivity, cross-talk limitations, and the need to have several different rf drive sources to generate a shaped optical output of reasonable complexity so as to be useful in optical CDMA.

Frequency domain encoding-decoding using pulse-shapers consisting of a pair of diffraction gratings placed at the focal planes of a pair of unit magnification plano-convex spherical lenses [23-26] was the encoding-decoding scheme of choice. It has the advantages of high-resolution pulse shaping [26], the flexibility to apply arbitrary programmable phase codes of different code length [24], and compact low-loss construction. Pulse shaping of picosecond pulses has been demonstrated before [25], and encoding-decoding of femtosecond pulses has also been demonstrated before at visible wavelength using two conjugate phase masks placed successively in the same free-space pulse-shaper [26]. The construction of the pulse-shapers used in optical CDMA was quite similar to the ones demonstrated before. Our pulse-shapers were however fiber-pigtailed to make them compatible with the rest of the fiber-optic system. Fiber-pigtailing increases the ease with which we can either connect the pulse-shapers in the whole system, or disconnect them for individual measurements. It also has the advantage that the pulse-shapers have to be aligned only once during the initial construction phase. Related to the construction of encoder-decoders, was the choice of phase codes for encoding-decoding. While several different phase codes could be used in theory [12-14],

M-sequence were the phase codes on choice. M-sequences are bit patterns of 1's and 0's of length $L = 2^N-1$ (N = integer), generated by using ordinary shift registers [46]. The number of 1's is always equal to the number of 0's plus 1, and M-sequences have the property that two sequences shifted by one bit are orthogonal to each other. By using cyclic shifts, an M-sequence of length L can accommodate L simultaneous users in the optical CDMA scheme. For all of the above reasons, the encoder-decoders were built using programmable pulse-shapers and M-sequence coding.

2.2. Pulse Shaper-Construction and Design

The experimental arrangement of the pulse-shaper is shown in Fig. 2.1. In the pulse-shaper, collimated light from the input fiber pigtail is first diffracted off a grating (1100 lines/mm) and the different spectral components are then collected and focussed by an achromatic lens (focal length = 190 mm). At the focal plane of the lens, the spectral components of the input pulse are linearly spatially separated. A liquid crystal modulator is used to set the spectral phases to a length 15, length 31, length 63, or length 127 M-sequence pseudorandom phase-code (which encodes the pulses into 5-15 ps wide pseudonoise bursts) or held constant leading to essentially unchanged uncoded pulses. Note that alternately fixed masks [47], holographic plates [48], or acousto-optic modulators [49] could be used instead of the LCM. The LCM has a fully programmable linear array of 128 pixels, and individual pixels can be controlled by applying upto 4096 (0-4095) different drive levels resulting in phase shifts from 0 to 4π. A length 31 M-sequence consists of a pattern of 1's and 0's 31 bits in length that is accommodated by the 128 pixels of the LCM by assigning 4 pixels to each bit. For M-sequence bits equal to 1, the phases of the corresponding LCM pixels are set to π radians; for bits equal to zero, the phase is set to 0 radians. The rest of the pulse-shaper consists of a second matched achromatic lens and grating which reassembles the different spectral components into a single collimated output beam which is then coupled back into an output fiber pigtail. Note that two half waveplates were used, before and after the LCM

respectively since the polarization state for operation of the LCM was orthogonal to that required by the gratings for optimum diffraction efficiency. The fiber-to-fiber insertion loss of the entire pulse-shaper (including LCM) was 5.3 dB.

The design of the pulse-shaper is relatively straightforward and involves determining the following five pulse-shaper parameters; incident angle, diffracted angle, input beam diameter, grating period, and focal length of the lenses. These five parameters are picked for the following three known quantities. The input signal bandwidth to be encoded (~ 12nm), spatial frequency spread in the mask plane (determined by the overall linear dimension of the LCM ~ 12.8mm), and spot size in the mask plane (determined by the linear dimension of individual LCM pixels ~ 100 microns). The following three equations [50] were iteratively solved for the above-mentioned five design parameters.

$$Sin\theta_d = Sin\theta_i + \frac{m\lambda}{d}$$

$$\alpha = \frac{\lambda^2 f}{2\pi c d Cos\theta_d}$$

$$w_o = \frac{Cos\theta_{in}}{Cos\theta_d}\frac{f\lambda}{\pi w_{in}}$$

Here θ_{in} and θ_{out} are the incident and diffracted angles respectively, λ is the wavelength, d is the grating period, c is the speed of light, α is the spatial dispersion in the mask plane (expressed in units of mm.fs), w_o is the beam radius (1/e field radius) in the mask plane, and w_{in} is the input beam radius. Using the above three equations, the pulse shaper was designed for incident and diffracted angles of 43 and 75 degrees respectively, and an input beam diameter of ~ 9mm. The grating period and lens focal lengths were chosen to be 1100 lines/mm and 190mm respectively. This gave a spatial dispersion parameter of α ~ 5900 mm.fs (or in terms of wavelength ~ 0.75 mm/nm), and a spot size (intensity FWHM) in the mask plane of ~ 140 microns.

Note that achieving a low insertion loss for the pulse shaper was crucial as it reduced the amplification requirement of the CDMA system. This was important not only from a systems point of view, but it also made possible for connecting two pulse shapers back-to-back without requiring an amplifier after the second pulse shaper. Femtosecond erbium doped fiber amplifiers are quite susceptible to effects of gain narrowing and consequently pulse broadening in the amplifier. By eliminating the amplifier we got a true indication of the fidelity of the encoding-decoding process. The key to achieving low loss insertion loss (fiber-to-fiber insertion loss of only ~ 5.3 dB) was the symmetry of the pulse shaper optics between the input and output fiber pigtails. The input fiber pigtail was simply a meter long piece of standard SMF and the optical beam exiting the pigtail was collected by a 40mm focal length positive achromat resulting in a 9mm collimated beam. The input optical beam was then passed through a carefully aligned pulse shaper and the beam exiting the pulse shaper was focussed into a standard SMF fiber pigtail by an identical 40mm focal length positive achromat. The almost perfect match of the input and output beam size and shape, along with the perfect symmetry of the set-up gave one of the lowest reported loss for pulse shapers.

2.3. Pulse Shaper-Experimental Results

The experimental arrangement used to demonstrate femtosecond encoding operation as well as femtosecond encoding-decoding operation is shown in bloack diagram for in Fig. 2.2. Input pulses to the pulse-shaper are derived from an erbium doped fiber laser which produces ~ 62fs pulses with a bandwidth of ~ 60nm at a repetition rate of ~ 30 MHz. The laser output is taken from a 80-20 coupler, with the pulses from the 80% port externally filtered by a bandpass filter (bandwidth ~ 11nm) and then amplified by a chirped pulse erbium doped fiber amplifier to produce near transform limited pulses having a pulse-width of ~ 375 fs and an average power of ~ 1.2mW. The 20% output port has 62fs pulses that are used in all the cross-correlation measurements. A more complete description of the femtosecond laser and amplifier will be given in

chapter 4. Fig. 2.3. (a) and (b) respectively show output cross-correlation and spectra for a constant phase applied to the LCM pixels. For comparison, the input spectra is shown in Fig. 2.3 (c). Note that the output pulse-width is ~ 440fs indicating a slight pulse broadening at the output of the pulse-shaper for a constant phase applied to all the LCM pixels, although theoretically there should not be any such pulse broadening for an ideal zero-dispersion pulse-shaper set-up. The cause of this pulse broadening is related to polarization effects in the fiber pigtails and its interaction with polarization sensitive elements (e.g. gratings) in the pulse-shaper, and also possibly due to the aberrations in the pulse-shaper optics due to the large diffraction angles. Some experimental evidence of the effects of aberration was seen when the diffraction angle of the first grating was increased to ~ 80 degrees. The output pulsewidth was now almost 35 % broader than the input pulse width. Decreasing the diffraction angle by a few degrees resulted in a reduction in the broadening factor of the output pulsewidth but it also detrimentally affected the spectral resolution of the pulse-shaper by reducing the bandwidth available (in the Fourier plane) for encoding with longer length M-sequences. Hence the diffraction angle was kept at 75 degrees as it showed only minimal broadening (10-20% depending on polarization effects) and also left enough bandwidth for coding. Fig. 2.4 shows output cross-correlations and Fig. 2.5 shows corresponding spectra for several different M-sequence phases applied to the pixels of the LCM. Note from Figs. 2.4 (a)-(d), that the process of encoding transforms an input femtosecond pulse into a noise-like signal several picoseconds in time duration. A longer length M-sequence increases the temporal spread of the output pulse, with a corresponding decrease in peak power. This is important for optical CDMA as it reduces the effects of nonlinearity in the transmission channel when such encoded pulses are propagated over several kilometer distances. Note the holes in the spectrum seen in Figs. 2.5 (a)-(d) which are related to diffraction effects arising from the frequency components of the input pulse which fall on the edges of individual pixels of the LCM's in the pulse shaper [50,51]. Each individual frequency component of the input pulse has a finite spatial extent at the mask plane (as determined by the input beam diameter), which may cause the different spatial regions of one particular frequency component to see different phase retardations. These effects are

more pronounced for the longer length M-sequences due to a larger number of 0 to π transitions. The numerical simulations presented in the next section will corroborate these results.

2.4. Pulse Shaper-Numerical Results

A numerical simulation program was written to model the effects of finite spot size on pulse-shaper operation. For the pulse shaper sketched in Fig. 2.1, the output pulse is the Fourier transform of the pattern transferred by the mask onto the input spectrum. In the frequency domain this is represented by the equation [50,51],

$$E_{out}(\omega) = E_{in}(\omega)H(\omega)$$

Here $E_{in}(\omega)$ is the Fourier transform of the input pulse, $H(\omega)$ is the transfer function of the pulse shaper and $E_{out}(\omega)$ is the output pulse in the Fourier domain. The transfer function is related to the phase transmission function in the mask plane by the equation [51],

$$H(\omega) = \left(\frac{2}{\pi w_o^2}\right)^{\frac{1}{2}} \int_{-\infty}^{+\infty} M(x) \exp\left(\frac{-2(x-\alpha\omega)^2}{w_0^2}\right) dx$$

Here M(x) is the filter transfer function in real space and the α is the linear spatial dispersion parameter of the pulse-shaper. This equation shows that the transfer function (mask function) in frequency space is the mask function in real space convolved with a Gaussian beam profile of effective spot size $w_0/(2)^{1/2}$, where w_o is the actual field spot size. This equation is valid under the assumption that the input pulse spatial profile can be represented by the lowest order Hermite-Gaussian mode, a very reasonable assumption in the current set-up considering that the input and output fiber pigtail will

filter out any higher order modes. The transfer function was solved numerically using MATLAB and the numerical results for 15, 31, 63 and 127 element M-sequence phase codes are shown in Fig.2.6 and Fig. 2.7. Note that the input pulse field $E_{in}(\omega)$ used in the simulation was the actual experimental input to the pulse-shaper as measured by an optical spectrum analyzer. The appearance of holes in the spectrum clearly indicates the effects of finite spot size on pulse-shaping operation. For comparison purposes, Fig. 2.8 shows both frequency domain experimental and numerical encoding data for 63 element M-sequence coding. With a linear approximation used in the simulations (the different frequency components in the mask plane are linearly dispersed in real space), the agreement between theory and experiment appears to be quite good.

Note that a value of $w_o = 120$ microns was used in the simulation which was determined by the following process. Experimentally, zero phase was applied to half the LCM pixels and π phase was applied to the remaining pixels resulting in a single notch in the output spectrum. Simulations were then performed for an identical mask pattern by using an initial guess for w_o, and the experimental and numerical data was compared to match the widths of the notches. After a trial and error process, the value of $w_o = 120$ microns was found to be the most appropriate.

2.5. Pulse-Shapers as Encoder-Decoders-Experimental and Numerical Results

The real test of pulse-shapers as encoding-decoding devices lied in the performance of two pulse shapers when connected in series. The two pulse-shapers had to be identical with respect to the five input design parameters listed in section 2.2. Of those five design parameters, the focal length of the lenses, and the grating period of the input and output gratings could be matched exactly by choosing identical lenses and gratings from vendors. The other three design parameters, namely the incident and diffracted angles, and the input beam diameter were made to match by careful construction of the second pulse-shaper. The following two step procedure was used to ensure a close match between the pulse-shapers. First, with no phase applied to the LCM

of either pulse-shaper the spectrum at the output of each pulse-shaper was recorded, and one pulse-shaper was tuned to create an almost exact match of the two spectra on the optical spectrum analyzer. Second, a π phase was applied to the 20^{th}, 64^{th}, and 110^{th} pixel of the LCM of each pulse shaper and zero phase applied to the remaining pixels. This created three notches in the output spectrum of each pulse-shaper at those particular pixel positions. Again one pulse-shaper was slightly tuned to match the three notches (from either spectra) in position and width on an optical spectrum analyzer. This ensured that the spatial dispersion parameter (α) and the spot size (w_o) was closely matched thus ensuring a close match of all five design parameters.

Fig. 2.9 shows experimental cross-correlation data and Fig. 2.10 the corresponding output spectra for the encoding-decoding operation for length 31 M-sequence phase codes. Fig. 2.9 (a) shows normalized intensity cross-correlation for an uncoded pulse where a constant phase is applied to the LCMs in both the encoder and the decoder. Fig. 2.9 (b) shows cross-correlation data for a properly decoded pulse for 31 element M-sequence encoding-decoding when the phase codes of the two LCMs match and Fig. 2.9 (c) shows an improperly decoded pulse when the phase codes on the two LCMs do not match. Note that the vertical axes in Figs 2.9 (b) is normalized to the peak intensity of Fig. 2.9 (a). It can be seen from Fig. 2.9 (a) and Fig. 2.9 (b) that although the encoding-decoding process restores the pulse-width of the properly decoded pulse to its original uncoded value, its peak intensity is reduced (measured second harmonic intensity ~ 60 % for length 31 M-sequence coding). As explained before for the single pulse shaper case, diffraction effects at the LCM cause a decrease in the peak intensity and the appearance of wings in the decoded pulse. Note also the dramatic difference in the pulse-width and peak intensities between the properly and improperly decoded pulse (compare Fig. 2.9 (b) with Fig. 2.9 (c)). Multiple-users can be accommodated in optical CDMA based on this contrast in intensity and pulse-width. Figs. 2.10 (a) - (c) show the output spectra corresponding to Figs. 2.9 (a) -(c) respectively. Note that the spectrum of the improperly decoded pulse shows more holes. This is because the M-sequences in the encoder and decoder do not match resulting in a larger number of 0-π transitions.

Although some diffraction effects are inevitable due to the discrete nature of the LCM pixels and the physical limitations on the diameter of the input beam, they do not appear to be a serious limitation for two reasons. First, the pulse-width of the properly decoded pulse is quite well restored (the decrease in the peak intensity can be compensated by amplification). Second, the intensity contrast between the properly and improperly decoded pulses is quite high (compare Fig. 2.9 (b) and Fig. 2.9 (c)) as is required for high contrast nonlinear thresholding in the receiver. As will be described in the final chapter, we can also obtain high fidelity encoding-decoding with a 2.5km dispersion compensated link between the two pulse-shapers. The numerical results for the encoding-decoding operation are shown in Figs. 2.11 and Figs. 2.12. Fig. 2.11 shows the temporal numerical results for 31-element M-sequence encoding-decoding and Fig. 2.12 shows the corresponding spectral numerical results. A comparison of Fig. 2.11 with Fig. 2.9, and Fig. 2.12 with Fig. 2.10 shows good agreement between the numerical and experimental results. Numerical simulations for length 15 and length 63 M-sequences were also performed and the numerical and experimental results are compared in Table 1 which clearly shows of the effect of the length of the M-sequence on the reduction in the peak intensity of the properly decoded pulse. This proves the validity of the numerical simulation program and establishes its usefulness as a simulation tool for analyzing multi-user encoding-decoding operation in optical CDMA.

Table 2.1
Comparison of numerical and experimental results for different length M-sequence coding. Γ is the ratio of the peak intensity of the properly decoded pulse to that of the uncoded pulse.

M-sequence length	Γ (expt.)	Γ (theory)
15	73.15%	74.07%
31	59.02%	65.50%
63	28.52%	35.69%

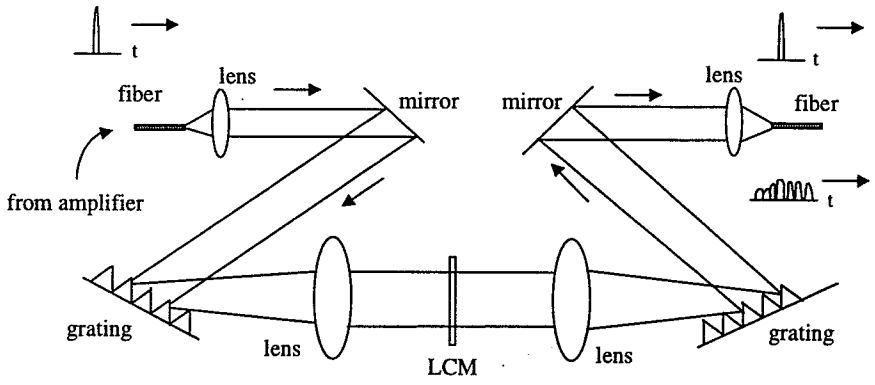

Fig. 2.1. Experimental arrangement of the pulse shaper (encoder).

(a)

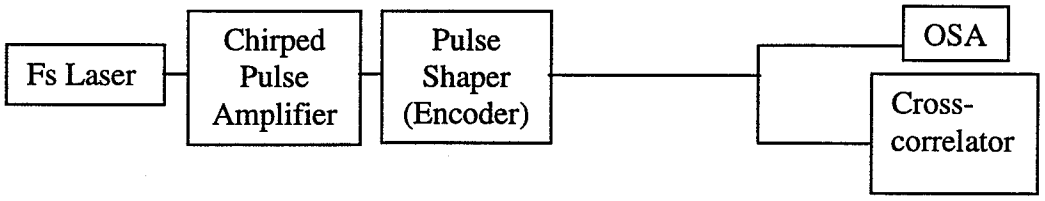

(b)

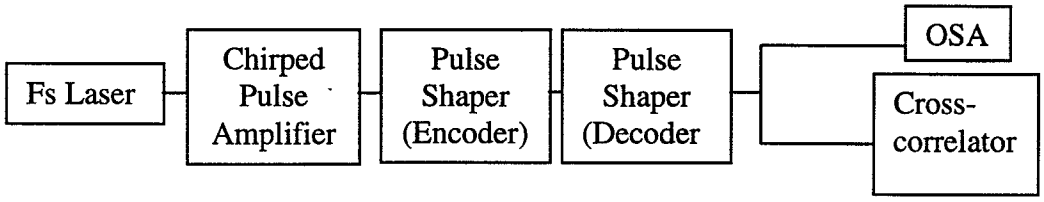

Fig. 2.2: (a) Experimental arrangement to demonstrate femtosecond encoding, (b) experimental arrangement to demonstrate femtosecond encoding-decoding.

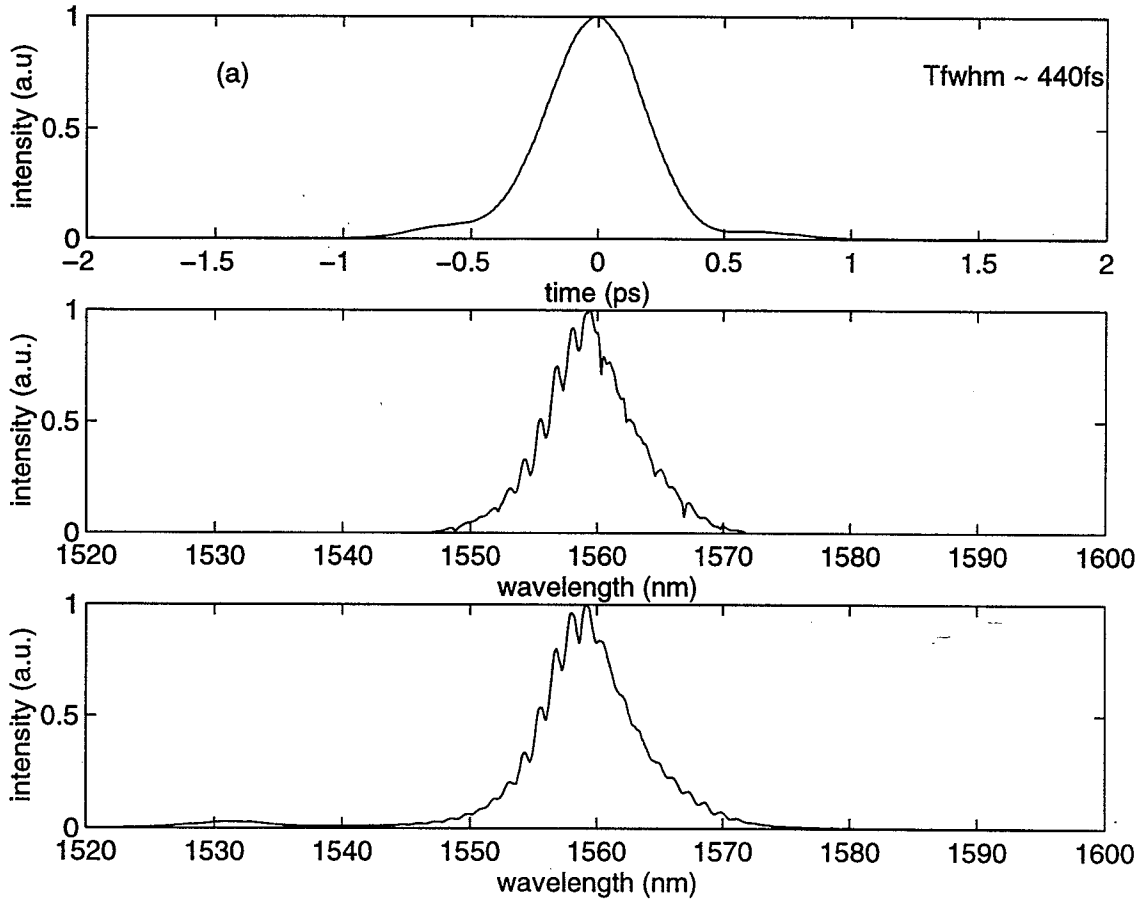

Fig. 2.3. (a) Cross-correlation data at the output of the pulse-shaper for constant phase applied to the LCM pixels, (b) power spectrum corresponding to (a), (c) power spectrum at the input of the pulse-shaper.

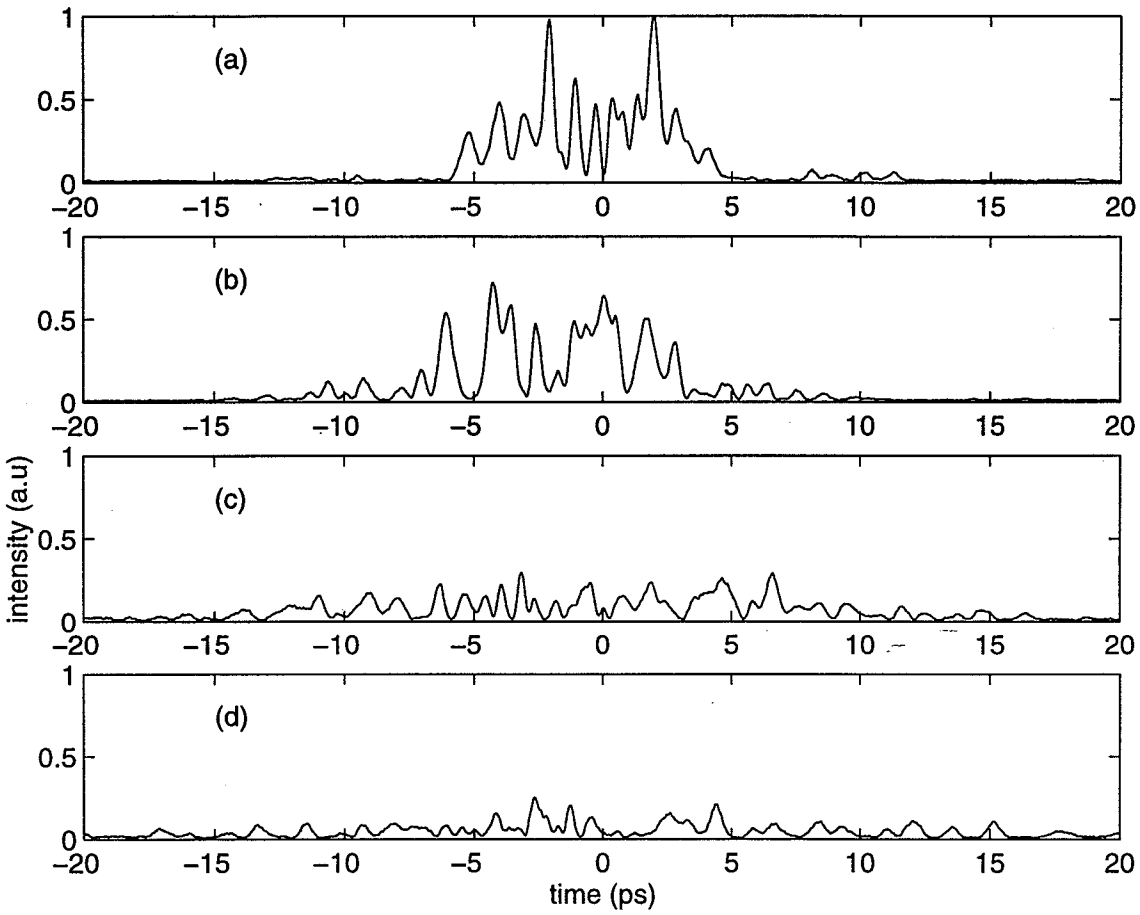

Fig. 2.4. Intensity cross-correlations at the output of the pulse-shaper for length 15, 31, 63, and 127 element M-sequence coding (corresponding to (a)-(d) respectively).

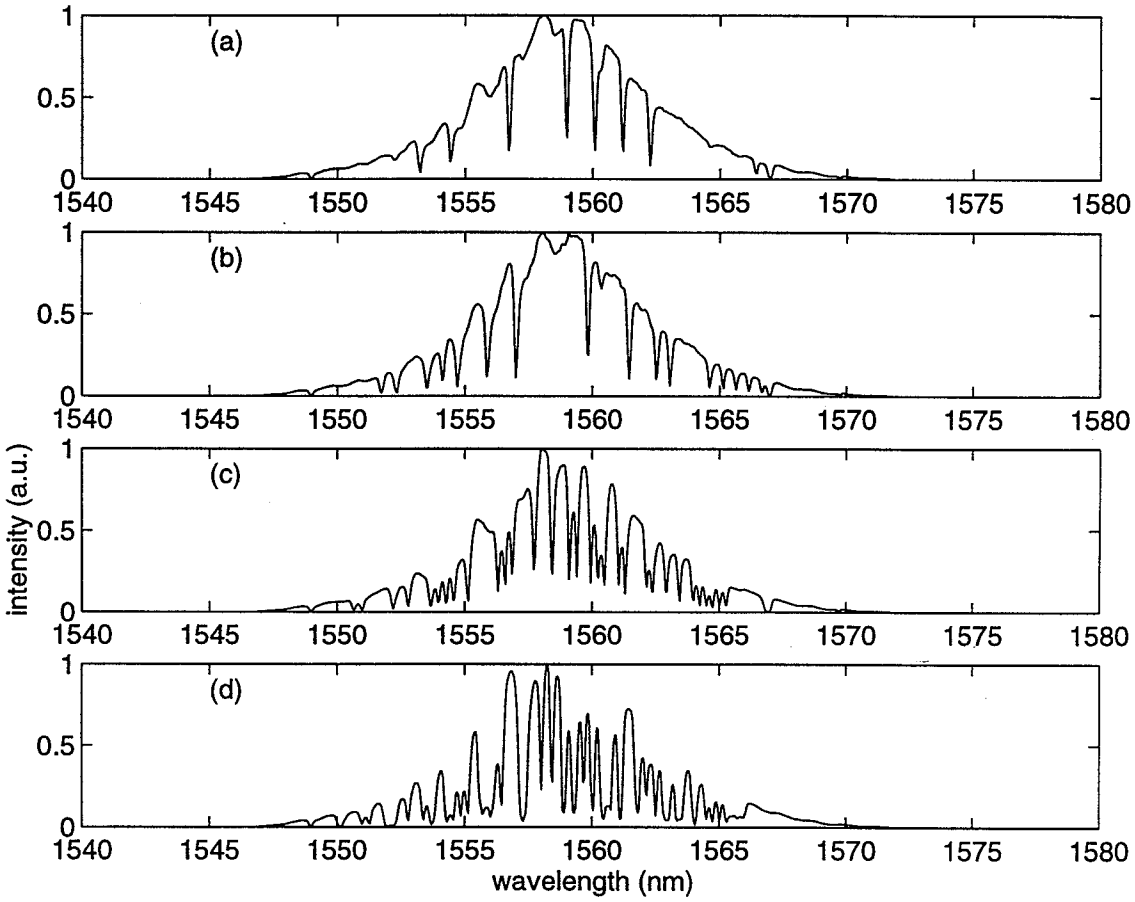

Fig. 2.5. Power spectra at the output of the pulse-shaper for length 15, 31, 63, and 127 element M-sequence coding (corresponding to plots (a)-(d) respectively).

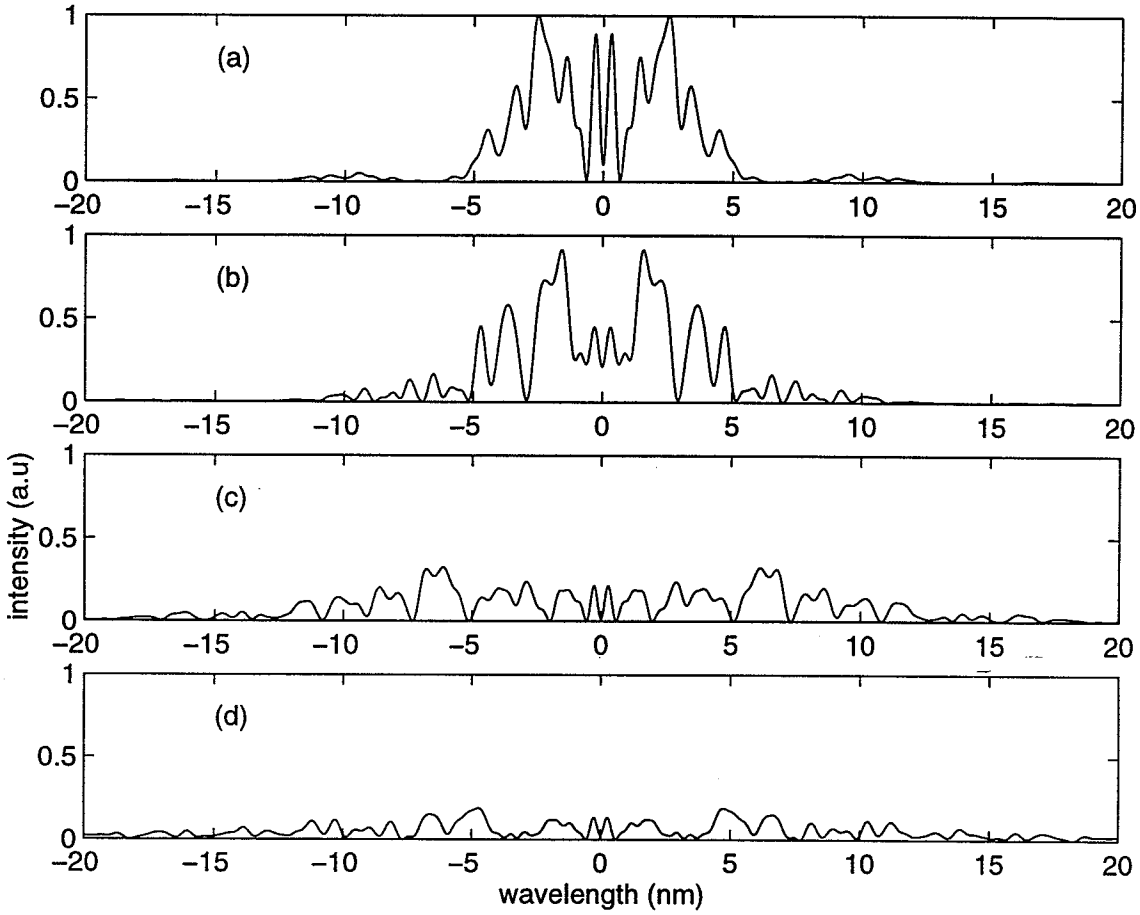

Fig. 2.6. Numerical temporal pulse shaping results for length 15,31,63, and 127 M-sequence coding. (corresponding to (a)-(d) respectively).

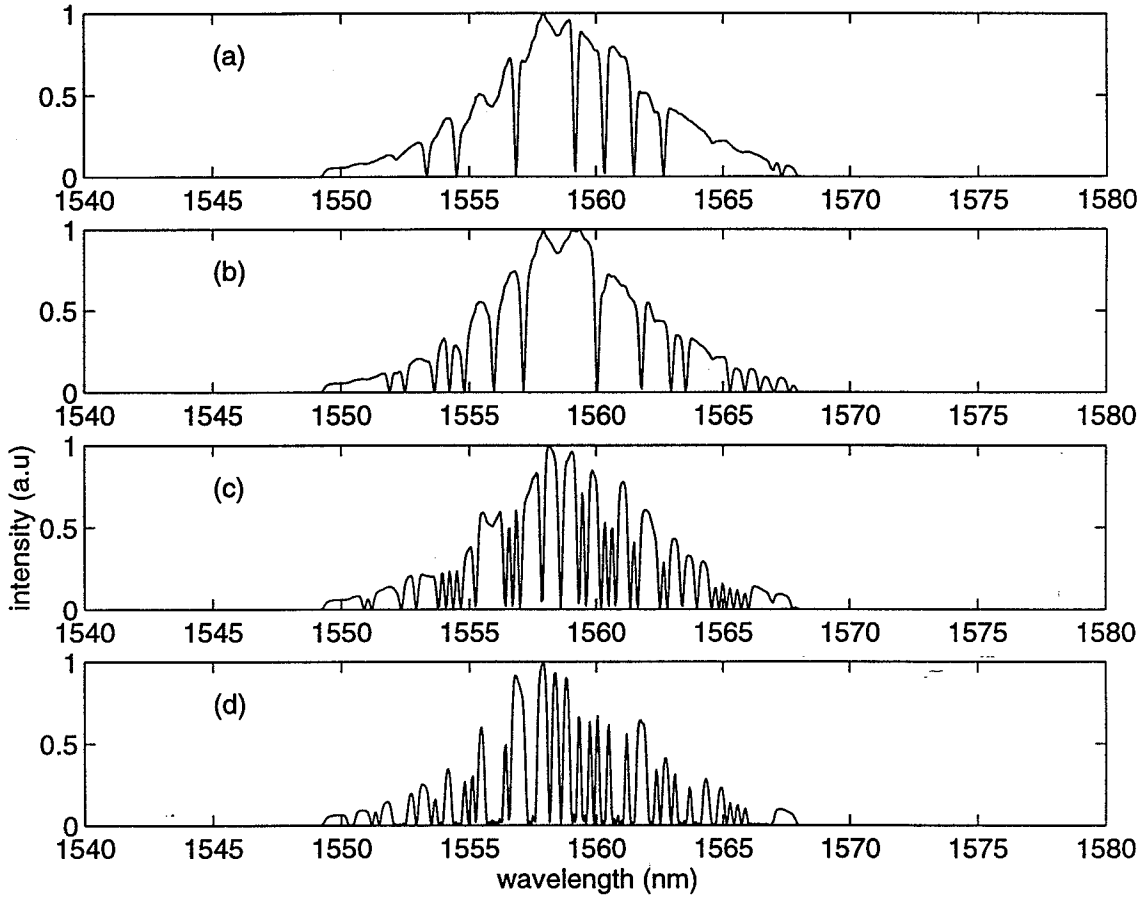

Fig 2.7. Numerical spectra at the output of the pulse-shaper for length 15, 31, 63, and 127 element M-sequence coding (corresponding to (a)-(d) respectively).

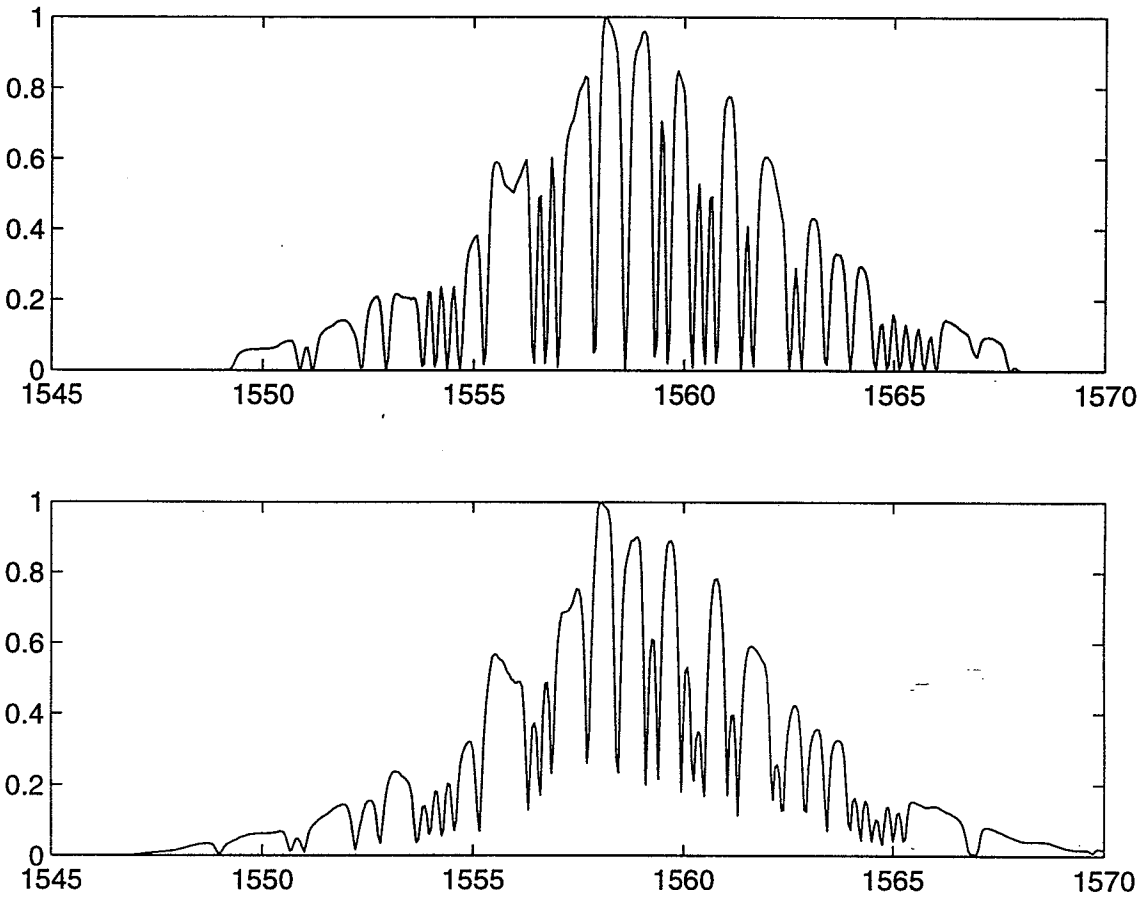

Fig. 2.8. Comparison of numerical (top figure) and experimental (bottom figure) power spectra for length 63 M-sequence coding.

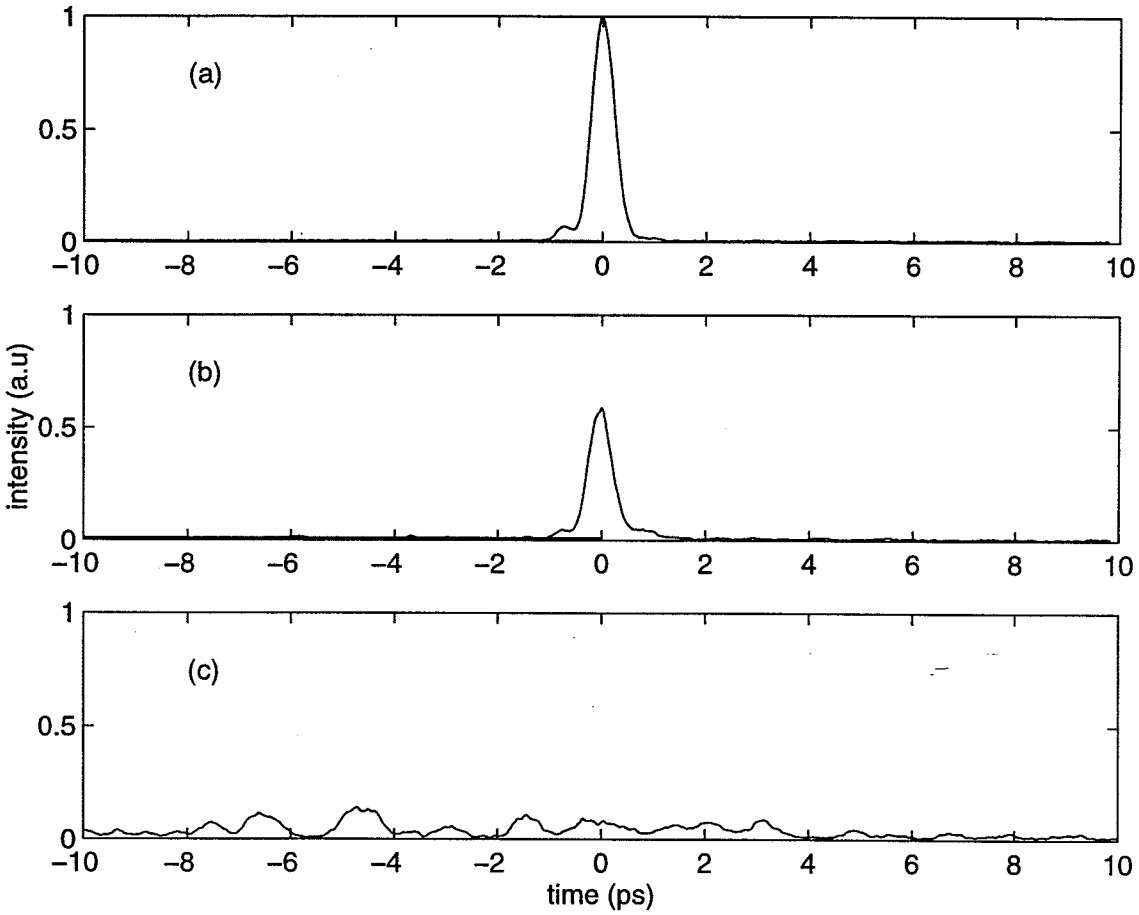

Fig. 2.9. Experimental encoding-decoding intensity cross-correlation data for length 31 M-sequences for two back to back connected pulse shapers. (a) Constant phase applied to LCM's in both pulse shapers, (b) conjugate phase applied to LCM's in both pulse shapers, (c) non-conjugate phase applied to LCM's in both pulse shapers.

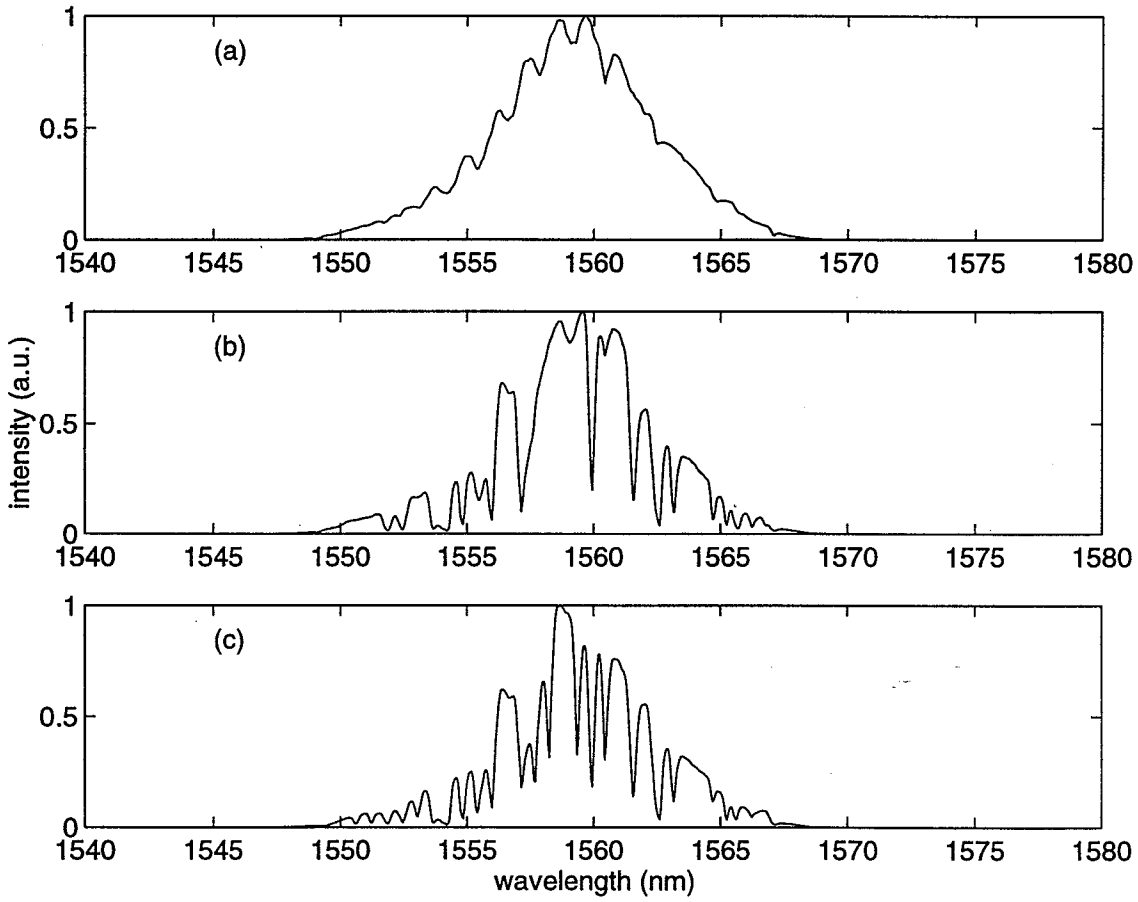

Fig. 2.10. Experimental encoding-decoding power spectral data for length 31 M-sequence encoding-decoding for two back to back connected pulse shapers. (a) Constant phase applied to LCM's in both pulse shapers, (b) conjugate phase applied to LCM's in both pulse shapers, (c) non-conjugate phase applied to LCM's in both pulse shapers.

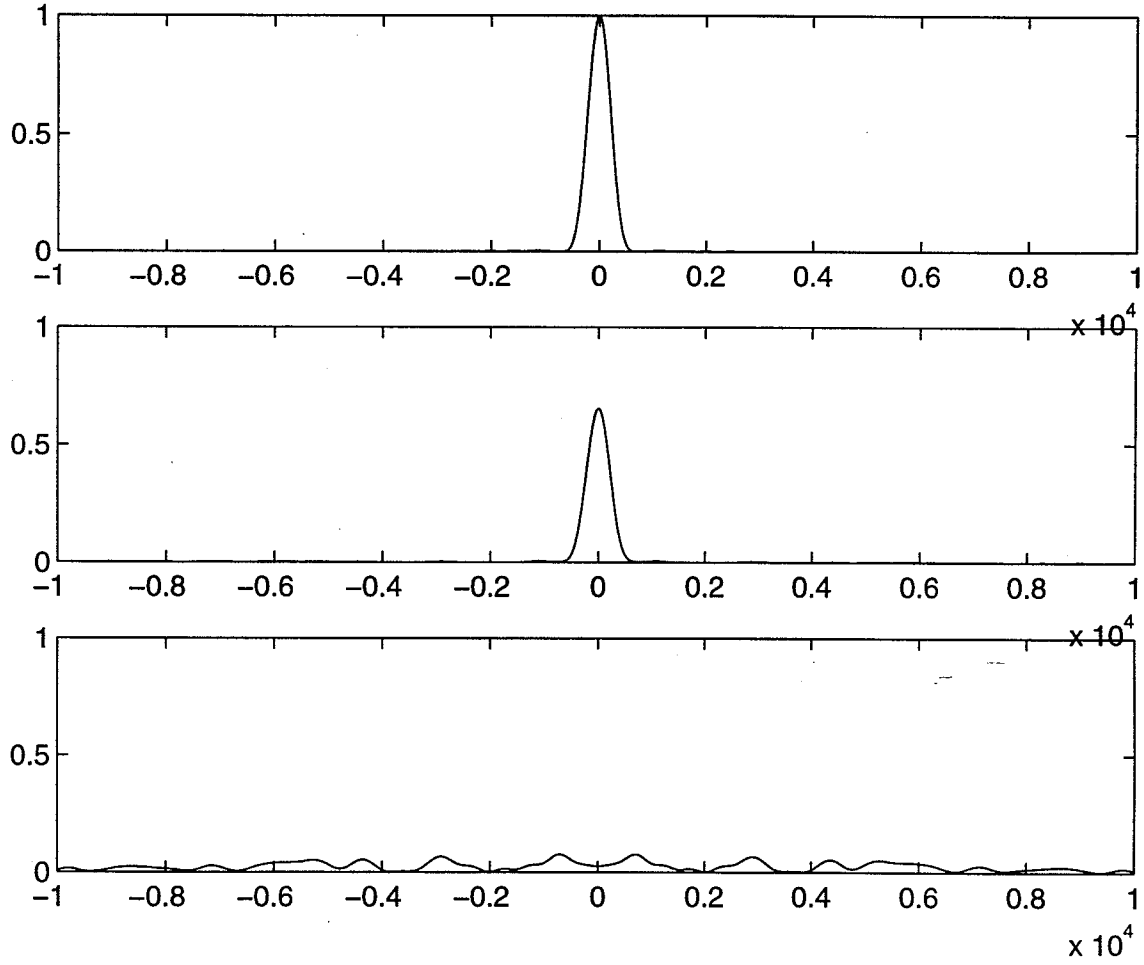

Fig. 2.11. Numerical encoding-decoding temporal intensity data for length 31 M-sequences for two back to back connected pulse shapers. (a) Constant phase applied to LCM's in both pulse shapers, (b) conjugate phase applied to LCM's in both pulse shapers, (c) non-conjugate phase applied to LCM's in both pulse shapers.

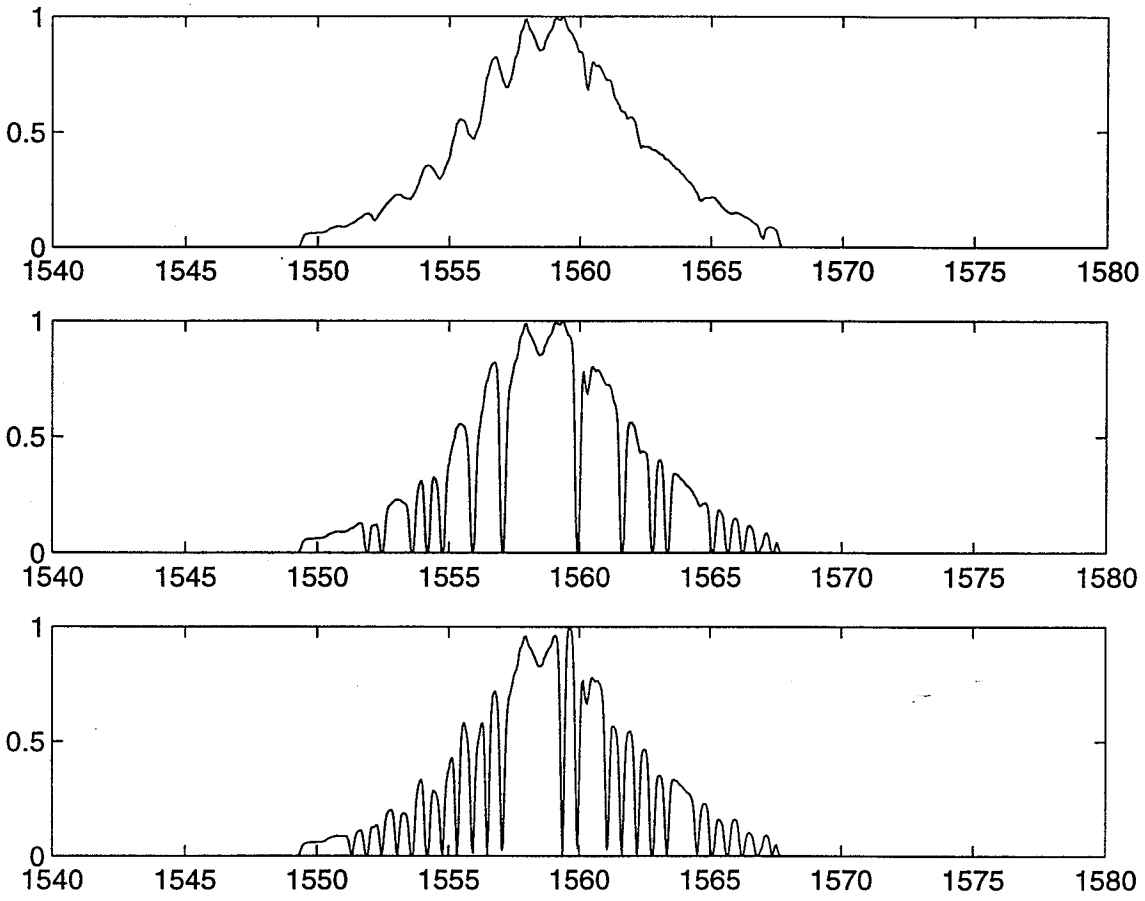

Fig. 2.12. Numerical encoding-decoding power spectral data for length 31 M-sequences for two back to back connected pulse shapers. (a) Constant phase applied to LCM's in both pulse shapers, (b) conjugate phase applied to LCM's in both pulse shapers, (c) non-conjugate phase applied to LCM's in both pulse shapers.

3. ULTRAFAST NONLINEAR THRESHOLDERS

The receiver in the optical CDMA scheme requires a thresholding device that is able to distinguish between properly decoded femtosecond signal pulses and improperly decoded picosecond interference. Since both the signal and interference are too short in duration to be distinguished by ordinary photodiodes, a nonlinear device is required which distinguishes on the basis of peak power (or pulse-width). This chapter describes such nonlinear thresholders that use the nonlinear effects in optical fibers to perform high contrast thresholding at relatively low average powers. The experimental arrangement used to perform this high contrast thresholding will be described, and the experimental results will be presented. Numerical simulations were also performed to understand the nonlinear effects in optical fibers. A brief description of the numerical solver and numerical results will also be presented.

3.1. Background And Literature Survey

To be useful in femtsecond CDMA systems, the ultrafast nonlinear thresholder should satisfy the following criteria. First, it should be able to discriminate between high peak power femtosecond pulses and low peak power picosecond interference with a very high contrast ratio. A high contrast ratio is critical in a multi-user environment where there would be only one signal pulse and several interfering users. To perform satisfactorily in a multi-user environment, for example in local area networks that may typically have several hundred users, a contrast ratio on the order of 30 dB or higher would be necessary to prevent erroneous detection. Second, the thresholder should be able to perform high contrast thresholding at relatively low average powers. This is also critical for multi-user operation since it would reduce the demands on the

amplifier preceding the thresholder. Most fiber amplifiers are limited in output saturation powers to a few tens of milliwatts. Hence to accommodate a reasonable number of users, the thresholder should be able to operate at average power levels of one milliwatt or less. Third, the thresholder design should be fairly insensitive to small changes in the power or pulse-width of the decoded signal. This is again necessary for a multi-user CDMA system where as it would reduce the requirement for precise power budgeting. Several different nonlinear effects (in different material media) have been used to perform the operations of switching and multi/demultiplexing, operations that are related to thresholding [36-38, 53-61]. A device based on two-photon absorption in GaAs waveguides was also reported that shows potential for ultrafast thresholding applications [62]. Some pertinent examples from the literature will be reviewed here, and their advantages and disadvantages will be discussed to motivate the final choice of using the nonlinear self-phase-modulation and soliton-self-frequency-shift effects in optical fibers to perform thresholding operation for the optical CDMA system.

One technique for femtosecond switching used nonlinear directional couplers fabricated in dual core optical fibers [36]. A nonlinear directional coupler consists of two closely spaced single mode waveguides with an intensity dependent index of refraction [56,57]. At low intensities, light in one waveguide gets coupled to the other waveguide over a distance called the coupling length. When the input intensity goes above a critical limit, the intensity dependent refractive index detunes the coupler and the light remains in the original waveguide. The device reported in 36 used a 0.5cm fused-quartz dual-core directional coupler and could switch 100fs pulses between the two cores for 32KW switching peak power. Although this device exhibited good switching performance it would not make a good thresholder due to its several limitations. The main limitation of this device was the low contrast ratio (~ 10 dB) obtained between the two output ports even at power levels greater than four times the switching power. This would limit its use in a multi-user environment. Other limitations were low fabrication and environmental tolerances, as well as the large energies required for achieving intensity dependent switching. Although by using longer interaction lengths and superior fabrication technology the limitations of switching energy and environmental tolerance could be alleviated, the low contrast ratio nevertheless remains a serious limitation for using this device as a thresholder in optical CDMA.

Another potential method of intensity discrimination used the intensity dependent state of polarization in birefringent fibers [37,58]. In this method, a long piece of birefringent fiber is

unequally excited at the input. The state of polarization at the output is dependent on the input intensity. By using a polarizer after the fiber, low intensity input can be blocked while a high intensity input pulse can be transmitted through the polarizer. Although this device could be used for such applications as pedestal removal of femtosecond pulses, and for shaping the pulse-width of soltion pulses, its usefulness as a thresholder is limited due to the following reasons. The main limitation of this device was again the low contrast ratio (on the order of ~ 10 dB) that was obtained for long fiber lengths (several hundred meters) and a carefully prepared state of input polarization, thus making it unsuitable for multi-user CDMA applications. Another limitation of this device was the sensitivity of the output to the input state of polarization, and also to the birefringences induced in the fiber itself due to temperature, stresses, and fiber twists and bends. Typically, the polarization state of light propagating in optical fibers varies randomly, and precise polarization control would be difficult to attain in practice.

A third method of intensity discrimination made use of the nonlinear optical loop mirror (NOLM) [59]. A NOLM can be thought of as a waveguide loop formed by connecting the two output ports of a conventional two input-two output coupler having a power coupling ratio of α:1-α at the coupler port. An input field is split into two fields that counter-propagate the loop and return in coincidence to recombine at the coupler. Linearly this device would act as a simple mirror, but nonlinearly when $\alpha \neq ½$, the effects of propagation in the two directions (in the waveguide loop) would be intensity dependent resulting in an unequal coupler output, a property that could be exploited to make an intensity dependent switch. NOLM's have been used in a variety of applications including extinction ratio improvement devices [38], and in all-optical switching [60] and demultiplexing [61]. Although NOLM's have the advantages of robust construction (no alignment is required), and low switching energies (100's of picojoules), they nevertheless have two limitations which would have to be overcome for use in CDMA thresholding applications. The first limitation is the sensitivity of the output to the input peak intensity that would limit the dynamic range of operation this device. Functionally, the output varies as the cosine of the input intensity, and under all other ideal condition this would cause serious changes in the output if the input power levels were to fall either above or below the critical power level. The second limitation of this device is the incomplete switching observed in actual experimental devices that would limit contrast ratios (high intensity-on against low intensity-off) in the 10-15 dB range [38,60], although some improvement in contrast ratio may

be obtained by a careful design of the NOLM (theoretically the NOLM should exhibit 100% switching) and by cascading two carefully constructed NOLM's. The above-mentioned limitations would limit the usefulness of NOLM's as thresholding devices for multi-user CDMA, nevertheless, NOLM's would be the most serious challenger to our present choice of thresholders.

Ultrafast thresholding in semiconductor waveguides at 1.55μm wavelength using two-photon absorption (TPA) was also recently demonstrated [62]. Two-photon absorption is an instantaneous effect where two photons are absorbed simultaneously to generate a single electron-hole pair. The TPA induced photocurrent is directly proportional to the square of the average input optical power and inversely proportional to the pulse-width of the incident optical field. Measurements done on GaAs waveguide devices indeed found a close match between theoretical predictions and experimental results [62] testing the viability of this technique for ultrafast thresholding applications. Although this technique has the advantages of using semiconductor technology and presents an interesting choice for ultrafast thresholding, its usage as an optical CDMA thresholder is limited due to some of its disadvantages. The main disadvantage of this technique is that the photocurrent shows only an inverse linear dependence on the input pulse-width. (For comparison, the soliton-self-frequency shift effect thresholder has an inverse fourth power dependence on the pulse-width). The thresholder in the optical CDMA scheme would have to distinguish between properly decoded femtosecond pulses and equal energy improperly decoded picosecond pulses, where the difference in the pulse-width between the two would normally be on the order of 10-50. It would be difficult to extend this pulse-width contrast ratio to several hundred. A TPA waveguide thresholder used in a multi-user CDMA environment would therefore exhibit low contrast ratio that may result in erroneous detection. A second disadvantage of this technique is the additional coupling optics required for interfacing an optical fiber to a waveguide device, but with advances in interconnect technology this should not be a very serious limitation.

3.2 Ultrafast Non-Linear Fiber Thresholder

The above section discussed competing designs for ultrafast CDMA thresholding and showed their limitations with respect to the three main design considerations, namely, high contrast ratio, good dynamic range, and low average power thresholding. This section will introduce the nonlinear fiber-optic thresholders used in CDMA experiments. Two different thresholders were constructed based on two different nonlinear effects in optical fibers. The principle of operation and experimental construction of the thresholders will be discussed here. The next two sections will present the experimental and numerical results for the two thresholders.

3.2.1 Fiber-optic thresholder based on nonlinear self-phase modulation

Self-phase modulation (SPM) in optical fibers refers to a self-induced intensity-dependent phase shift experienced by an optical field propagating in the fiber resulting from an intensity dependence of the fiber refractive index [35]. This effect causes a spectral broadening of the output optical field with the magnitude of the spectral broadening proportional to the intensity of the incident field. Further, the spectral broadening is symmetric around the center wavelength for a spectrally symmetric input pulse. Before describing the use of SPM for thresholding applications, two other effects that affect femtosecond pulses propagation in optical fibers, namely, group velocity dispersion and solitons will be described. In general, dispersion is defined as the wavelength dependence of the refractive index of the medium, causing different wavelength (or frequency) components of a light pulse to travel at different velocities. The above definition typically describes chromatic dispersion, and for single-mode optical fibers, an additional factor that accounts for the effects of guided wave propagation needs to be considered. Fiber GVD is then made up of two terms, chromatic dispersion that is related to the fiber material, and waveguide dispersion that is related to the geometrical construction of the fiber and the core-cladding index difference. Fiber GVD has two important characteristics, namely, it is a function of wavelength, and it has a magnitude of zero for a particular wavelength called the zero-dispersion wavelength. An optical pulse having its center wavelength less than the zero-dispersion wavelength is said to propagate in the normal dispersion regime of the fiber, while an

optical pulse having its center wavelength greater than the zero-dispersion wavelength is said to propagate in the anomalous dispersion regime of the fiber. In general, both normal and anomalous GVD acting alone would cause the input pulse to be temporally broadened as it propagates through the fiber, the difference being in the opposite signs of chirp on the output pulse for the two cases.

The combined effects of SPM and GVD can give rise to interesting pulse behaviour depending on the relative positioning of the center wavelength of the incident pulse and the zero-dispersion wavelength of the optical fiber in which it is propagating. For pulses propagating at 1.55 μm in standard single mode fiber (that has a zero dispersion wavelength ~ 1.32 μm), the combined action of SPM and GVD can give rise to solitons. A soliton is a non-dispersive pulse that makes use of the nonlinearity in a fiber to cancel out chromatic dispersion effects. For a fundamental soliton the two effects are ideally balanced as a result of which it maintains its temporal and spectral shape as it propagates through the optical fiber. For a higher order soliton, the input pulse periodically returns back to its original temporal and spectral shape at certain positions along the fiber length, the separation between two such adjacent positions called the soliton period. Within one soliton period, the temporal and spectral shapes undergo complex structural changes governed by the exact order of the soliton.

A thresholder for optical CDMA based on the self-phase modulation effect can be ideally constructed by propagating the properly decoded femtosecond pulse as a higher order soliton over a length of optical fiber such that the output pulse over the propagation length is maximally spectrally broadened. The larger time duration improperly decoded pulse would propagate at peak power levels much less than a fundamental soliton (almost linear propagation) and would see negligible self-phase modulation effects, and subsequently negligible spectral broadening. A suitable spectral filter after the thresholder fiber can filter out the spectrally broadened femtosecond pulse and reject the picosecond interference giving high contrast thresholding. Although this scheme would work in principle, to obtain a reasonable amount of spectral broadening, either very long lengths of optical fibers or very high levels of input peak power (for the properly decoded pulse) would be required [35]. An interesting variation of this basic idea was used where the zero-dispersion wavelength of the fiber was matched to the center wavelength of the input pulse. The main motivation for this variation was the considerable reduction in the input optical power necessary to cause SPM induced spectral broadening. In this

case a femtosecond pulse propagating in the fiber would have the longer wavelength part of its spectrum in the anomalous dispersion regime, and the shorter wavelength part in the normal regime of fiber propagation. This would cause the output spectrum to split on either side of the zero-dispersion point, with the red-shifted components propagating as solitons and the blue-shifted components propagating as dispersive waves. A properly positioned long wavelength pass spectral filter would now filter out the red-shifted part. The picosecond interference due to its much lower peak power would see the fiber as an almost linear medium, would have negligible spectral changes, and would get blocked by the output spectral filter giving rise to high contrast thresholding. A schematic of the nonlinear thresholder based on the nonlinear frequency shift effects is shown in Fig. 3.1.

3.2.2 Fiber-optic thresholder based on soliton-self-frequency-shift

The soliton-self-frequency-shift is due to the Raman effect in optical fibers that causes a conversion of a small fraction of the incident power from an optical beam to another optical beam at a frequency shifted from the original frequency. This process also called as Raman scattering can be described as a scattering of the incident photon by a molecule of the medium to a lower frequency photon, along with the molecule making a transition between vibrational states in the medium [38,63]. The incident light beam can be thought as acting like a pump to generate the lower frequency light beam that is called the Stokes wave. (Although theoretically it is possible to generate an anti-Stokes wave having a frequency higher than the incident frequency, it is difficult to obtain it in practice due to the difficulty in satisfying the energy conservation principle). If the intensity of the incident beam is increased beyond a particular threshold value, this can cause the Stokes beam to grow rapidly inside the medium at the expense of the incident (pump) beam a process called stimulated Raman scattering (SRS). The process of SRS gets slightly modified when the incident light beam is an ultrashort light pulse. For a short pulse, the correspondingly broad spectral bandwidth allows the lower frequency or red shifted components of the pulse spectrum to experience Raman gain at the expense of the blue shifted components [43,64] resulting in a spectral shift towards the lower frequency or the red side. This self induced SRS phenomena can occur before the Raman threshold of noise induced SRS is reached.

In the case when the center wavelength of the incident pulse falls in the anomalous dispersion regime of the optical fiber, as is true for the 1550nm optical communication band, the pump pulse and the SRS generated Stokes pulse can experience certain novel soliton effects. If the input pulse is conditioned to match a fundamental soliton, the result is an ever-increasing red shift as the pulse propagates through the fiber. This effect which is called the Soliton Self Frequency Shift (SSFS) [43] is the primary mechanism responsible for the operation of the Raman effect thresholder. For a fundamental soliton, the SSFS is inversely proportional to the fourth power of the pulse-width and this strong dependence forms the basis for achieving high-contrast thresholding between a femtosecond signal pulse and picosecond interference signal. For a soliton of any order, the pulse width and the peak power are mathematically related and hence cannot be independently chosen, but the SSFS still shows a strong inverse dependence on pulse-width, hence the same optical fiber can provide high contrast thresholding even with higher-order solitons. The time domain picture of the Raman effect can be explained as follows. The energy in the red shifted components appears as a pulse that lags behind the input pulse since the red shifted components travel slower in the anomalous dispersion regime. This time delay increases with an increase in the frequency shift of the input pulse and puts an upper bound on the allowed frequency shift in an optical CDMA system. The time delay is not a very serious limitation as long as it is much less than the bit rate at which the system operates.

3.3. Experimental Arrangement

Fig. 3.2. shows the construction of the nonlinear thresholder which is combination of a suitable length of optical fiber followed by a long wavelength pass spectral filter and a photodetector. Two optical fibers were used, a 500m length of dispersion shifted fiber with zero-dispersion wavelength at 1559nm (which coincided with the center wavelength of the transmission laser), and a 340m length of dispersion shifted fiber with zero-dispersion wavelength at 1547nm. The first fiber was used to demonstrate the nonlinear self-phase modulation thresholder, and the second fiber was used to demonstrate the nonlinear Raman effect thresholder. The spectral shifts obtained in the fiber are converted into a contrast in energy by the long-wavelength pass filter and a photodetector. The long wavelength pass filter is

one half of a pulse shaper, with the LCM replaced by a knife-edge mounted on a translation stage. This arrangement allows us to change the filter cut-off wavelength by simply moving the spatial position of the knife-edge. The knife-edge is positioned to block most of the wavelength components of the unshifted picosecond interference, and pass most of the long wavelength components of the shifted femtosecond signal pulse. As will be seen in the next section the exact position of the cut-off wavelength is critical to achieve high contrast thresholding. The spectrally filtered pulse exiting the long wavelength pass filter is focussed into a photodetector. The combination of spectral filter and photodetector thus converts any frequency shifts occurring in the thresholder fiber into amplitude variations which can be detected by the photodetector.

Fig. 3.3 shows in block diagram form the experimental arrangement used for demonstrating nonlinear thresholder operation. Input pulses to the experiment are generated by a stretched pulse modelocked fiber ring laser [21] which are spectrally filtered to yield pulse durations of ~ 275 fs, a repetition rate of ~ 30 MHz, and pulse energies of ~ 1 pJ. These pulses are amplified using chirped pulsed amplification technique by a two-stage erbium doped fiber amplifier that uses a dispersion-compensating fiber in the final compression stage. The first stage has a gain of ~ 15 dB and gives close to transform limited ~ 350fs output pulses with a spectral bandwidth ~ 7.5 nm. The slight pulse broadening is due to the gain narrowing effects in the amplifier. In the second stage, the pulses are amplified by ~ 10 - 13 dB and are further broadened to between ~ 600fs - 900fs respectively. This stronger broadening occurs both due to further gain narrowing and due to nonlinear effects in the compression fiber. Note the amplifier could be used in either one stage or two-stage configuration depending on the thresholder fiber. For the nonlinear self-phase modulation effect thresholder only one amplifier stage was used, while for the SSFS effect thresholder both amplifier stages were used. This was simply dictated by the degree of amplification necessary for thresholder operation.

The amplified pulses are passed through a low-loss fiber pigtailed pulse shaper that was described earlier in Chapter 2. In the pulse shaper, the programmable liquid crystal modulator (LCM) was used to set the spectral phases either to a length 63 M-sequence pseudorandom phase code (which encodes the pulses into 10 -12 ps wide pseudorandom bursts) or held constant leading to essentially unchanged uncoded pulses. For M-sequence bits equal to 1, the phases of the corresponding LCM pixels are set to π radians; for bits equal to zero, the phase is set to 0 radians. The entire M-sequence is accommodated by the LCM with two pixels of the LCM

corresponding to every bit of the M-sequence. Note that we obtain a slight pulse broadening (~ 10%) between the output and input of the pulse shaper when a constant phase is applied to the LCM, although ideally there should be no pulse broadening [10]. This may arise due to interactions of polarization mode dispersion effects in the fiber components with polarization sensitive devices (e.g. gratings) in the pulse shaper.

3.4. Ultrafast Nonlinear Thresholder-Experimental Results

To demonstrate the first thresholder design, coded and uncoded pulses from the pulse-shaper were propagated over 500 m of dispersion shifted optical fiber with zero dispersion wavelength λ_0 ~ 1559 nm (which is near the center of the amplified spectrum). Note that for a full CDMA system consisting of an encoder and a decoder, the coded pulse here would correspond to an improperly decoded signal in the full system; the uncoded pulses would similarly correspond to properly decoded pulses in the full system. Nonlinear propagation effects cause the spectrum of the uncoded pulse to split and spread to either side of λ_0 [41,42]. Varying the intensity and time duration of the pulse and the propagation distance through the fiber can control the magnitude of the spectral split. The coded pulse with a lower intensity and larger time duration propagates through the same length of the thresholder fiber but exhibits negligible spectral shifts. Figs. 3.4 (b) and (c) shows the power spectral data for 0.44 mW average power in the thresholder fiber clearly revealing the differences in the output spectra for coded and uncoded pulses. The power spectrum at the input of the decoder is also shown for comparison in Fig. 3.4(a). Note that the emission at 1530nm and the long wavelength tail at 1570nm of the amplifier output spectrum are suppressed in the pulse shaper due to the finite aperture of the pulse shaper optics. These frequency shifts are converted into a contrast in energy by using a long wavelength pass filter followed by a conventional photodetector operating at speeds comparable to the repetition rate of the system. By optimally choosing the average power and the filter cutoff wavelength, a high contrast ratio is obtained. The contrast ratio is defined as the ratio of energy of the uncoded pulses to that of the coded pulses at the output of the thresholder. As seen in Fig. 3.5 a contrast ratio of nearly 1000 is achieved for a 1569 nm cutoff wavelength, a 0.44 mW average power for a fixed M-sequence code. It should

be noted that the higher contrast ratio at longer cutoff wavelengths comes at the expense of lower energy at the output of the thresholder. Fig. 3.6 shows the conversion efficiency of the nonlinear thresholder defined as the ratio of the energy at the output of the thresholder to the energy at the input of the thresholder. As shown in the figure, for 0.44 mW average power at the thresholder input, we get almost 50 % conversion efficiency for lower cutoff wavelengths, but the efficiency drops down to about 10 % when the cutoff wavelength is ~ 1569nm.

An additional test was performed to demonstrate the relative insensitivity of the contrast ratio to the exact bit pattern make-up of the 63 element M-sequence. This was done by cyclically shifting one bit at a time all the 63 bits of the M-sequence resulting in 63 different M-sequences. For a full CDMA system these 63 different M-sequences (obtained by such cyclic shifts) may represent 63 different addresses given to 63 different users. The contrast ratio was now plotted for a fixed average power of 0.44 mW in the thresholder fiber, but for 63 different M-sequence coded pulses. The results are shown in Fig. 3.7 for two different cut-off wavelengths of the spectral filter. Note that the variation in contrast ratio is less than 2 dB when the cut-off is ~ 1569nm, and less than 4 dB when the cut-off wavelength is ~ 1567nm. These results can be explained in the following manner. The pulses coded by the 63 different M-sequences have different nonlinear shifts in the thresholder fiber relative to each other, (the absolute spectral shifts are very small as compared to the uncoded pulse) giving the small variation in the contrast ratio. As the cut-off wavelength of the spectral filter is increased, more of the uncoded pulse spectrum is blocked (except possibly for some small spectral tails), making the differences in the nonlinear shifts for the different coded pulses less important, giving a more uniform contrast ratio.

To demonstrate the second thresholder design, coded and uncoded pulses from the pulse-shaper were propagated over 340 m of dispersion shifted optical fiber with zero dispersion wavelength λ_0 ~ 1547nm. The power spectra at the input of the thresholder fiber are shown in Figs. 3.8(a) and Figs. 3.8(b) for coded and uncoded pulses respectively. Figs. 3.8 (c) and 3.8 (d) show the corresponding output power spectra for ~ 1.84 mW average power in the thresholder fiber. As seen in Fig. 3.8(d), the nonlinear Raman effect has caused a part of the spectrum to shift to longer wavelengths. The coded pulse with a lower intensity and larger time duration propagates the same length of thresholder fiber but exhibits negligible spectral shift as seen in Fig. 3.8(c). Fig. 3.9 shows contrast ratio between the uncoded and coded pulses at the output of

the nonlinear thresholder for different positions of the long wavelength spectral filter. By optimally choosing the average power and the filter cutoff wavelength, a high contrast ratio between coded and uncoded pulses is obtained for a fixed m-sequence code. As seen in the figure, a contrast ratio of nearly 36 dB is achieved for 1577 nm cutoff wavelength and 1.84 mW average power. Note that the change in contrast ratio is less than 3 dB for almost a factor of two variation in the average signal power in the thresholder fiber. For this design only a small fraction of the incident energy (of the uncoded pulse) is transmitted by the spectral filter for photodetection, giving an energy conversion efficiency value of ~ 1% at the highest contrast ratio. Although this is significantly lower as compared to the earlier design, in absolute terms it is more than sufficient energy for photodetection, and is also significantly higher than the sensitivities of most receivers used in optical communication systems.

Note that for the uncoded pulses, only part of the spectrum shifts to longer wavelengths. This behavior is explained as follows. For the spectra corresponding to Fig. 3.8(d), measurements of the average power and autocorrelation pulse width at the input of the thresholder fiber yielded an approximate soliton number N ~ 5.5 and a soliton period z_0 ~ 677 m (assuming sech shaped unchirped pulses). It is well known that for powers levels corresponding to higher order solitons, input femtosecond pulses breakup into several Stokes shifted constituent pulses and a dispersive wave as they propagate along the fiber, a phenomenon called soliton decay [65]. The dispersive wave represents the energy shed by the launched pulse as it evolves into constituent solitons, and it does not shift in frequency [44]. The energy content and the center wavelength of the Stokes shifted pulses depend critically on factors like soliton number, input pulse duration, input chirp, fiber length, and the polarization maintaining properties of the fiber [65-67,44,35]. For instance, it was shown [44] that the magnitude of SSFS in polarization preserving fibers was much greater than that in standard fibers under same input conditions. Further, it was also shown [44] that for higher order solitons, a significant amount of energy existed between the shifted and unshifted spectral peaks in standard fibers as against polarization preserving fibers, the effect being more severe the higher the soliton number. The effect of input chirp on the evolution of soliton pulses in optical fibers [66,67] showed that an initial linear chirp resulted in broader solitons, with a larger amount of input energy being transferred into the dispersive wave. Although the severity of this effect is expected to be less the higher the input soliton number [67], it will nevertheless be a contributing factor. The fiber length will also affect

the SSFS, with greater shifts expected for longer propagation distances (several soliton periods). Hence for a given set of input conditions and fiber type, due to the reasons outlined above only a part of the input spectrum will shift to longer wavelengths due to the soliton self-frequency shift effect. Our experimental observations appear to be consistent with simulations and experiments conducted by others [65-67,44,35] that show similar behavior for higher order soliton propagation.

3.3. Ultrafast Nonlinear Thresholder-Numerical Results

A mathematically elegant way of analyzing nonlinear self-phase modulation and the soliton-self-frequency-shift effect in optical fibers is by using the Generalized NonLinear Schrodinger Equation (GNLSE) [35]. The GNLSE is a nonlinear partial differential equation that describes the evolution of light pulses propagating in a single mode optical fiber in the presence of dispersion and nonlinearity and except for very simple cases it can only be solved numerically. The derivation of the GNLSE from Maxwell's equations is not a trivial task and hence only the final form of the equation will be considered. Each term in the equation affects the pulse propagation in the optical fiber and the individual and collective contributions of different terms will be considered using qualitative arguments and numerical results. This section describes the numerical solution technique and presents the simulation results.

3.4.1 The Generalized Nonlinear Schrodinger Equation (GNLSE)

The GNLSE is a nonlinear partial differential equation and can be rigorously derived from the vector Helmholtz wave equation. In its most general form it can be written as [35],

$$\frac{\partial A}{\partial z}+\frac{\alpha}{2}A+\beta_1\frac{\partial A}{\partial t}+\frac{j\beta_2}{2}\frac{\partial^2 A}{\partial t^2}-\frac{\beta_3}{6}\frac{\partial^3 A}{\partial t^3}= \tag{3.1}$$

$$j\gamma\left[(1-\alpha_r)|A|^2A+\alpha_R A\int_0^\infty h_R(t')|A(t-t')|^2\,dt'+\frac{j}{\omega}\frac{\partial}{\partial t}\left((1-\alpha_r)|A|^2A+\alpha_R A\int_0^\infty h_R(t')|A(t-t')|^2\,dt'\right)\right]$$

Here z is the distance along the direction of propagation in the fiber and t is the time. A (z,t) is the slowly varying amplitude of the optical electric field vector **E**(**r**,t) which is written as,

$$E(r,t) = \hat{x}\frac{1}{2}\{F(x,y)A(z,t)\exp(j(\omega t - \beta_0 z)) + c.c\} \tag{3.2}$$

Here F(x,y) is the transverse field distribution and the other symbols have their usual meaning. The first term on the left-hand side of Eq. (3.1) describes the evolution of the pulse amplitude with distance along the fiber. The second term includes the effect of fiber loss through the loss parameter α. The next three terms account for the chromatic dispersion through the parameters β_1, β_2 and β_3 which are related respectively to the group velocity of the pulse, the group velocity dispersion and the slope of the group velocity dispersion. The terms on the right hand side account for the effects of fiber nonlinearity through the fiber nonlinearity parameter γ. The first term describes the lowest order instantaneous nonlinear effect and is due to the nonlinear refractive index of the optical fiber. The second term describes the higher order nonlinear Raman effect and is represented by a delayed response function $h_R(t)$. The function $h_R(t)$ has been modeled in several different ways [68-71] to accurately reflect the actual delayed Raman response of a silica fiber. The constant α_R is a scaling constant and indicates the contribution of the Raman nonlinearity towards the total nonlinearity. Its exact value is dependent on the functional form of $h_R(t)$ and a value of 0.18 is most commonly used [70]. The third and fourth terms describe the higher order nonlinear effect of self steepening or shock formation at a pulse edge and acting alone make negligible contributions [72] unless the pulse duration is on the order of a few tens of femtoseconds [35,72].

It is necessary to make several simplifying assumptions to arrive at the form of the GNLSE as written above. First, the incident optical field is considered to be linearly polarized and is assumed to maintain its polarization as it propagates along the fiber length so that light can be treated as a scalar phenomenon. Second, the interaction of the optical field with the optical fiber is mathematically described by a macroscopic induced electric polarization and quantum mechanical effects are neglected. The induced polarization consists of a linear part that is proportional to the electric field, and a nonlinear part, which is proportional to higher powers of

the electric field. The nonlinear part is considered as a small perturbation to the linear part. Third, the slowly varying approximation for the incident electric field is used which treats the electric field as a slowly varying function of time relative to the optical period and a slowly varying function of spatial distance relative to the propagation distance along the fiber. Although some of these approximations may seem restrictive at first, the simplifications due to them make the solution of the GNLSE tractable and these solutions have been shown to agree well with experimental data for several different cases [35,70,71,72,73].

3.4.2 Numerical Simulation of the Generalized Nonlinear Schrodinger Equation

Before attempting to solve the GNLSE as given by Eq.(3.1), it is useful to employ a frame of reference moving with the optical field at the group velocity v_g and use a normalized amplitude U(z,t). This can be respectively achieved by making the transformations,

$$T = t - z/v_g = t - \beta_1 z \tag{3.3}$$

$$A = \sqrt{P_0}\,U(z,t) \tag{3.4}$$

Here Po is the incident peak power. The GNLSE can now be written in the form,

$$\frac{\partial U}{\partial z} + \frac{\alpha}{2}U + + \frac{j\beta_2}{2}\frac{\partial^2 U}{\partial T^2} - \frac{\beta_3}{6}\frac{\partial^3 U}{\partial T^3} = \tag{3.5}$$

$$j\gamma P_0\left[(1-\alpha_r)|U|^2 U + \alpha_R U\int_0^\infty h_R(T')|U(T-T')|^2\,dt' + \frac{j}{w_0}\frac{\partial}{\partial T}\left((1-\alpha_r)|U|^2 U + \alpha_R U\int_0^\infty h_R(T')|U(T'-T')|^2\,dT'\right)\right]$$

The split step Fourier method [35] was used to solve the GNLSE. It is based on the premise that in propagating the optical field over a small distance h, the dispersive and the nonlinear effects can be assumed to act independently. This can be better understood by writing the GNLSE in the following form,

$$\frac{\partial U}{\partial z} = (\hat{D} + \hat{N})U \tag{3.6}$$

Here $\hat{D}$ is a differential operator that accounts for the effects of fiber dispersion and loss in a linear medium and $\hat{N}$ is a nonlinear operator that accounts for the effect of fiber nonlinearity. Using Eq. (3.5) these operators can be written as,

$$\hat{D} = -\frac{j\beta_2}{2}\frac{\partial^2}{\partial t^2} + \frac{\beta_3}{6}\frac{\partial^3}{\partial t^3} - \frac{\alpha}{2} \tag{3.7}$$

$$\hat{N} = j\gamma P_0\left[(1-\alpha_r)|U|^2 + \alpha_R\int_0^\infty h_R(t')|U(T-T')|^2\,dt' + \frac{j}{w_0 U}\frac{\partial}{\partial T}\left((1-\alpha_r)|U|^2 U + \alpha_R U\int_0^\infty h_R(T')|U(T-T')|^2\,dT'\right)\right] \tag{3.8}$$

Now consider the propagation of the optical field a small distance h in the optical fiber, from z to z+h. If $\hat{N}$ is assumed to be independent of z, a formal exact solution of Eq. (3.6) is given by,

$$U(z+h,T) = \exp(h(\hat{D}+\hat{N}))U(z,T) \tag{3.9}$$

According to the split step Fourier method the solution can be arrived at in two steps: in the first step, the nonlinearity acts alone and the dispersion is zero, and in the second step, dispersion acts alone and the nonlinearity is zero. The solution of Eq. (3.6) can then be simply written as,

$$U(z+h,T) = \exp(h\hat{D})\exp(h\hat{N})U(z,T) \tag{3.10}$$

A comparison of Eqs. (3.9) and (3.10) shows that the split step Fourier method ignores the noncommuting nature of the operators $\hat{D}$ and $\hat{N}$. For any two noncommuting operators $\hat{a}$ and $\hat{b}$, we can write [35],

$$\exp(\hat{a})\exp(\hat{b}) = \exp\left[\hat{a}+\hat{b}+\frac{1}{2}[\hat{a},\hat{b}]+\frac{1}{12}[\hat{a}-\hat{b},[\hat{a},\hat{b}]]+\ldots\ldots\ldots\right] \tag{3.11}$$

Here $[\hat{a},\hat{b}] = \hat{a}\,\hat{b} - \hat{b}\,\hat{a}$. By using $\hat{a} = h\hat{D}$ and $\hat{b} = h\hat{N}$, the dominant error term when the solution is written in the form of Eq. (10) results from the commutator $h^2/2\,[\hat{D},\hat{N}]$ and the split step Fourier method is said to be accurate to the second order in step size h.

To improve the accuracy of the split step Fourier method the solution is arrived at in three steps. In the first step the optical field is propagated over a distance h/2 where the dispersion acts alone and the nonlinearity is taken as zero. In the second step, at the midplane z + h/2 the effect of nonlinearity over the entire distance h is considered with the dispersion taken as zero. In the third step, the optical field is again propagated over a distance h/2 with the dispersion acting alone and the nonlinearity being zero. Using this recipe, we can mathematically express the solution as,

$$U(z+h,T) = \exp(\frac{h}{2}\hat{D})\exp(h\hat{N})\exp(\frac{h}{2}\hat{D})U(z,T) \tag{3.12}$$

A comparison of Eq. (3.9) and (3.12) shows that the dominant error term is of the third order in step size h. Because of the symmetric form of the exponential operators in Eq. (3.12), this method is known as the symmetric split step Fourier method. The solution to the linear part $\exp(\frac{h}{2}\hat{D})$ is obtained by integration in frequency space and the solution to the nonlinear part $\exp(h\hat{N})$ is obtained by direct time integration. The symmetrized split step method is straightforward to implement and only requires that the step size in z and the total time window T be selected judiciously to maintain the required accuracy. The details of the algorithm are illustrated in the flowchart of Fig. 3.10.

3.4.2. Numerical Results

Before the GNLSE was used to design ultrafast nonlinear thresholders, it was initially solved for certain known test cases to establish the validity of the numerical solver. The effects of dispersion and nonlinearity were considered both separately and jointly, and in all instances they compared well with numerical results obtained by others [35,44,71,72]. Numerically the

effect of dispersion can be observed by solving the GNLSE with the nonlinearity parameters $\gamma = 0$. Fig. 3.11 shows the effect of group velocity dispersion for a 250fs Sech shaped optical pulse, $U(T) = \mathrm{Sech}(T/T_o)$ after it has propagated a distance of 10LD in standard fiber ($\beta_2 < 0$). The parameter LD is called the dispersion length and is formally defined as $T_o^2/|\beta_2|$, where To is the initial incident pulse width parameter. T_o is related to the full width at half maximum by the expression $T_{FWHM} = 1.763\ T_o$ for Sech shaped pulses and by the expression $T_{FWHM} = 1.665\ T_o$ for Gaussian pulses. LD provides a convenient length scale over which the dispersive effects become important. For this example in real units 10LD corresponds to a distance of about 10 meters. Two observations can be made from the figures: first, as expected, the pulse has considerably broadened in the time domain but has retained its Sech shaped profile, second, the spectral bandwidth of the transmitted pulse is unchanged and therefore the pulse has become chirped. Fig. 3.12 shows the effects of third order dispersion on the pulse after it has propagated a distance equivalent to 100LD in standard fiber. As seen, the effect of higher order dispersion is to distort the pulse shape such that an oscillatory structure develops near the pulse edge. The bottom part of Fig. 3.12 shows the effects of both β_2 and β_3 on the pulse after it has propagated a distance of 100LD in standard fiber. For convenience the output pulse has been magnified 10 times. It can be seen that the parameter β_2 totally dominates the parameter β_3. Third order dispersion becomes significant if the magnitude of the parameter β_2 decreases or if the pulse width is decreased.

Numerically the effect of loss enters the GNLSE through the parameter α. Due to advances in fiber fabrication technologies, fused silica fibers have a very low value of loss. Typically the attenuation constant has a value of 0.2 dB/km and loss plays an important role only when the propagation distance is over several kilometers. This can be observed from the GNLSE by setting the nonlinearity and dispersion parameters equal to zero. We then have the simple equation,

$$\frac{\partial U}{\partial z} = -\frac{\alpha}{2}U \tag{3.13}$$

that has the solution,

$$U = U_0 \exp(\frac{-\alpha z}{2}) \tag{3.14}$$

For a typical attenuation constant of 0.05 km^{-1}, we can see that the output power has decreased by about 4% after propagating through 1 kilometer of fiber. Since the thresholder fiber is typically under a kilometer in length the effect of loss can be neglected.

Numerically the effect of nonlinearity can be observed by solving the GNLSE without the dispersion and loss terms. The GNLSE be then written in the following form.

$$\frac{\partial U}{\partial z} = j\gamma P_0\left[(1-\alpha_r)|U|^2 U + \alpha_R U\int_0^\infty h_R(T')|U(T-T')|^2\,dt' + \frac{j}{w_0}\frac{\partial}{\partial T}\left((1-\alpha_r)|U|^2 U + \alpha_R U\int_0^\infty h_R(T')|U(T'-T')|^2\,dT'\right)\right] \tag{3.15}$$

Here the various terms on the right side constitute the various nonlinear effects observed in optical fibers. The effect of SPM can be observed by solving the above equation keeping only the first term and setting $\alpha_R = 0$. This is equivalent to assuming an instantaneous nonlinearity, a questionable assumption for pulses shorter than 1 psec. Fig. 3.13 shows the effect of SPM on a 250fs Sech pulse after it has propagated a distance of 10LNL. The parameter LNL is called the nonlinear length and is defined as $(\gamma Po)^{-1}$ where γ is the nonlinearity parameter and Po is the incident pulse peak power. At the transmission wavelength of 1550 nm, γ takes on a value of 1.62 W^{-1} km^{-1} [35] and for a peak power of about 614W, the physical distance of 10LNL corresponds to about 10m. Two observations can be made from the figures: first, SPM causes a considerable amount of symmetric spectral broadening, second, the temporal width of the pulse is unchanged, implying that the pulse has become chirped.

If the same pulse is propagated in a negative dispersion fiber with second order dispersion added to the GNLSE soliton effects are observed. To see this, a parameter N is introduced by the definition,

$$N^2 = \frac{LD}{LNL} = \frac{\gamma PoTo^2}{|\beta_2|} \tag{3.16}$$

If N=1, a fundamental soliton is said to propagate due to the exact balance of dispersion and nonlinearity. Dispersion dominates when N << 1 and nonlinearity dominates when N >> 1. Although not apparent from equation (3.16), the sign of the dispersion parameter and the shape of the incident pulse are important criteria for the pulse to propagate as a soliton. This is because for soliton propagation the chirp introduced by dispersion has to be equal in magnitude and opposite in sign to that induced by SPM and this is only possible if the dispersion is negative and the pulse profile is secant hyperbolic. The bottom part of Fig. 3.13 shows the propagation of the same 250fs pulse for a distance of 10 meters (10 LD) in a negative disperson fiber. The input and output spectral and temporal shapes are indistinguishable.

A higher order nonlinear effect that results from the intensity dependence of the group velocity is called the nonlinear shock effect. Physically, the group velocity becomes such that the peak moves at a lower speed than the wings and the trailing edge of the pulse becomes steeper and steeper as the pulse propagates. This self-steepening of the trailing edge eventually creates an optical shock and hence this effect is called the nonlinear shock effect. Numerically this effect can be observed by keeping only the first and third terms on the right side of Eq. (3.15) and again treating the nonlinearity as being instantaneous. Fig. 3.14 shows the effect of self-steepening for a 125fs sech shaped optical pulse after it has propagated a distance of 20 LNL. The input peak power was such that this physically corresponds to propagation distance of 5 meters. The effect of self-steeping on the trailing edge is evident. Also seen is the asymmetric spread of the spectral frequencies. The magnitude of the optical shock is dependent on the pulse width and the peak power. The bottom traces in Figs. 3.14 show a 250fs Sech pulse propagated through 5 meters of fiber. The input peak power is reduced by a factor of 2 to keep the pulse energy constant to that of the 125fs pulse. The figures show that the shock effect is much less pronounced. The optical shock effect is considerably affected by the group velocity dispersion. GVD tends to dissipate the shock by broadening the steepened trailing edge of the pulse thus making it more symmetric. When the temporal asymmetry is reduced, the spectral asymmetry reduces correspondingly. Figs. 3.15 shows the combined effects of shock and GVD for the same

input pulse parameters and propagation distance as in Fig. 3.14. GVD tends to cancel the effects of optical shock with the cancellation being more complete for longer pulse widths.

A third nonlinear effect in optical fibers is the nonlinear Raman effect. Physically this is due the scattering of the incident photon by a molecule of the medium to a lower frequency photon, along with the molecule making a transition between vibrational energy states of the medium. If the incident pulse is a soliton then this results in an ever increasing frequency down shift as the pulse propagates, a phenomenon called the soliton self frequency shift (SSFS). Since a fraction of the energy is transferred between the pulse and the medium, energy between the input and the output pulse is not conserved. The Raman effect takes a finite amount of time and hence it is mathematically modeled by a delayed response function. The second term on the right side of the GNLSE describes the Raman effect with the parameter α_R characterizing the fraction of the contribution of the Raman effect towards the total nonlinearity and is normally taken as 0.18. In Fig. 3.16 two forms of the Raman response function $h_R(t)$ are plotted. The top plot corresponds to the mathematical function often called the Lorentzian response function.

$$h_R(t) = \frac{\tau_1^2 + \tau_2^2}{\tau_1 \tau_2^3} \exp\left(\frac{-t}{\tau_2}\right) Sin\left(\frac{t}{\tau_1}\right) \tag{3.17}$$

Here τ_1 and τ_2 are constants chosen to match the response function to actual data and their typical values are 12.2fs and 32fs respectively [71]. The bottom plot corresponds to the response function obtained from measured data on fused silica fibers. Both the functions have been normalized such that the area under the curve is equal to unity, and the functions are causal to correspond to physical reality. The normalization explains the slight differences in the magnitudes of the two functions. It can be seen that while the mathematical function is quite identical to the actual response function for times less than 150fs, the actual response function has more detail for longer times. It was found from the simulations that the mathematical function gave good results for pulse width between 100fs - 400fs when the value of the parameter α_R was taken as 0.36. For other pulse widths, this value had to be suitably modified. The actual response function gave good results when tested for pulse widths between 100fs - 1 ps with the value of α_R being 0.18. For pulse widths longer than 1 ps, the Raman effect has a negligible effect on the nonlinearity, as for longer pulses the response no longer appears to be

delayed and the entire nonlinearity can be treated as instantaneous. The Raman contribution to the nonlinearity decreases for pulsewidths shorter than 100fs and even becomes negative for pulsewidths shorter than 30fs [70]. Thus the choice between the use of the mathematical function and the actual response function depends on the availability of measured data, range of pulse widths over which results are desired and the slight added computational complexity and delay due to the use of the actual response function. Since the actual response function was available, it was used in generating the simulation results.

Fig. 3.17 show the effect of the soliton-self-frequency shift on a 250fs optical pulse propagating in standard fiber over a distance of 50 LD's which corresponds to a physical distance of 50 meters in the presence of negative GVD. The input peak power corresponds to that of a fundamental soliton. Note the frequency downshift of the output pulse and the associated time delay. The effects of third order dispersion and shock on the soliton self-frequency shift are shown in the bottom traces in Fig. 3.17. Note that these higher order effects have minimal effect on the properties of the output pulse. For comparison Fig. 3.18 shows a 125fs fundamental soliton propagating for 50 LD's in the presence of Raman nonlinearity. This corresponds to a physical distance of 12.5 meters. Note that the frequency shift is considerably higher than that obtained for the 250fs pulse. It has been shown that for a fundamental soliton, the frequency shift scales inversely with the fourth power of the pulsewidth [43]. The bottom traces in Fig. 3.18 again show the influence of higher order effects on the soliton-self-frequency shift. Note that there is now a noticeable difference in the output pulse especially in the frequency domain where the frequency shift is seen to decrease. The peak power is also reduced and since the effects of the SSFS are cumulative over the propagation distance, the differences will be more pronounced for longer propagation distances.

To design the SSFS effect thresholder we initially start by numerically simulating N=1 soliton pulses of pulse widths 125fs, 250fs and 500fs propagating over 300 LD's of standard fiber. All the terms in the GNLSE were used in the simulations. The frequency down shift incurred by each pulse as a function of distance is shown in Fig 3.19. The horizontal dashed lines indicate the transform limited spectral width of the corresponding pulses. Since the pulse propagates in the anomalous dispersion regime, this frequency downshift results in time delay. The time delay associated with the propagation of each of the pulses is plotted in Fig. 3.19. Several general trends can be observed from the figures. First, note that the frequency shift

increases as the propagation distance is increased. Second, the frequency shift increases as the pulse width is decreased. Note that the parameter LD is dependent on the pulse width and scales inversely with it as $LD = To^2/|\beta_2|$. In terms of real distance, 100 LD for a 125fs pulse is about 25 meters while that for a 250fs pulse is about 100 meters. The time delay is not a very important consideration as long as it is much less that the round trip time of the laser. For a laser operating at 1Gb/s, a maximum limit on the time delay of 100ps corresponding to one tenth of the round trip period would be considered tolerable for the thresholder design. The N=1 soliton case is used for illustrative purposes only and is not very useful for thresholding purposes primarily because the fiber lengths required to obtain a reasonable frequency shift are quite long. Also, for small fluctuations in input power, the input pulse energy may no longer be enough to sustain a fundamental soliton. This will cause the pulse to spread as it propagates which in turn will reduce the frequency shift. This situation is drastically changed if the input power is increased. Fig. 3.20 show plots of frequency shifts against distance for an N=1.2 and an N=2 soliton. The maximum time delay was less than 10 ps and was therefore not plotted. A comparison of the horizontal axes of the two figures indicates that much larger frequency shifts for the same propagation distance are obtained with an increase in input power.

Another way of obtaining high frequency shifts over reasonable fiber lengths with reduced input power requirement is by using a dispersion-shifted fiber. This fiber has close to zero group velocity dispersion at 1550nm and the third order dispersion plays an important role in defining the output properties of the pulse. This forms the basis of the second thresholder design. Fig. 3.21 shows the temporal and spectral evolution of a 250fs sech shaped input pulse after it has propagated in dispersion shifted fiber a distance equivalent to about 40 LD's in standard SMF. The equivalent soliton parameter for the same pulsewidth in standard SMF would approximately N = 0.6, and we will refer to this as the Neq = 0.6 soliton. Note the characteristic oscillations of the trailing edge due to third order dispersion. The pulse spectrum is seen to split into two spectral peaks. The lower frequency peak lies in the anomalous dispersion regime and can form a soliton. The high frequency peak lies in the normal dispersion regime and disperses away with propagation. Fig. 3.22 shows the frequency shift incurred by the input pulse propagating in the dispersion shifted fiber where LD' is defined as $To^3/|\beta_3|$. Note that a frequency shift of almost three times the spectral width can be obtained and the curves tend to saturate with increasing pulsewidths.

The frequency shifts obtained in the above thresholder designs can be converted into a contrast in energy by using a spectral filter and phototodiode after the thresholder fiber. We define a contrast ratio parameter S as the ratio of the energy in the shifted signal to the energy in the unshifted signal for a particular output filter cut-off frequency. The contrast ratio parameter would indicate how well we can discriminate between a properly decoded femtosecond signal (that would encounter large frequency shifts) and improperly decoded picosecond interference (that would encounter minimal frequency shifts). Fig. 3.23 shows the numerically evaluated variation of the contrast parameter S as a function of propagation distance for the 250fs N=1.2 soliton. The different curves correspond to different cutoff frequencies of the long wavelength pass filter after the thresholder fiber. A filter cutoff of $0.5\Delta\omega_0$ implies than the filter cutoff frequency is at half a spectral width below the center frequency. The filter is assumed to be ideal, i.e., all frequencies above the cutoff frequency are blocked and all frequencies below the cutoff frequency are passed. As can be seen from the figure, for smaller propagation distances the contrast ratio is low since the signal pulse has not downshifted much in frequency and most of the pulse energy is cut-off. As the propagation distance increases, the pulse shifts more and the contrast ratio is increased. Finally the contrast ratio saturates when the pulse has shifted much beyond the cutoff point. The lower the cut-off frequency (the farther away it is from the center frequency point) the higher the overall contrast. This is because the filter now cuts off most of the unshifted pulse energy. One way to increase the contrast ratio without moving too far away from the center frequency is to use an amplitude filter to cut off the spectral wings of the unshifted pulse before propagating in the thresholder fiber. The amplitude filter is characterized by a parameter W. The solid line in that figure is for a detector having a long wavelength pass filter at a cut off frequency $1.5\ \Delta\omega_0$ below the center frequency without any amplitude filtering. The dashed line is for the same detector with an amplitude filter which cuts out the input spectral amplitude at the 10% point (W=0.1). If an amplitude filter with W=0.2 is used, the contrast ratio is increased further to values above 1000 for a propagation distance of about 75 LD. This was because for W=0.2 the spectral wings of the unshifted pulse were almost cut-off for frequencies$1.5\ \Delta\omega_0$ below the center frequency.

3.4.3. Comparison between numerical and experimental results

Although the numerical simulations of the GNLSE showed excellent agreement with similar simulations performed by others [35,44,71,72], they showed only qualitative agreement with experimental results for both the nonlinear self-phase modulation and SSFS effect thresholder designs. This lack of quantitative agreement between numerical and experimental results has also been observed in [44] for SSFS in various communication fibers. The main reason for the discrepancy is the assumption that the input light signal is linearly polarized and stays linearly polarized as it propagates through the optical fiber. In practice optical fibers exhibit a randomly varying birefringence, causing the polarization state of an input light signal to vary randomly during propagation. To obtain a better agreement between theory and experiment, these polarization effects need to be considered while formulating and solving the GNLSE. The scalar approach that was used for solving the GNLSE would also have to be replaced with a more rigorous vector approach. Another factor that can influence the simulation results is the numerical value of the nonlinear refractive index and the effective area, which would determine the value of the nonlinearity co-efficient γ. These values are not standardized, and depend on wavelength and the fiber properties. A 30-50% difference in the effective area and the nonlinear index is not uncommon to find [44], and could give quite different simulation results. The above-mentioned factors are non-trivial and cannot be accommodated by making simple changes to the GNLSE. Although the numerical results did not show perfect agreement with experiments, they however guided the development of the two thresholders. The different qualitative aspects that determined the final thresholder design and construction are listed below. First, it was clear from numerical simulations that unless power budgeting was not an issue, it would be necessary to construct the self-phase modulation thresholder. This was borne out by the experiments that revealed that the self-phase modulation thresholder indeed required almost a factor of 4 less average power than the SSFS effect thresholder. This advantage of low average power operation made it the thresholder of choice in system experiments. Second, it was also clear from numerical simulations that a practical SSFS effect thresholder would require the properly decoded pulse to propagate at power levels corresponding to higher order solitons. This was also shown to be true by the experiments. Third, it was numerically shown that the effect of amplitude filtering would increase the thresholder contrast ratio for a given spectral filter cut-off frequency. Experimentally the function of amplitude filtering was performed by the pulse-shaper, which due to its limited spectral aperture cut off the short and long frequency tails of the

properly decoded pulse giving high contrast ratios. In the next chapter it will be shown that when these tails were not removed (as was the case when an amplifier after the pulse-shaper introduced ASE components), the contrast ratio was much lower.

The success of the ultrafast nonlinear thresholders demonstrated that high contrast ratio thresholders operating at relatively low average powers could indeed be built. Hence further numerical development of the thresholder model was not undertaken, but focus was shifted to system integration since the focus of this thesis was not only the construction of thresholders, but also femtosecond encoder-decoders and an optical CDMA test-bed.

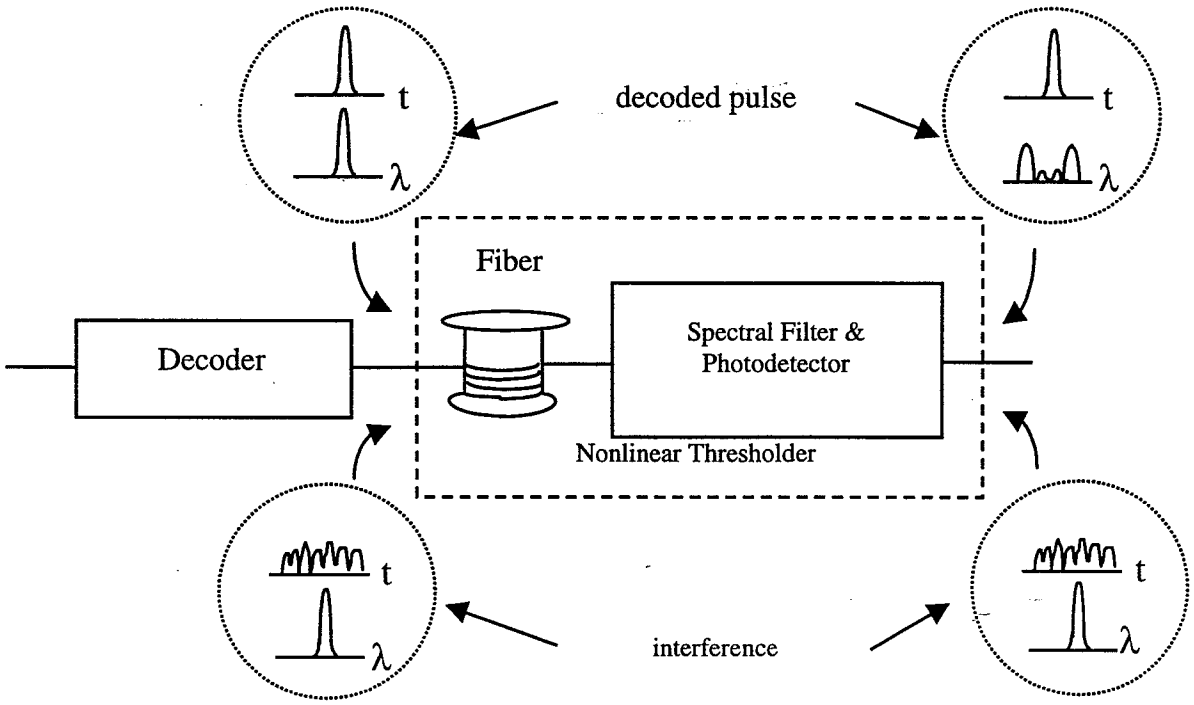

Figure 3.1: Schematic of the nonlinear thresholder.

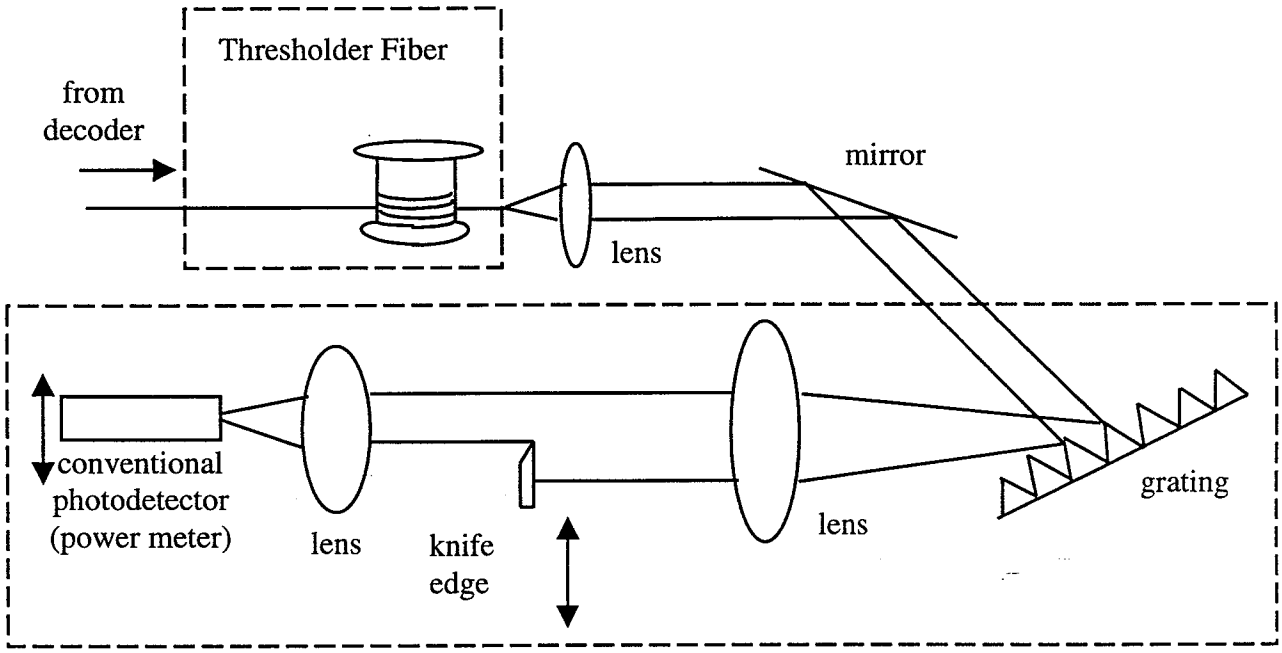

Figure 3.2: Construction of the nonlinear thresholder.

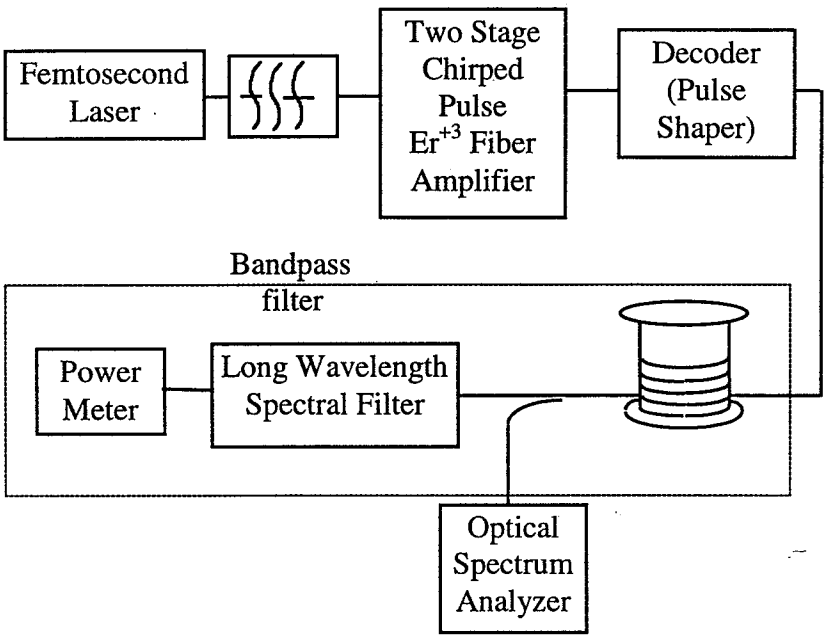

Figure 3.3: Experimental arrangement for demonstrating thresholder operation.

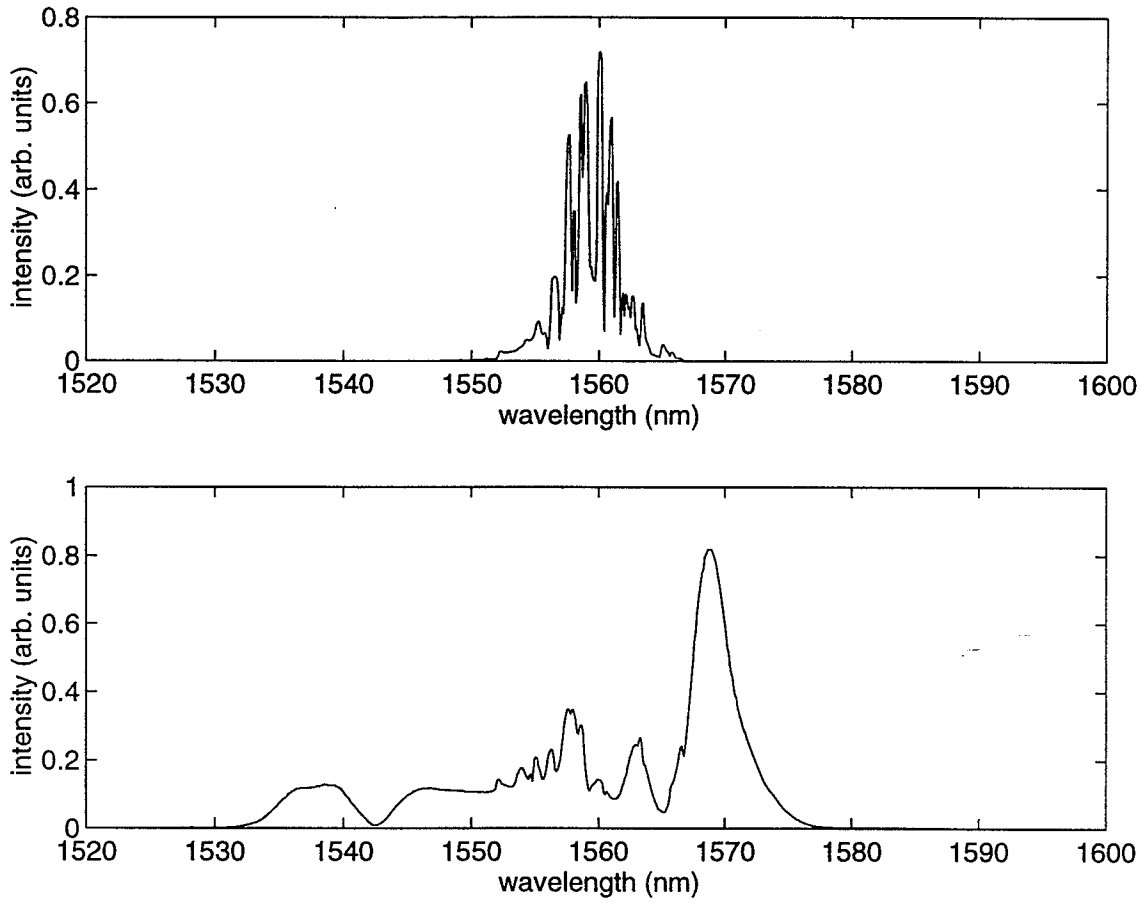

Figure 3.4: Power spectra, (a) coded signal at the output of the thresholder, (b) uncoded signal at the output of the thresholder. The average power in the thresholder fiber is 0.44 mW for both cases.

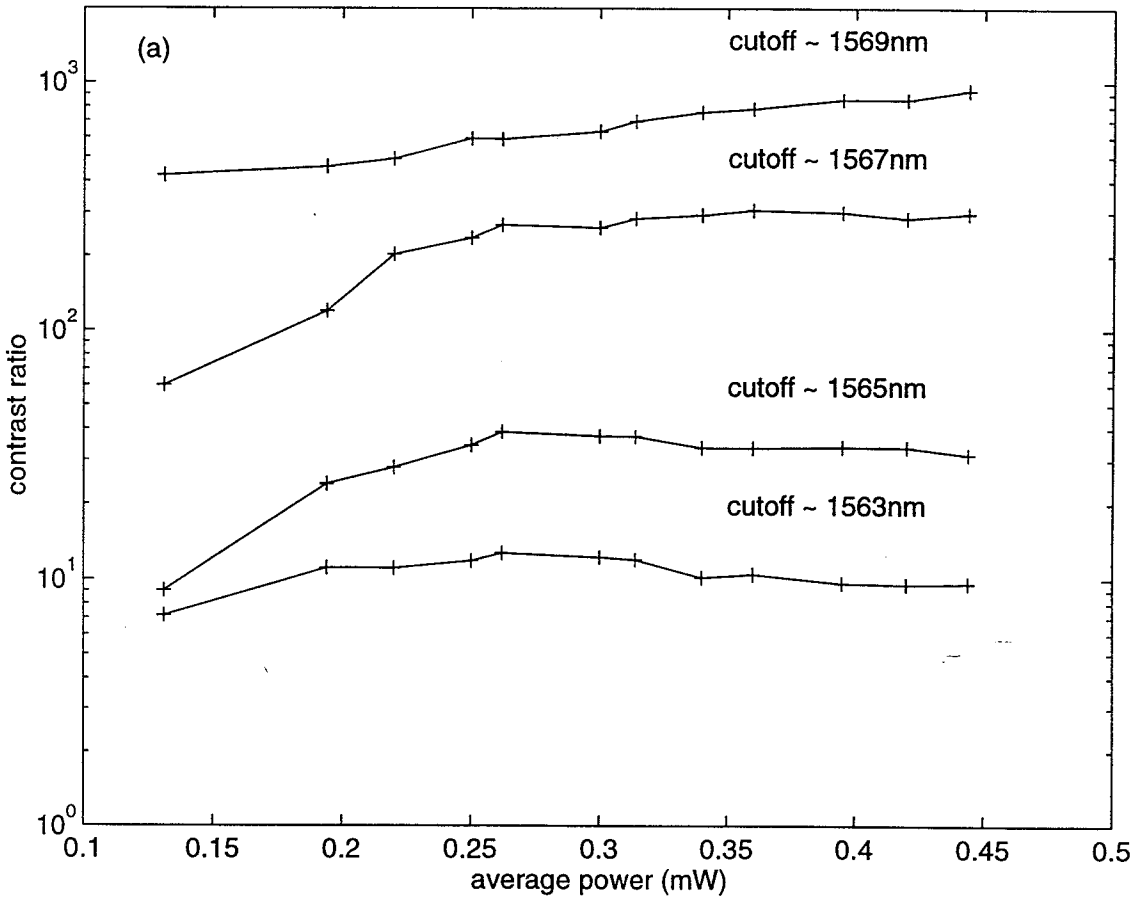

Figure 3.5: Contrast ratio of the nonlinear thresholder for different cutoff wavelengths of the long wavelength pass filter against average signal power at the input of the nonlinear thresholder fiber.

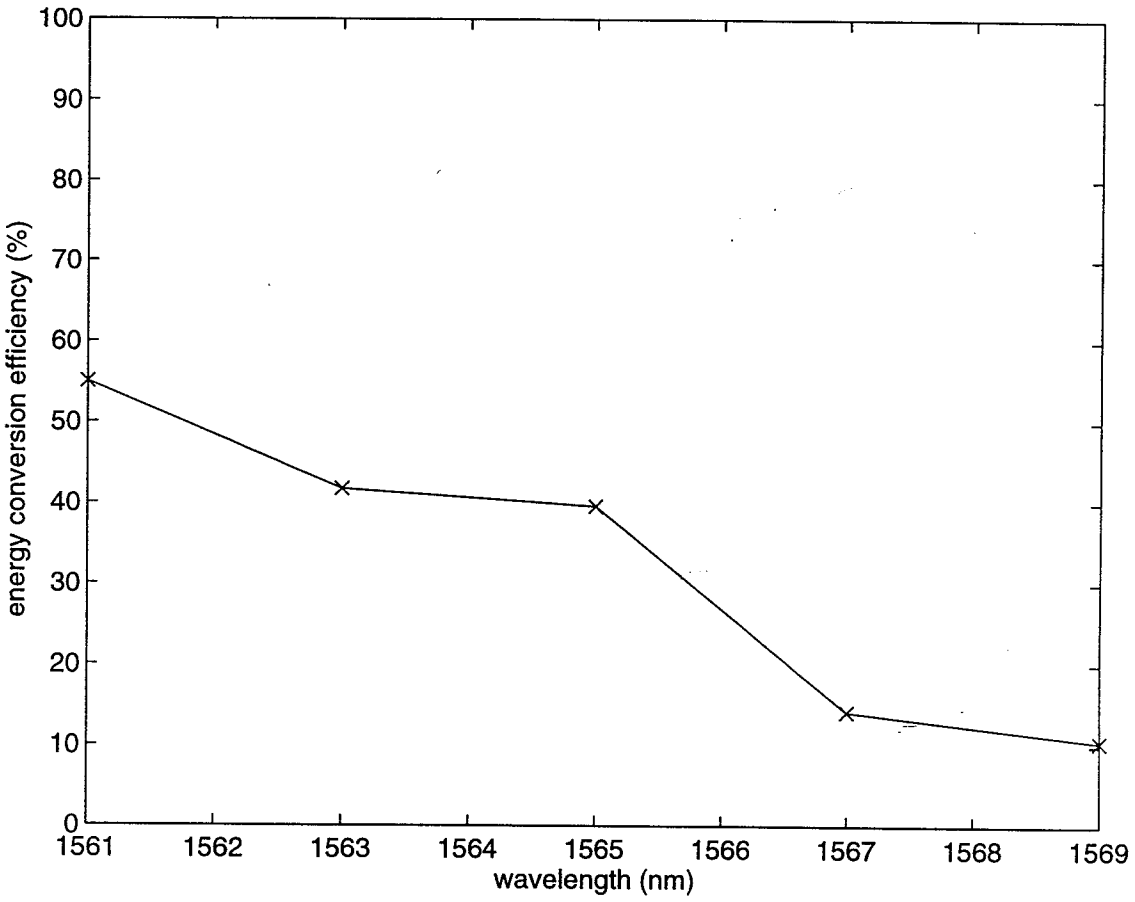

Figure 3.6: Energy conversion efficiency of nonlinear thresholder for different cut-off wavelengths of the long wavelength pass filter.

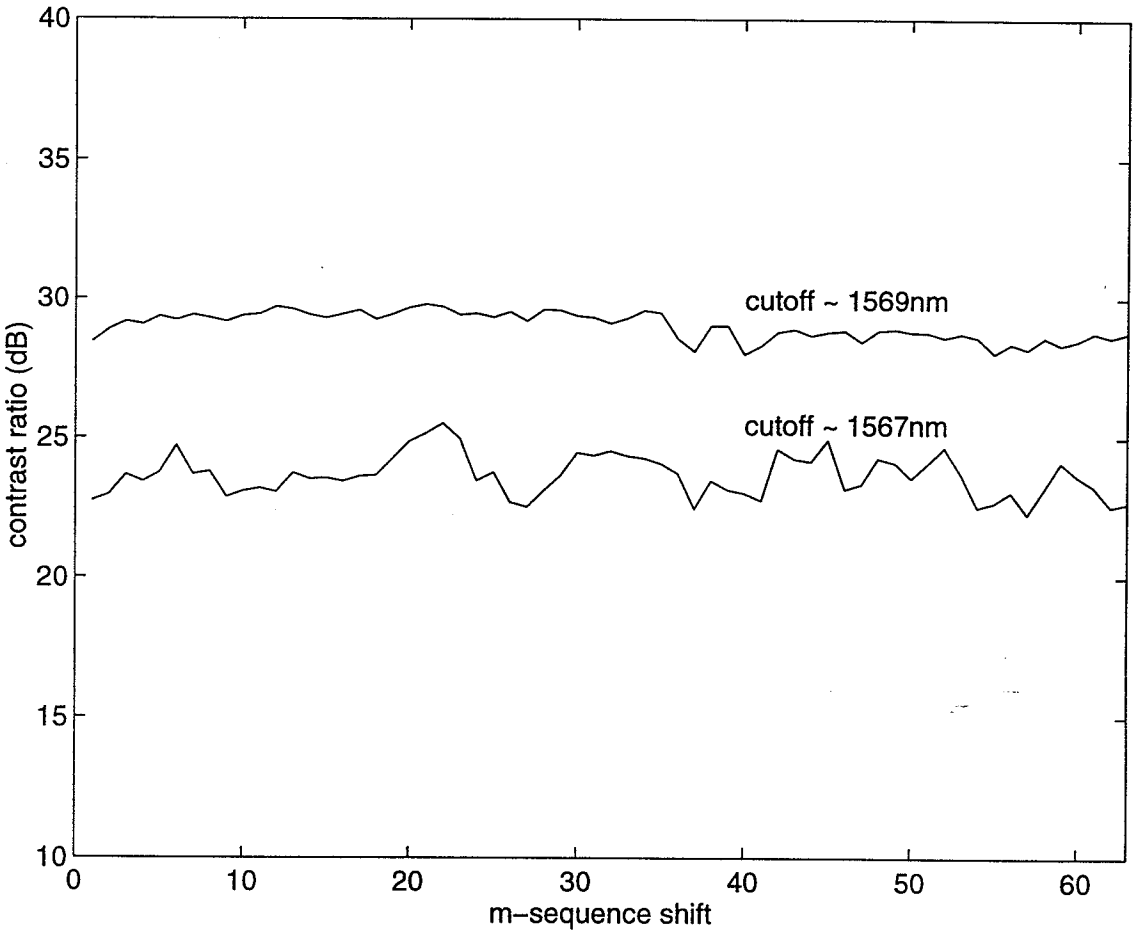

Figure 3.7: Contrast ratio variation at the output of the nonlinear thresholder for 63 different length 63 M-sequences at two different filter cutoff positions.

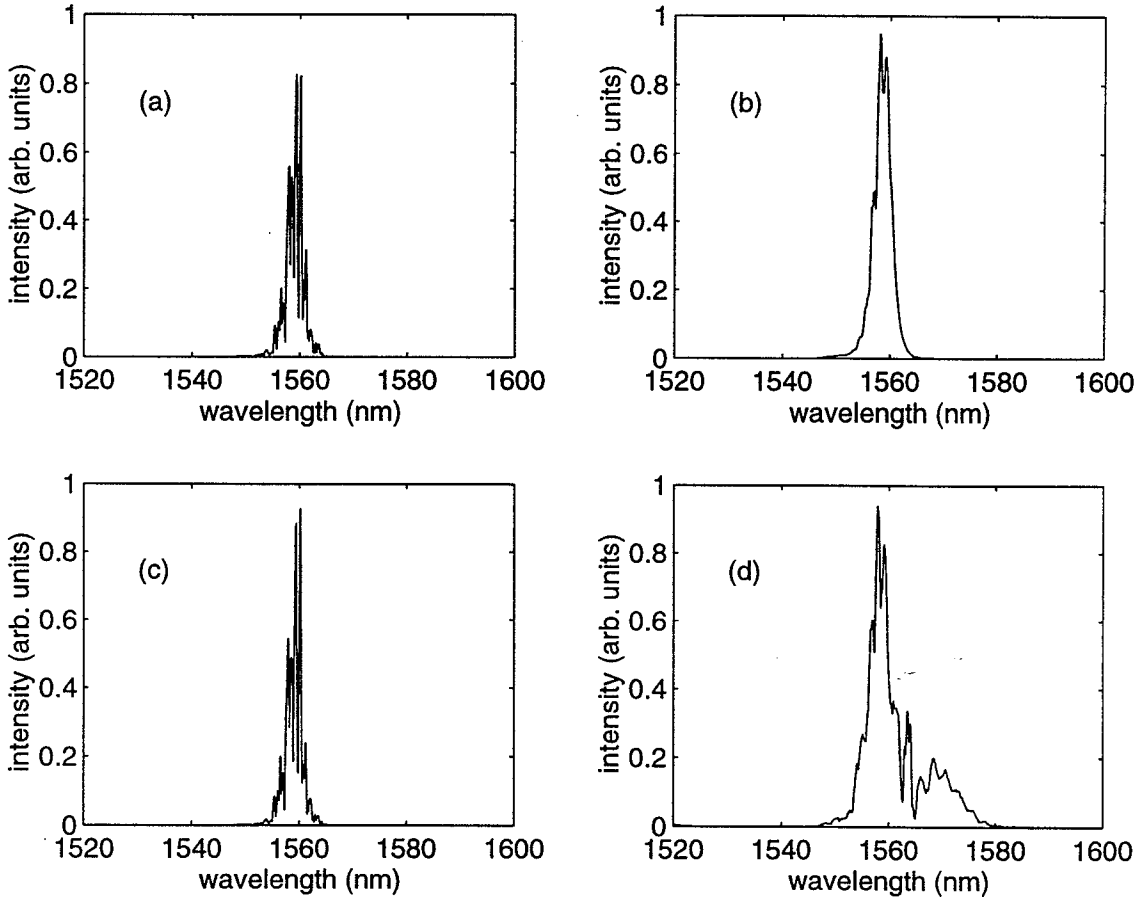

Figure 3.8: Power spectra, (a) coded pulse at input of the thresholder, (b) uncoded pulse at input of the thresholder, (c) coded pulse at output of the thresholder, (d) uncoded pulse at the output of the thresholder. The average power in the thresholder fiber is 1.84 mW in each case.

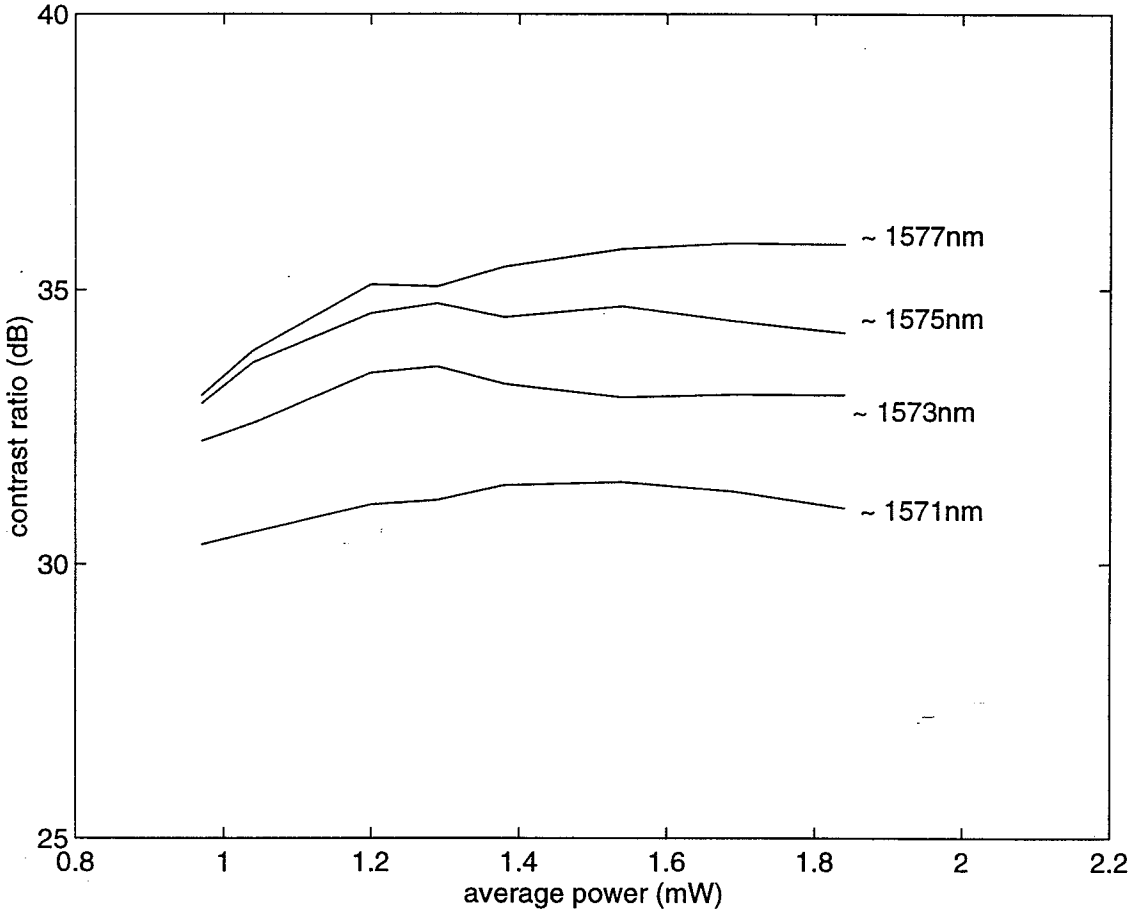

Figure 3.9: Contrast ratio of the nonlinear thresholder for different cutoff wavelengths of the long wavelength pass filter against average signal power at the input of the nonlinear thresholder fiber.

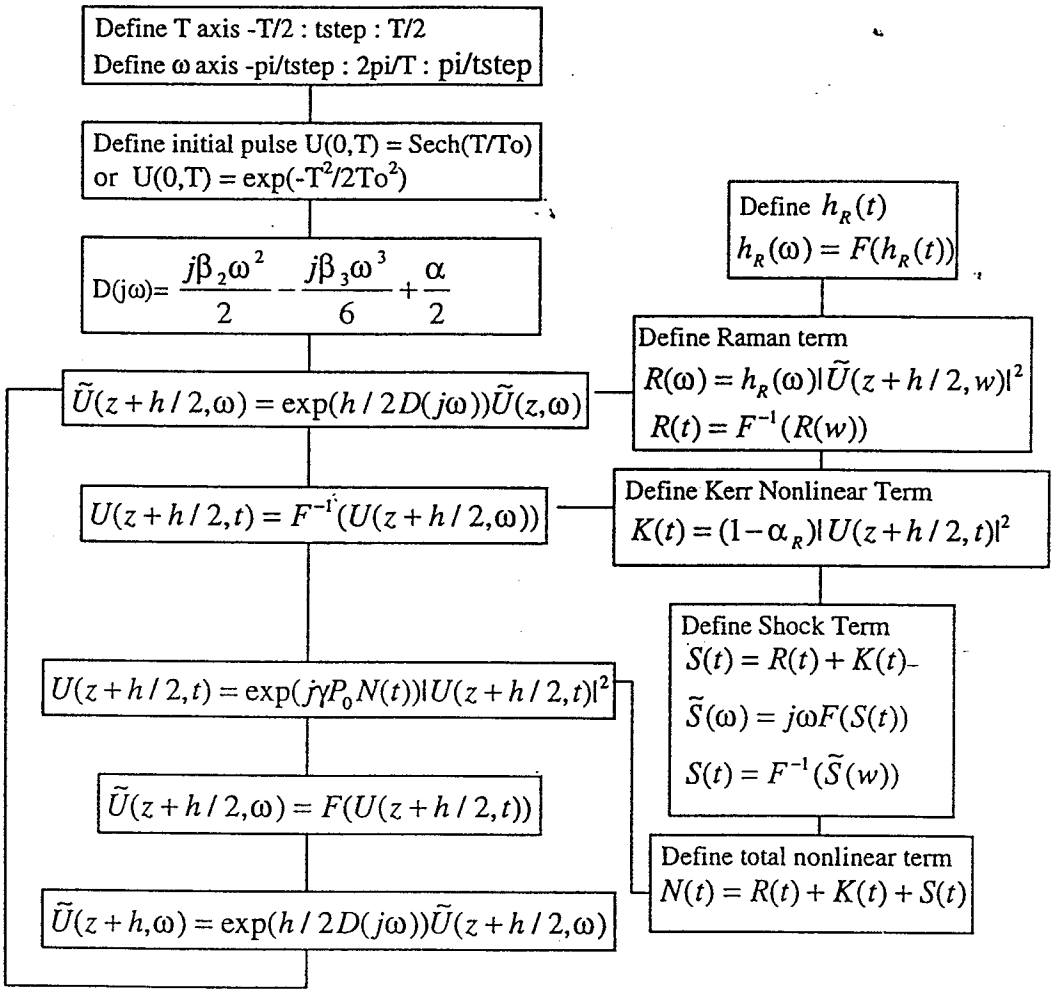

Figure 3.10: Flowchart of the algorithm to solve the GNLSE.

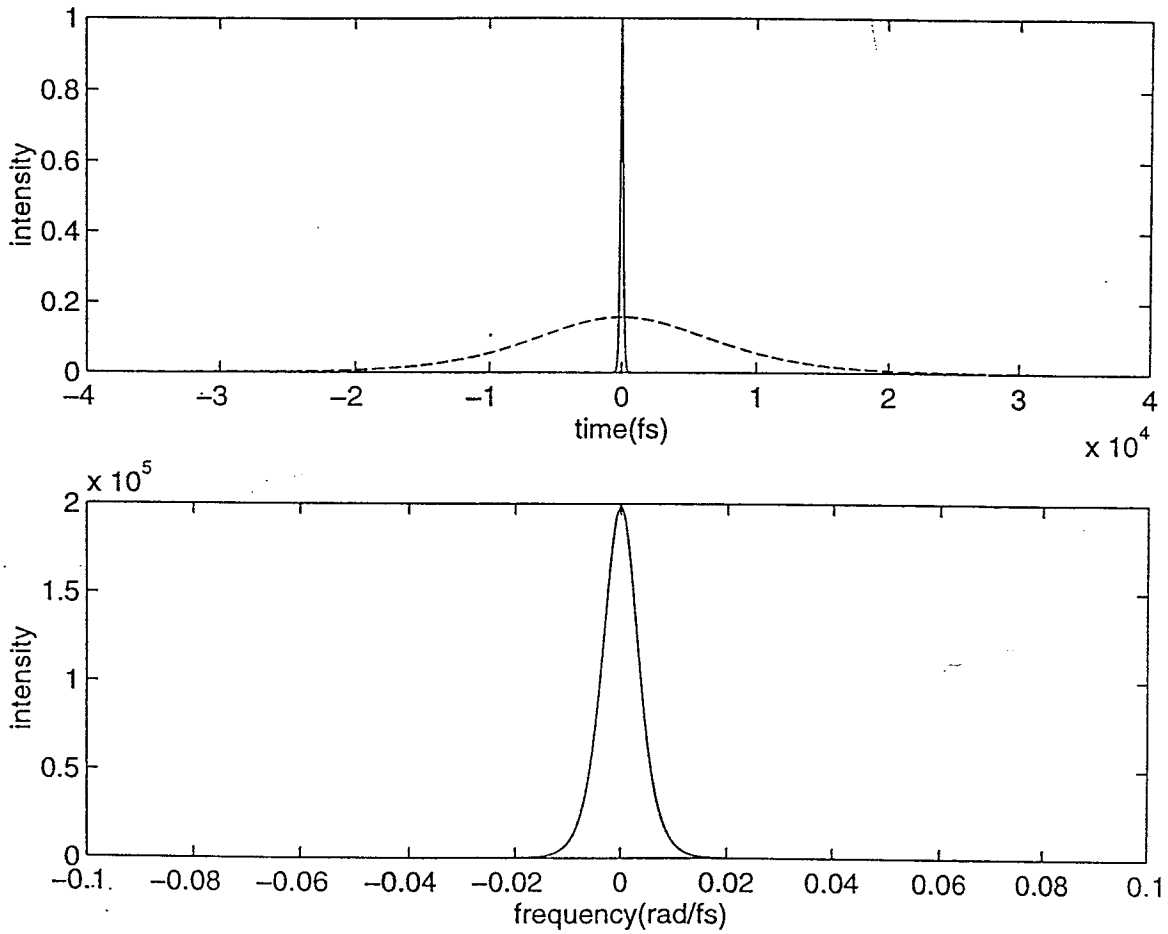

Figure 3.11: Effect of dispersion on a 250fs Sech shaped pulse after propagating in 10LD (10 meters) of standard single mode fiber. Top figure shows input (solid) and output (dashed) pulse intensity against time and bottom figure shows the corresponding power spectra.

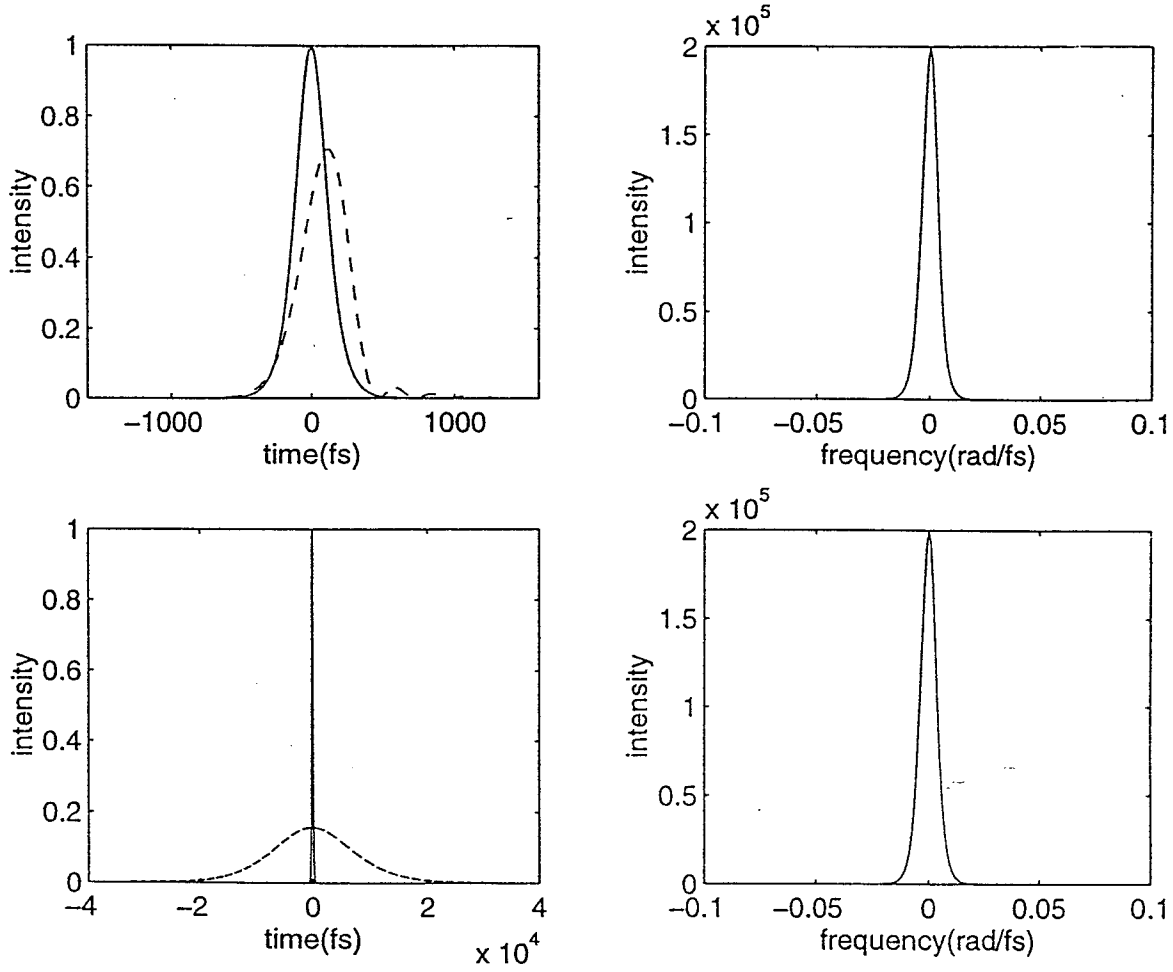

Figure 3.12: Effect dispersion on a 250fs Sech shaped pulse after propagating in 100 meters of standard single mode fiber. Top left figure shows input (solid) and output (dashed) pulse intensity against time with only third order dispersion present, and top right figure shows corresponding power spectra. Bottom left figure shows input (solid) and output (dashed magnified 10 times) pulse intensity against time when both second order and third order dispersion are present, and bottom right figure shows the corresponding power spectra.

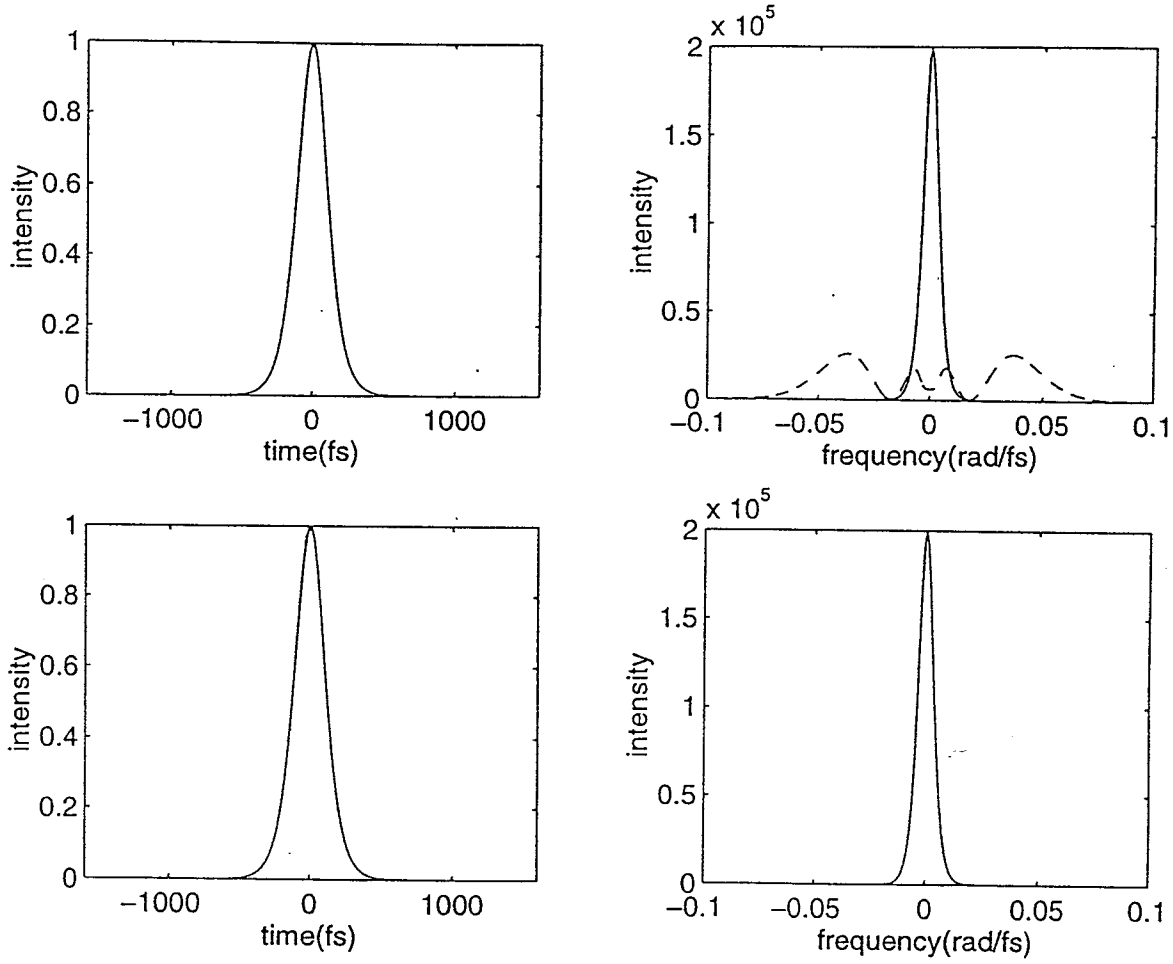

Figure 3.13: Effect of self-phase modulation for a 250fs pulse propagating in 10 meters of standard single mode fiber without and with dispersion. Top left figure shows input and output pulse intensity against time, and top right figure shows corresponding input (solid) and output (dashed) spectra when fiber dispersion was ignored. Bottom figures show the input and output temporal and spectral shapes (indistinguishable) when fiber dispersion was considered, and the pulse power was made equal to a fundamental soliton.

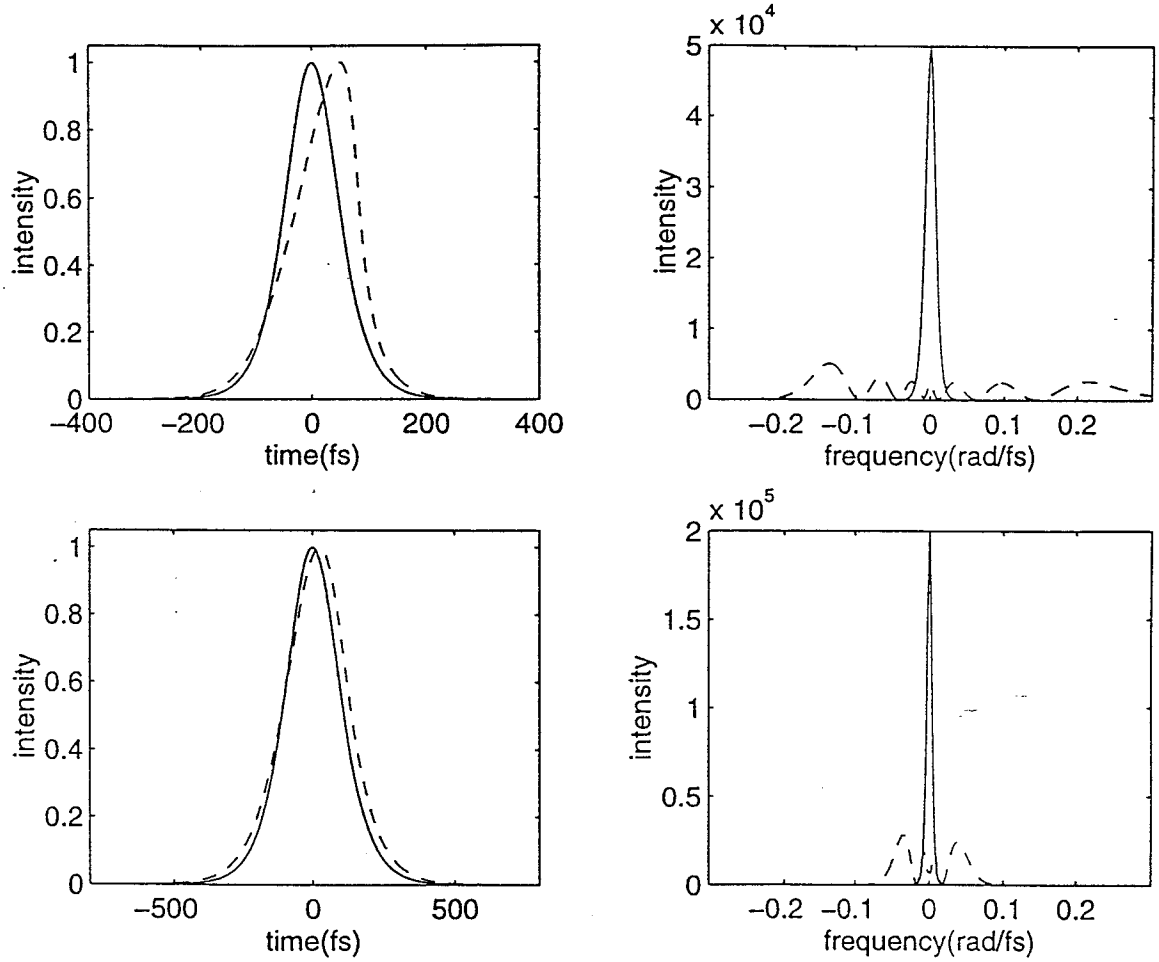

Figure 3.14: Effect of optical shock for a 125fs (top) and 250fs (bottom) pulse propagation in 5 meters of standard single-mode fiber when dispersion is ignored.

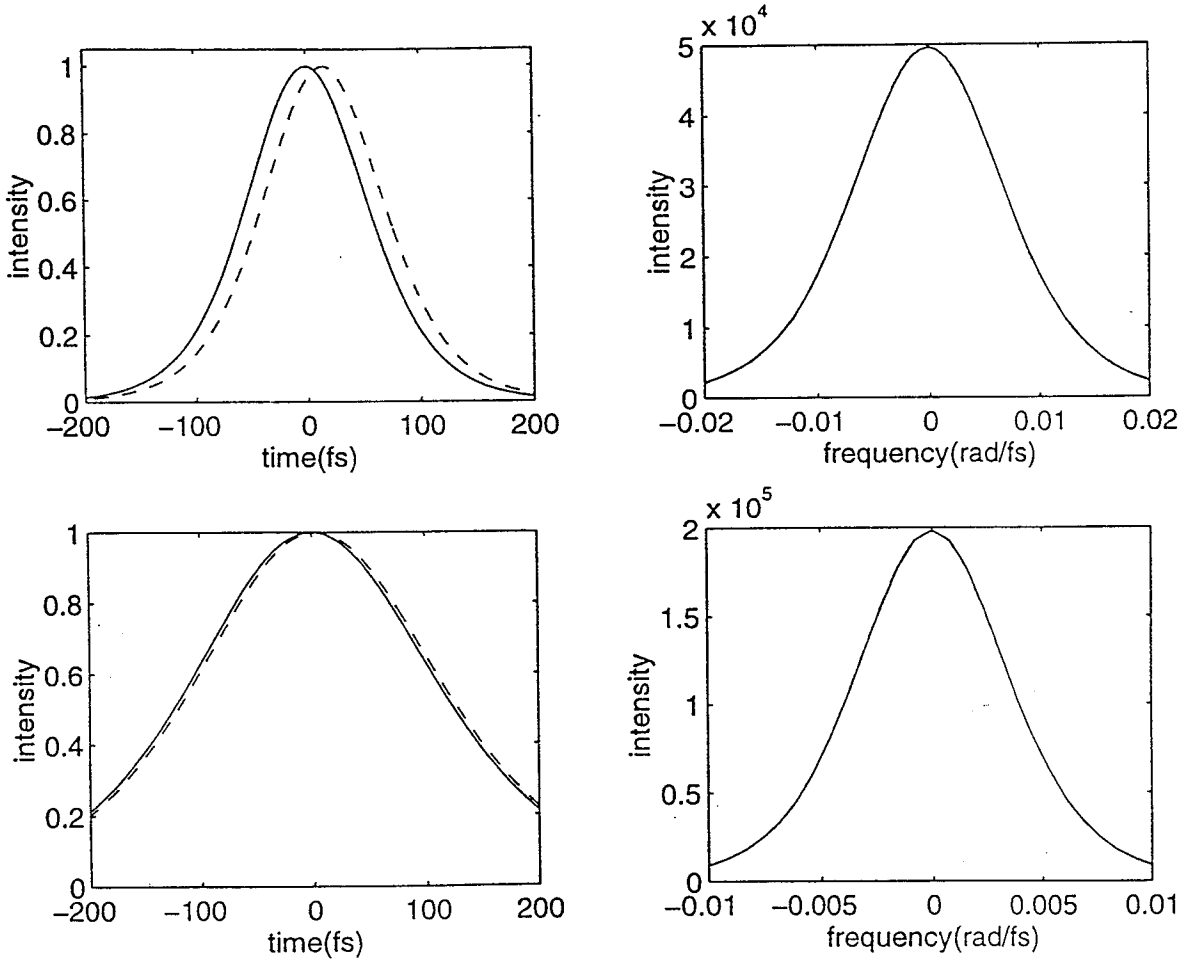

Figure 3.15: Effect of optical shock for 125fs (top) and 250fs (bottom) pulse propagation in the same 5 meters of optical fiber (corresponding to Figure 3.14) when second order fiber dispersion is considered.

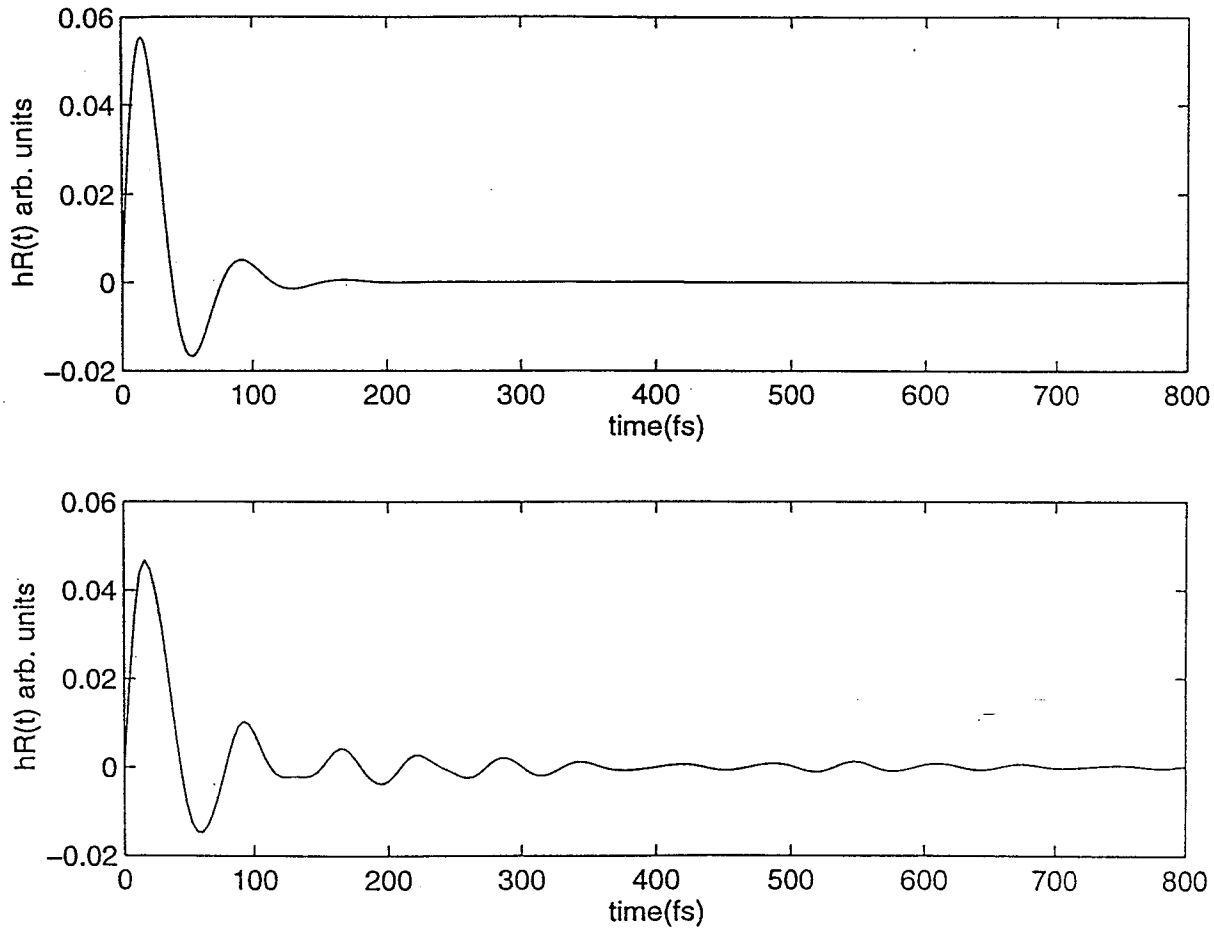

Figure 3.16: Raman response function of fused silica optical fiber. Top figure shows a mathematically generated response function, and bottom figure shows a response function generated from actual measurements on fused silica fibers.

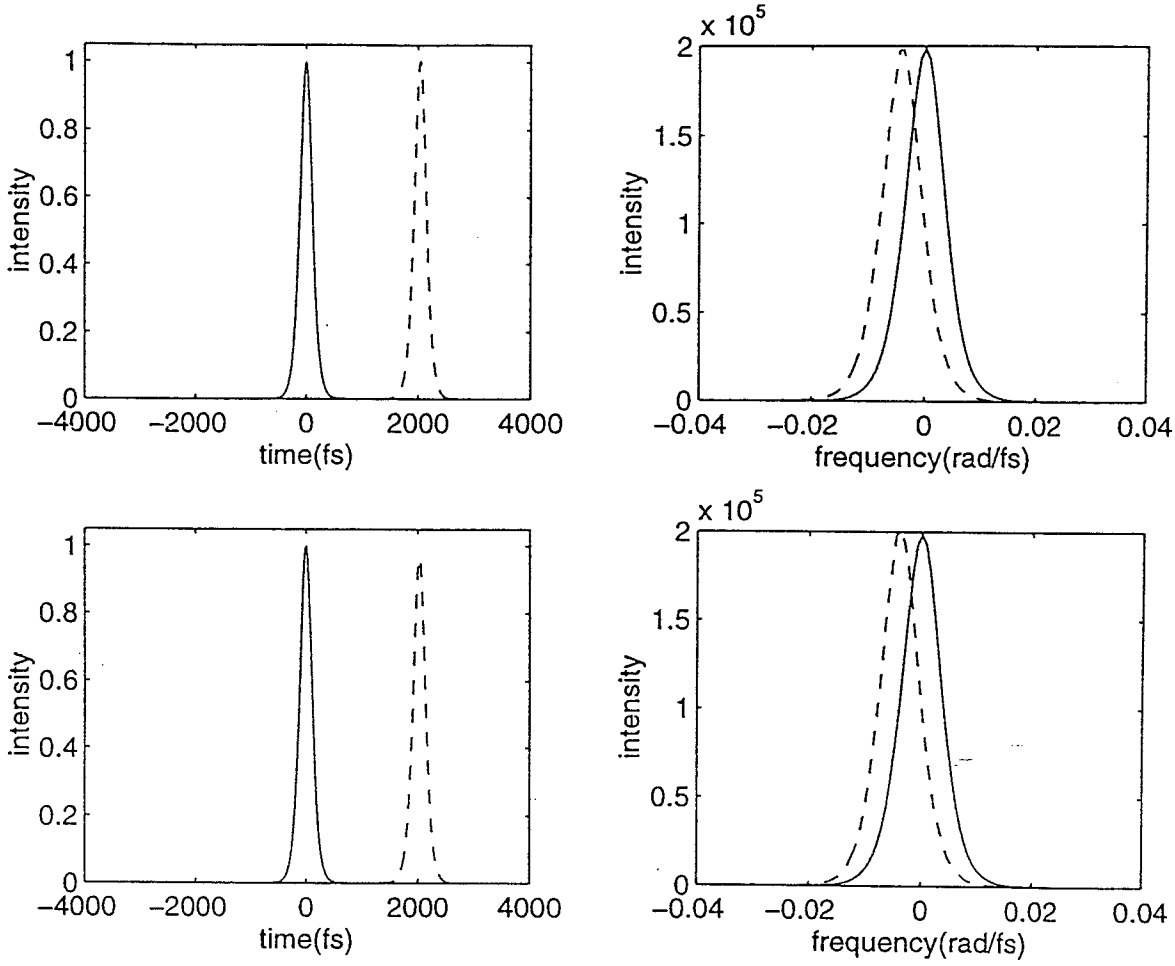

Figure 3.17: Effect of the soliton-self-frequency-shift for a 250fs N=1 soliton pulse after propagating 50 meters of standard single-mode fiber. The top figure shows input (solid) and output (dashed) temporal and spectral profiles when higher order effects were ignored, and the bottom figure shows the input and output profiles when higher order effects were considered.

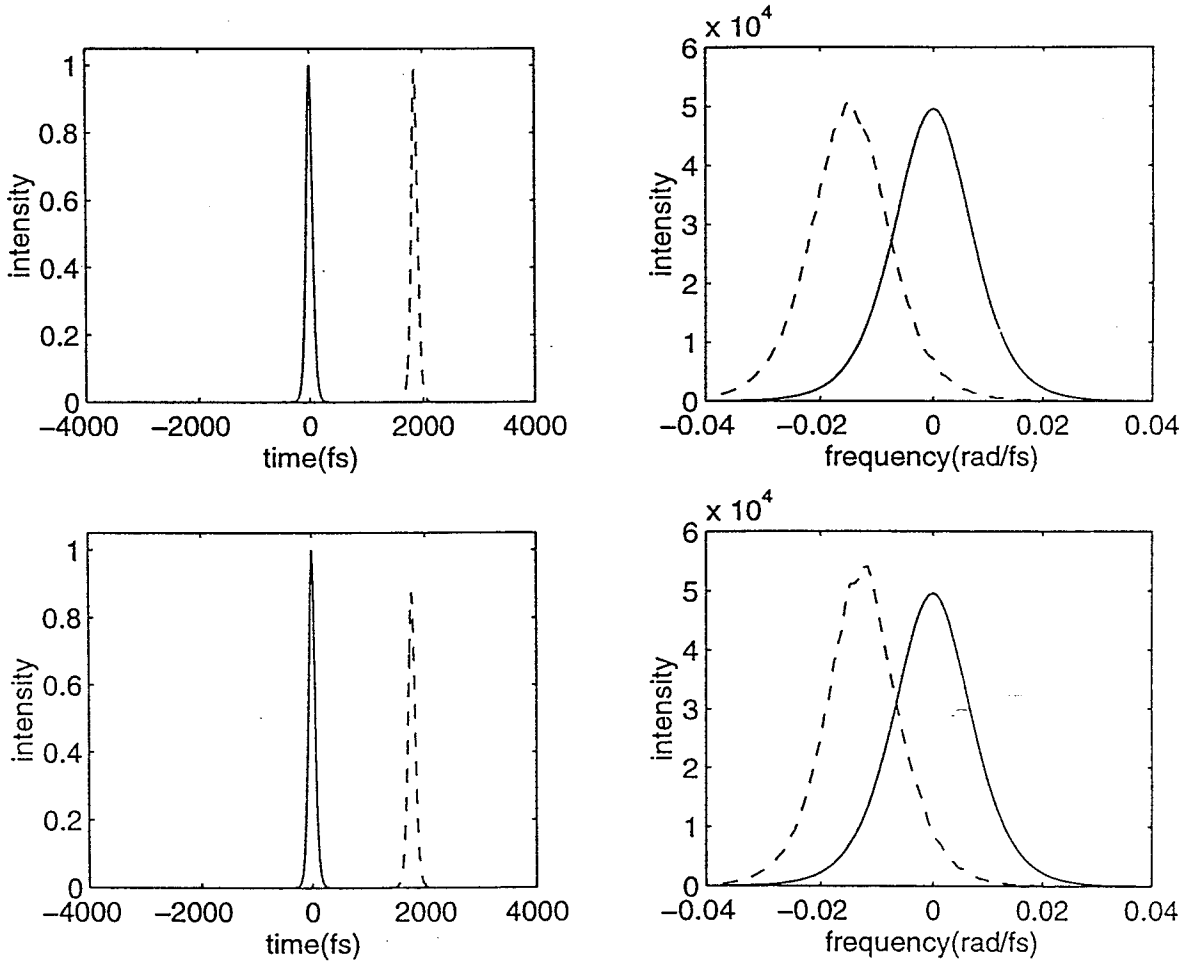

Figure 3.18: Effect of the soliton-self-frequency-shift for a 125fs N=1 soliton pulse after propagating 12.5 meters of standard single-mode fiber. The top figure shows input (solid) and output (dashed) temporal and spectral profiles when higher order effects were ignored, and the bottom figure shows the input and output profiles when higher order effects were considered.

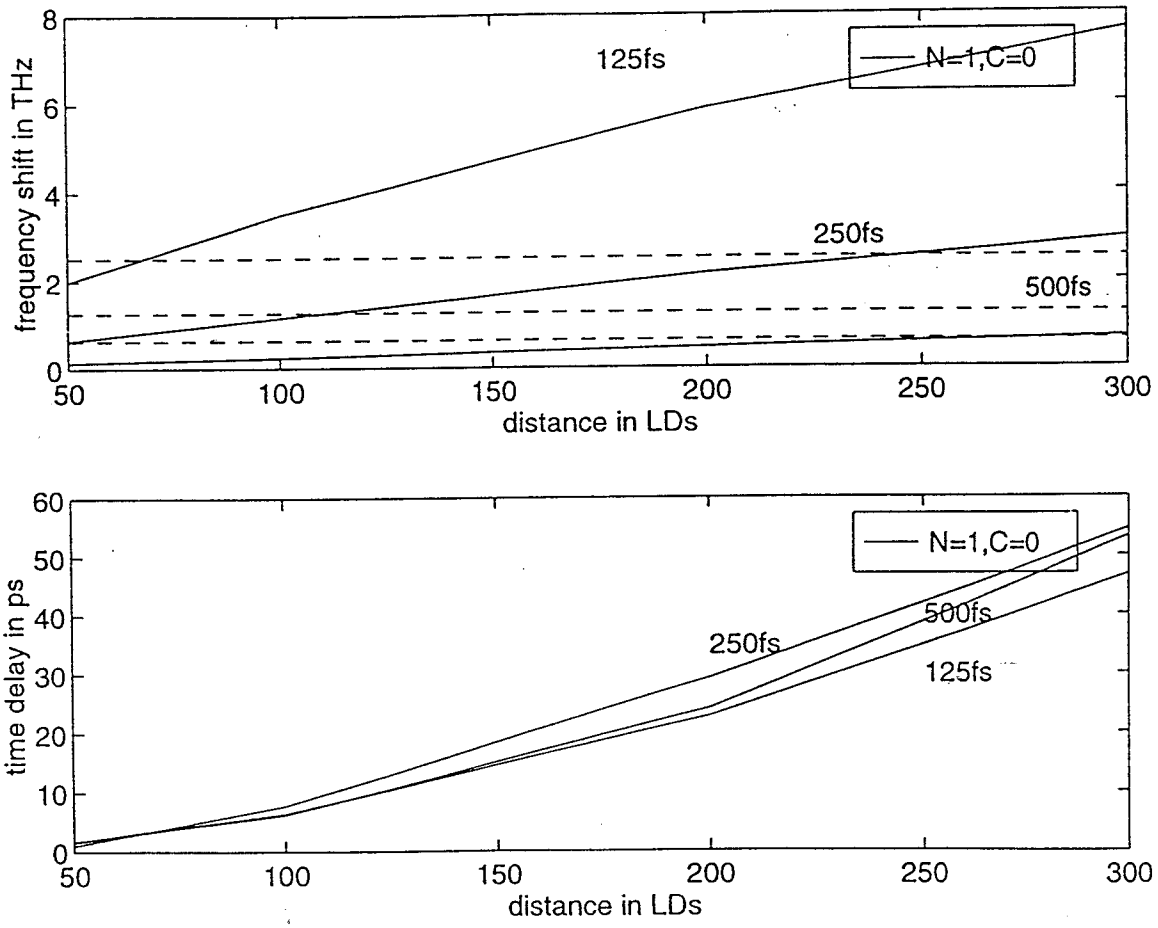

Figure 3.19: Effect of soliton-self-frequency shift for different pulse-width N=1 solitons as a function of propagation distance. Top figure shows the frequency downshift and the bottom figure shows corresponding propagation delay. The input chirp on the pulse is zero in each case (C=0).

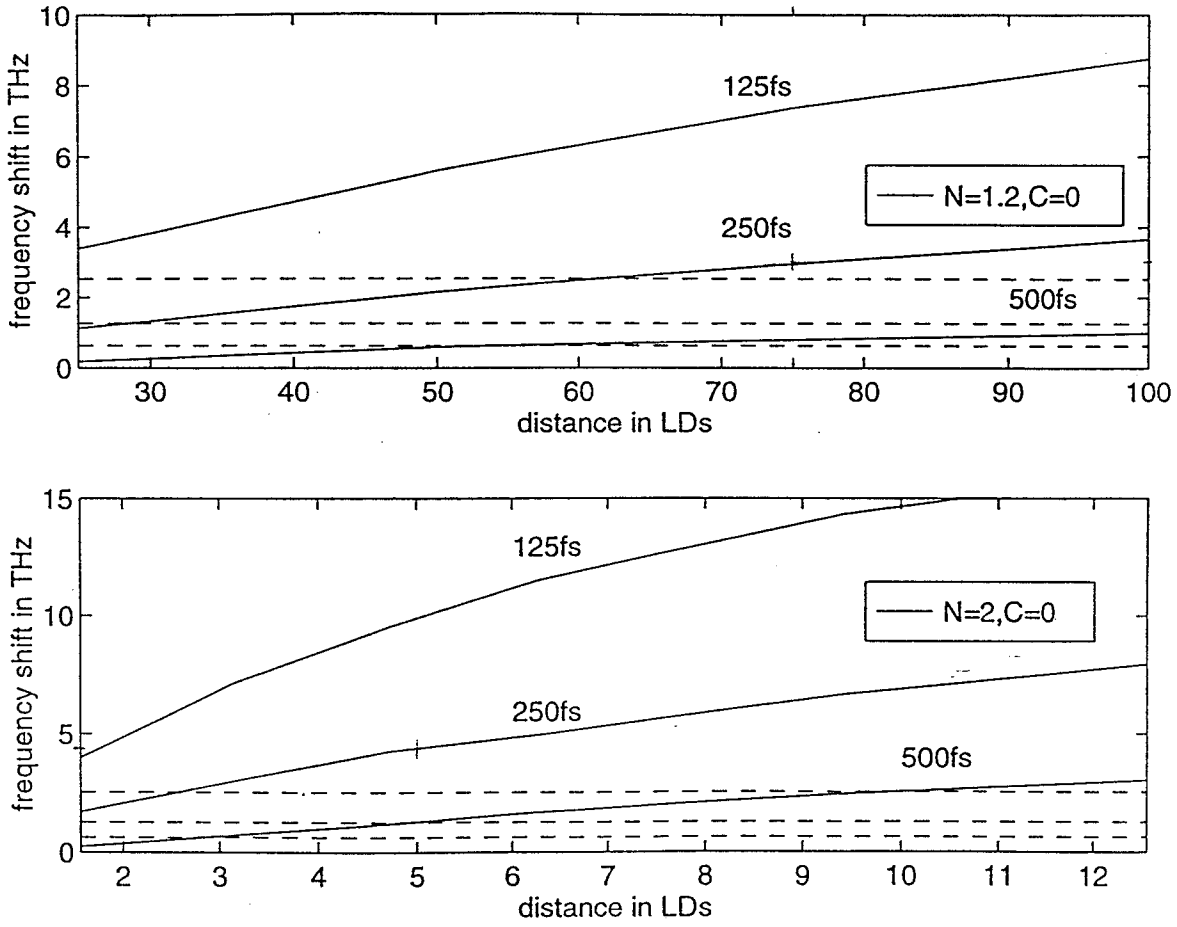

Figure 3.20: Effect of soliton-self-frequency shift for different pulse-width N=1.2 (top figure) and N=2 solitons. The input chirp on the pulse is zero in each case (C=0).

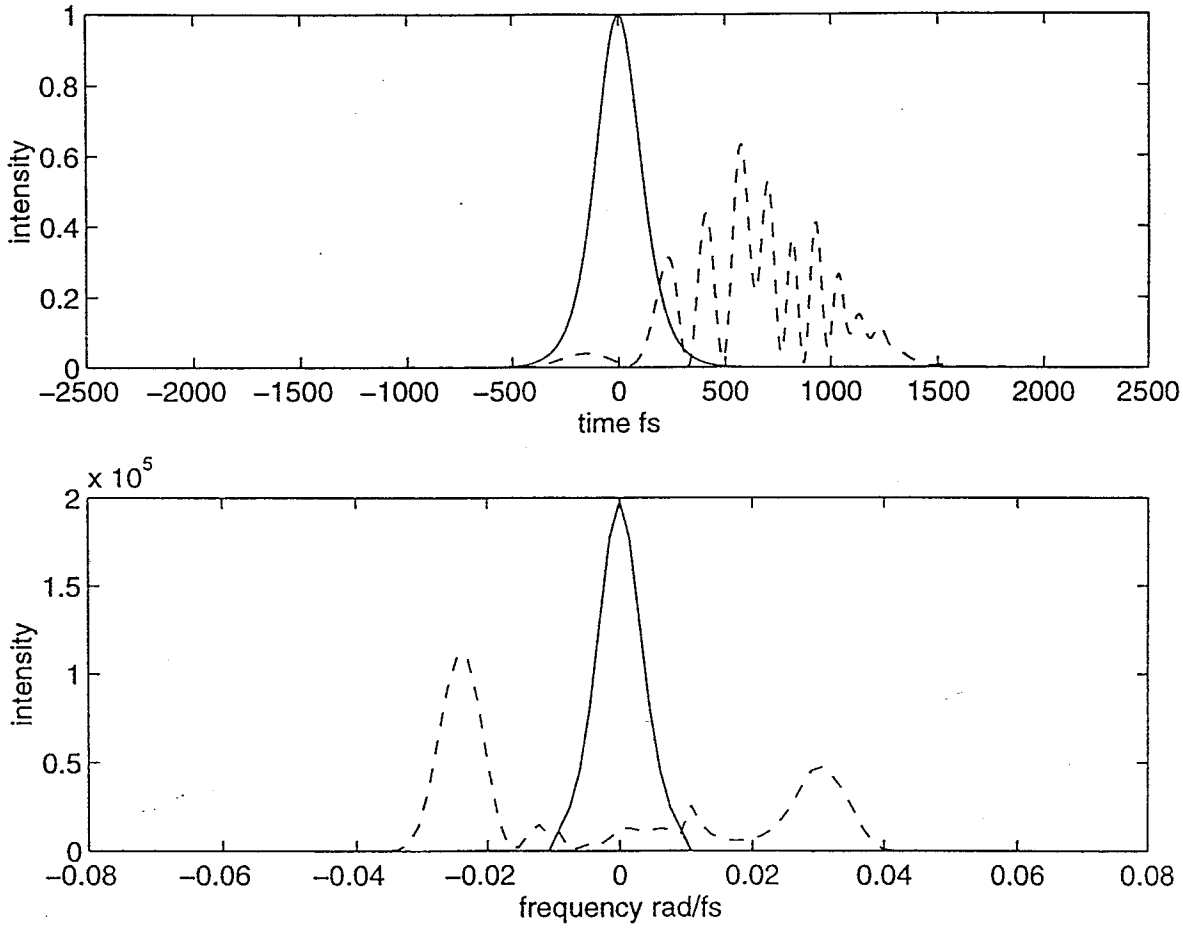

Figure 3.21: Effect of nonlinear self-phase modulation on a 250fs having an equivalent soliton parameter of N=0.6 and propagating an equivalent distance of 40LD's in dispersion shifted fiber. Top figure shows input (solid) and output (dashed) temporal profiles and bottom figure shows corresponding spectral profiles.

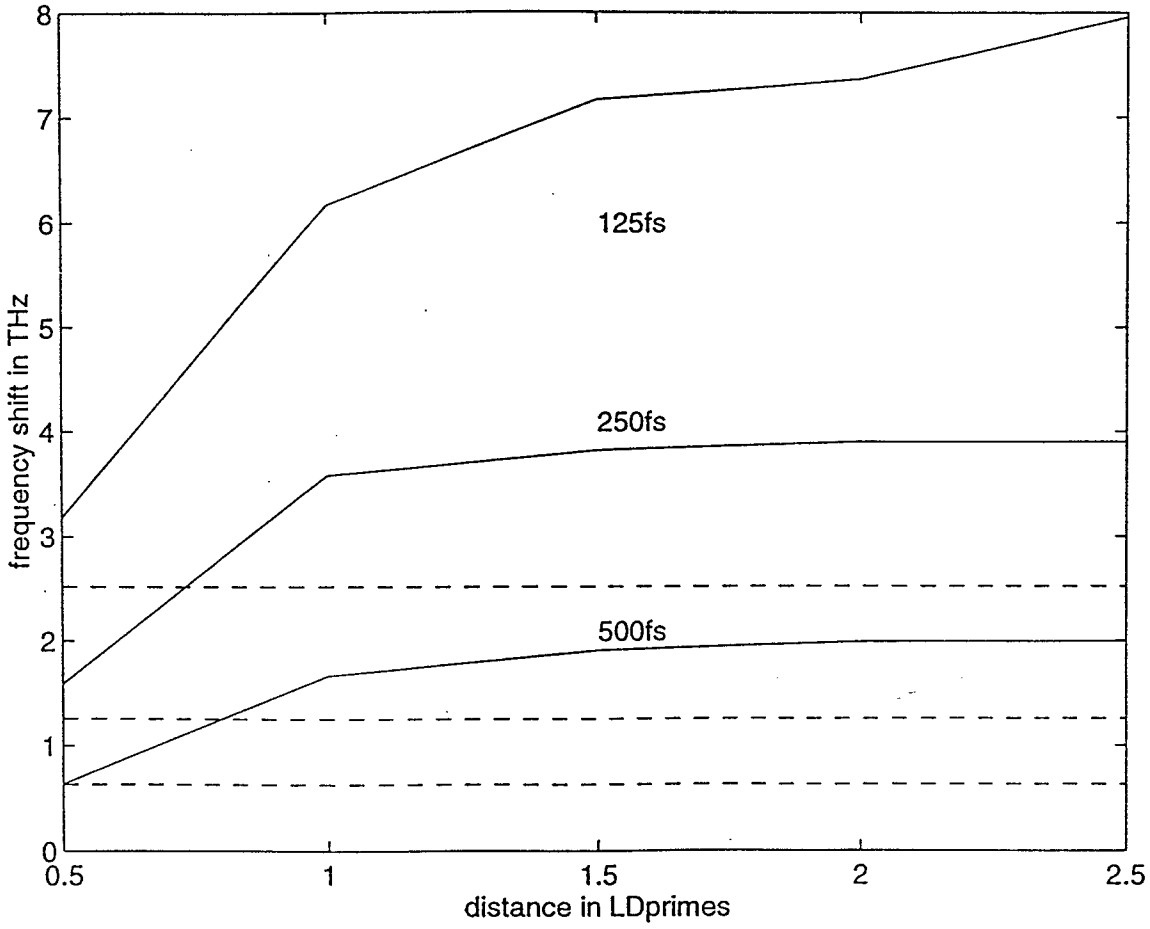

Figure 3.22: The frequency downshift of the pulse corresponding to Figure 3.21 as a function of distance for different pulsewidths.

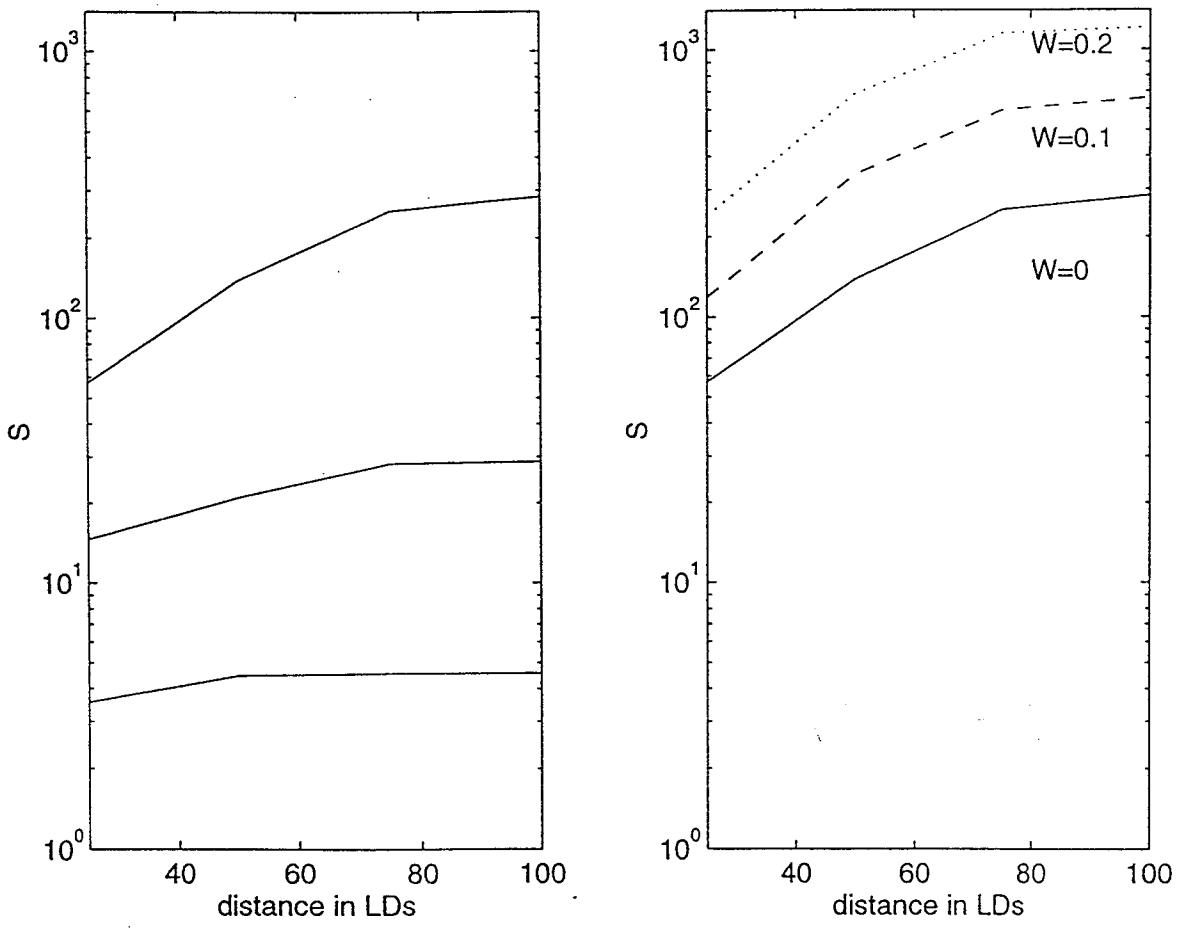

Figure 3.23: Contrast ratios for a 250fs N=1.2 soliton-self-frequency shift thresholder as a function of propagation distance. Left figure shows contrast ratio variation without amplitude filtering when the spectral filter after the thresholder fiber has a cutoff frequency 0.5 $\Delta\omega_0$ below center frequency (bottom trace), $\Delta\omega_0$ below center frequency (middle trace) and 1.5 $\Delta\omega_0$ below center frequency (top trace). Right figure shows the effect of amplitude filtering for the 1.5 $\Delta\omega_0$ cutoff position.

4. SYSTEM RESULTS

The previous two chapters described the femtosecond encoder-decoders and ultrafast nonlinear thresholders that constitute two of the four component technologies that make-up the femtosecond CDMA test-bed. This chapter will briefly describe the other two component technologies, namely, femtosecond laser sources and femtosecond fiber dispersion compensation, and also present system level results. Note that research on these two component technologies was conducted by a colleague and the four component technologies were successfully integrated (in a joint effort) to conduct system-level experiments.

4.1. Femtosecond Fiber Lasers

Ultrashort optical CDMA requires femtosecond laser pulses as they provide the wide bandwidth necessary for the encoding-decoding operation. The lower limit on the shortest femtosecond pulse that can be used is placed by the effectiveness of the dispersion compensation scheme over the transmission distance. The upper limit on the longest femtosecond pulse that can be used is placed by the minimum bandwidth required to code the ultrashort pulses, especially with multiple users, and the short pulsewidth required for effective high contrast thresholding. Due to these conflicting requirements for optimal operation of the different sub-systems that make up the CDMA system, a pulsewidth of several hundred femtoseconds appears to be the best compromise. Although several different techniques for femtosecond pulse generation in the 1.55μm

communication band exist, a passively mode-locked fiber laser was used due to its advantages of ease of construction and compatibility with all-fiber systems. Our femtosecond laser source, as shown in Fig. 4.1 is a passively mode-locked stretched-pulse all-fiber ring laser [21]. The laser is pumped by 980 nm light from a Ti-sapphire laser and the output is taken from the 20% port of a 20% - 80% output coupler. The erbium fiber in the cavity serves as the gain medium and the combination of single mode fiber and dispersion compensating fiber ensures overall positive group velocity dispersion in the cavity. The alternating pieces of negative and positive dispersion fiber cause the pulse to temporally stretch and compress in one round trip. The stretching lowers the peak power of the pulse avoiding nonlinear and saturation effects in the gain medium, effectively giving higher pulse energies. The mode-locking mechanism is additive pulse modelocking that converts the Kerr nonlinearity in the fiber into a fast saturable absorber type action [21,74-76]. The polarization controller and the polarization sensitive isolator initiate and sustain the mode-locking respectively generating ~ 62 fs pulses with a bandwidth of ~ 60 nm. As these pulses are too short for propagation over kilometer distances, the laser output is externally filtered by a bandpass filter resulting in ~ 275 fs pulses, with an average power of ~ 40 μW, at a repetition rate of ~ 30 MHz. Fig. 4.2 shows the intensity autocorrelation traces and spectra from the laser before and after the bandpass filter.

4.2 Femtosecond dispersion compensation

Transmission of femtosecond pulses over kilometer distances requires the simultaneous compensation of both the quadratic dispersion and most of cubic dispersion of the input pulse. In femtosecond optical CDMA dispersion compensation is necessary for two reasons. First, since the CDMA scheme needs linear pulse transmission due to the phase sensitive encoding-decoding operation, we cannot use soliton propagation. Second, if dispersion compensation were not used, the properly decoded pulses in the receiver after propagating through few kilometer of optical fiber would be far too wide

for successful nonlinear thresholder operation. Several dispersion compensation schemes have been demonstrated before that can compensate the chromatic dispersion of standard single mode fibers [27-30]. Our dispersion compensation scheme involves the use of dispersion compensating fiber (DCF) [30] to compensate the quadratic dispersion and most of the cubic dispersion of standard single mode fiber (SMF) [31-32]. A schematic of this dispersion compensation scheme is shown in Fig. 4.3. Such an SMF-DCF fiber link has much lower third order dispersion than conventional dispersion shifted fiber. Further, by applying a cubic phase to the pixels of the programmable liquid crystal (LCM) in the encoder, we can almost completely remove the residual third order dispersion of the SMF-DCF link resulting in almost dispersion free transmission of sub-500 fs pulses over 2.5 km of optical fiber [77]. To our knowledge, these were the first experiments of dispersion compensation on a femtosecond time scale using dispersion compensating fiber [31], and the first demonstration of almost dispersion free transmission by applying residual phase correction to a programmable liquid crystal modulator [77]. In addition to their applicability in femtosecond CDMA systems, this dispersion compensation scheme can be used in any other transmission scheme that uses ultrashort pulses.

Fig. 4.4 shows cross-correlation data for pulses at the input and output of the 2.5 km SMF-DCF link. The link is composed of ~ 2060 m of SMF and ~ 445 m of DCF fiber, dispersion optimized by adjusting the lengths of the individual fibers to give the shortest output pulse. The cross-correlation measurements are done using the 62 fs laser pulse as the reference. Fig. 4.3(a) shows the input pulse and Fig. 4.3 (b) shows data for the same pulse after the 2.5km link. The output pulse is broadened to ~ 580 fs with some small oscillation in the tail indicating residual positive third-order dispersion. This residual dispersion is further compensated by applying an appropriate phase variation across the pixels of the LCM in the encoder, resulting in almost complete dispersion compensation as seen in Fig. 4.3(c). The phase pattern applied to the LCM (see Fig. 4.3 (d)) is discretely sampled over the entire 128 LCM pixels, but since the phase difference between the first and last pixel is quite small (~ 2.1 π), the sampling can be considered almost continuous. This leads to the almost exact phase correction of the residual third

order dispersion in the link and thus to almost complete restoration of the output pulse. Note that we had earlier performed spectral interferometry experiments [32] and had determined the residual third order dispersion co-efficient of the DCF-SMF link to be β_3 = +0.018 ps^3/km. In the current experiments, the cubic phase applied to the LCM pixels corresponds to a residual third order dispersion coefficient of β_3 = 0.024 (± 0.006) ps^3/km, a value consistent with our earlier measurements. This flexible way of trimming out residual dispersion of an already nearly compensated fiber link can lead to increased transmission distances for future CDMA experiments.

4.3 Femtosecond Fiber Amplifiers

Two amplifiers are used in the ultrashort pulse optical CDMA link. First, a pre-amplifier directly after the filtered laser source to compensate for the insertion loss of the encoder and the link, and second a post-amplifier after the decoder to ensure adequate contrast between the properly and improperly decoded pulses in the nonlinear thresholder. Although the two amplifiers were designed to provide different levels of amplification and output saturation powers, their general construction is quite similar. Fig. 4.4 shows a schematic of the amplifier that is modification of a conventional erbium doped fiber amplifier (EDFA). This modification is due to using the chirped pulse amplification (CPA) technique [78,79] to reduce the nonlinear effects in the EDFA. If a conventional EDFA is used for femtosecond pulse amplification, a combination of self-phase modulation, Raman effects, and higher order soliton effects have been shown to cause distortion of both the temporal shape and the spectrum of the pulse exiting the amplifier [80-82]. The CPA technique avoids the nonlinearities associated with short pulse amplification by initially stretching the input pulse in the time domain by several orders of magnitude before passing it though the gain medium. After amplification the pulse is externally compressed to its time-bandwidth product. In the CPA-EDFA shown in Fig. 4.4, input pulses from the laser are first stretched by passing them through ~ 60 m of single mode fiber. They are then amplified by about ~ 15 dB by passing through ~ 18

m of erbium fiber (Corning type II T-8533-301) which serves as the gain medium. The erbium fiber is pumped by 980nm light from a Ti-Sapphire laser coupled to the amplifier through a WDM coupler. Monitors for both the pump and input signal are provided to measure input signal and pump power levels. Isolators at the input and output are used to reduce any feedback effects that can reduce the gain and output power. The pre-amplifier was designed to generate ~ 1.2 mW of power at 1550 nm when pumped by ~ 24 mW of pump power. The amplified pulse is compressed by using a dispersion-compensating fiber that compresses the pulse to its transform limited value. The amplifier produces ~ 375 fs pulses, the pulse being broadened due to gain narrowing effects in the erbium fiber. The output pulses are taken from the 90% port of a 10%-90% output coupler. The post-amplifier follows the same construction as the pre-amplifier, with the longer length (~ 25 m) of erbium fiber to give higher output powers. The post-amplifier is designed to deliver upto ~ 20mW of output power when pumped by ~ 130 mW of pump power. At higher output power levels, in addition to gain narrowing in the amplifier, we see some nonlinear effects in the compressed pulses and the pulses are further broadened to between ~ 600 fs - 900 fs. Fig. 4.6 (a) shows the variation of the output pulsewidth, and Fig. 4.6 (b) shows the corresponding variation of the output signal power for the post-amplifier as a function of the applied pump power. Fig. 4.6 (a) and (b) show the output pulsewidth at two different values of signal power clearly revealing the effects of nonlinearities at higher powers. Figure 4.7 shows the variation of the gain with respect to fiber length and input signal power for the post-amplifier. Note from the top figure that the fiber length was optimized to about 25m by cutting the erbium fiber at a pump power level about 25% lower than the maximum available pump power. This ensures good overall pump efficiency at different power levels. The bottom part of the figure shows the onset of amplifier saturation effects for input signal power levels greater than few tens of microwatts. This figure also shows the importance of using an isolator at the output of the amplifier to prevent feedback from saturating the gain. Note that with > 35 dB gain in the erbium medium, spurious reflections from some output port of the amplifier (like the end of the SMF fiber FC-PC connector which typically have back reflections of – 40 dB) would considerably decrease the gain for a forward propagating signal.

4.4 The femtosecond CDMA test-bed

We have so far discussed the various CDMA sub-systems and presented experimental data for their performance. Before discussing system results the femtosecond CDMA test-bed with all the sub-systems connected is described here. Our femtosecond CDMA test-bed is shown in Fig. 4.8. In the transmitter, femtosecond pulses generated by a stretched-pulse modelocked fiber ring laser are spectrally sliced to yield ~ 275 fs pulses which are first pre-amplified by a CPA-EDFA resulting in slightly broadened (due to gain narrowing in the amplifier) ~ 350 fs transform limited pulses. The amplified pulses are passed through an encoder which is a low loss (measured fiber-to-fiber insertion loss as low as 5.3 dB) fiber-pigtailed pulse-shaper containing a 128 element liquid crystal phase modulator (LCM) as a programmable phase encoder. In the pulse-shaper, the spectral phases are set either to a length 31 or length 63 M-sequence pseudorandom phase code which encodes the pulses into ~ 10-12 ps wide pseudonoise bursts. After the transmitter, the encoded pulses are propagated over a 2.5 km fiber link which uses dispersion compensating fiber to compensate both the second and most of the third order dispersion of the standard telecom fiber. Note that dispersion compensation is crucial as soliton propagation cannot be employed in the femtosecond CDMA scheme, since the encoding-decoding operation requires linear pulse propagation. For 350 fs input pulses, the pulses exiting the fiber link are broadened to ~ 600 fs (due to residual third order dispersion in the link), the pulses being first stretched and then recompressed by a factor of 800! Furthermore, the third order dispersion in our experiments is ~ 6 times less than that for dispersion shifted fibers. We also note that we have obtained experimental results in which the residual third order dispersion in the fiber link is reduced by applying a cubic phase to the encoder (along with the M-sequence).

In the receiver, pulses from the link are first decoded by a second fiber-pigtailed pulse-shaper. To properly decode the pulse, the LCM in the decoder is programmed with a phase code that is the conjugate of that applied to the encoder. This operation restores the original femtosecond pulse. If the pulse is improperly decoded (by a non-conjugate phase code in the decoder, as would be the case with an interfering user), the pulse remains as a pseudonoise burst. Properly and improperly decoded pulses are amplified

by a second CPA-EDFA and then distinguished on the basis of intensity and pulse-width by a nonlinear fiber-optic thresholder. The nonlinear thresholder is simply a 500 m long dispersion shifted fiber with zero dispersion wavelength of 1559 nm (which coincides with the mean wavelength for the CDMA transmitter), followed by a spectral filter and power meter. Nonlinear effects in the fiber cause the spectrum of the properly decoded pulse to split and spread on either side of the zero dispersion point. The improperly decoded pulse propagates the same length of the thresholder fiber but experiences negligible spectral shifts due to its lower intensity and a larger pulse width. These frequency shifts are converted into a contrast in energy by using a long wavelength pass filter followed by a slower photodetector that can operate at speeds comparable to the repetition rate of the system. By optimally choosing the average power and the filter cutoff wavelength, high contrast ratio's between coded and uncoded pulses can be obtained.

4.5. System Results

Most system level results of the femtosecond CDMA test-bed are for a single transmitter-single receiver system. Some preliminary experiments simulating a two-user system were also conducted to test ultrafast thresholder operation in the presence of an interfering user. The preliminary results of the two-user system are included at the end of this section. For single user operation, the following three parameters will chiefly determine the system performance. First, the fidelity of the encoding-decoding operation with the 2.5km fiber link in-between the encoder and decoder. Second, the effectiveness of the dispersion compensation scheme for coded pulse propagation with and without residual third-order dispersion correction, and finally, the contrast ratio after the nonlinear thresholder between a properly and improperly decoded pulse.

Fig. 4.9 shows autocorrelation data of the encoding-decoding operation for 31element M-sequence phase coding with the 2.5km dispersion compensated fiber link in between the encoder and the decoder. In Fig. 4.9 (a) the decoder has a matching phase

code that is the complex conjugate of the phase code on the encoder (representing a properly decoded pulse). In Fig. 4.9 (b) the decoder has an unmatched phase code that is a cyclically shifted version of the phase code on the encoder (representing an improperly decoded pulse). Note again the high intensity contrast (Fig. 4.9 (b) normalized with respect to Fig. 4.9 (a)) and the large pulsewidth difference between the two cases. Fig. 4.9 (c) shows a properly decoded pulse when the encoder in the testbed has a cubic phase correction applied to it (to trim out the residual third order dispersion of the link), superimposed on the M-sequence phase code, and Fig. 4.9 (d) shows the corresponding improperly decoded case. Although the cubic phase correction has resulted in only marginal improvement of the properly decoded pulse over the uncorrected case (the properly decoded pulsewidth is shorter by about 10%), these results prove the viability of the phase correction technique for coded pulse propagation. Note also the coherence spike at the origin for the improperly decoded pulses (see Figs. 4.9(b) and (d)) as is expected in autocorrelation traces for pseudonoise bursts. Third order dispersion compensation may become important for longer propagation distances. Also, like cubic phase correction, the LCM can be programmed for quadratic phase correction (to compensate second order dispersion), thus allowing some flexibility when users with dispersive transmitters (or receivers) get connected to a well-compensated transmission link. Note that these were the first experiments that showed encoding-decoding in two separate pulse-shapers for M-sequence coding [83] and also the first experiments that showed residual higher-order dispersion compensation using a liquid crystal modulator [77].

Fig. 4.10 shows power spectral data at the output of the thresholder for properly and improperly decoded pulses for 31 element M-sequence phase coding. In the system experiments, the thresholder fiber with zero dispersion wavelength at 1559nm was used, primarily because it requires lower average powers to give high contrast thresholding. By comparing Figs. 4.10 (a) and (b) we note that the spectrum of the properly decoded pulse has split to either side of the zero dispersion point. The peak at 1530nm observed on both the spectra is due to the amplified spontaneous emission from the erbium doped fiber amplifier in the receiver. Fig. 4.11 shows the encoding-decoding autocorrelation

data after the decoder and the corresponding power spectral data after the threholder for 63 element M-sequence encoding-decoding, clearly demonstrating CDMA operation for longer code lengths. The contrast ratios (defined as the ratio of the energy of the properly decoded pulse to that of the improperly decoded pulse) after spectral filtering in the nonlinear thresholder are plotted Fig. 4.12 for length 31 and length 63 M-sequence phase coding. The cutoff wavelength of the spectral filter is ~ 1573nm. The horizontal axis in the figure is the pump power applied to the EDFA in the receiver, and the corresponding variation of the average signal power in the thresholder fiber would be from ~ 1 - 2.5 mW. As seen in the figure, a slight increase in the contrast ratio is observed when third order dispersion correction is employed. Note that the contrast ratio for 31 element M-sequence encoding-decoding is larger than that for 63 element M-sequence encoding-decoding, and the difference between the two is more prominent at lower pump powers. This is because the properly decoded pulse has a larger peak power (and also larger average power) for 31 element M-sequence coding than for 63 element M-sequence coding. At lower pump powers the EDFA gain is fairly constant, resulting in the amplified properly decoded pulse for 31-element coding having a larger peak power, and therefore higher frequency shifts, and higher contrast ratios. At higher pump powers, gain saturation effects come into play and the differences in the contrast ratios are smaller. The contrast ratio in both cases is limited by the long wavelength ASE components of the EDFA in the receiver. Note also that for 31 element M-sequence coding, the contrast ratio curve is quite flat over the entire range of average powers in the thresholder fiber indicating that the contrast ratio is not very sensitive to the exact value of the average power. This is important as it gives some design margin for constructing the receiver amplifier especially under multiple user operation.

To get around the ASE limitation, we have two choices. First, we can install a bandpass filter after the receiver EDFA that eliminates the long wavelength ASE components. Second, we can engineer the spectral filter in the thresholder and set its cut-off wavelength to a much longer wavelength (> 1573 nm) effectively blocking out as much long wavelength ASE as possible. Note that in the second approach we also reduce some of the signal from the properly decoded pulse. This is however not a serious

limitation as long as we have sufficient signal for detection, and the reduction of the long wavelength ASE is greater than the reduction in the properly decoded signal. Using the second approach we increased the contrast ratio of the CDMA testbed to 27.5 dB and 25 dB for 31 element and 63 element M-sequence coding respectively (compared with ~ 18 dB and ~ 15dB in Fig. 4.12) as shown by the solid lines in Fig. 4.13. Note again that the horizontal axis in the figure is the pump power applied to the EDFA in the receiver, and the corresponding variation of the average signal power in the thresholder fiber would be from ~ 1.5 - 2.75 mW.

We also tested one more variation of the code length dependence on the contrast ratio, namely when the interfering user has encoded its data using a different length code-sequence than the intended user. We can now have some users who encode their data with length 31 M-sequences transmitting information over the same optical channel with other users who encode their data with length 63 M-sequences. Note that in optical CDMA the intended receiver has to be provided with a-priori information about the exact nature of the code sequence of the transmitter. Hence having different users encoding their data bits with different length M-sequence does not add any more complexity to the system. When the CDMA receiver decodes an incoming interference signal, its output remains as a low intensity pseudonoise burst irrespective of the exact nature of the code length of the interfering user. This can be observed from Fig. 4.13, where it should be noted that the contrast ratio has actually increased for length 31 M-sequence coding when the interfering user has its bits coded with a length 63 M-sequence. This can be attributed to a combination of two factors. First, an interfering user with 63 element M-sequence coding has a longer temporal spread of its encoded pulse than an interfering user with 31 element M-sequence coding. Hence after decoding, a length 31-length 63 M-sequence improper decoding results in a longer duration improperly decoded pulse than a length 31-length 31 M-sequence improper decoding. Since the thresholder is a nonlinear device, a longer duration improperly decoded pseudonoise signal has relatively less spectral shifts than a shorter duration improperly decoded pseudonoise signal. (Note that the absolute spectral shifts in either case are much less than that for a properly decoded pulse). This explains the increase in contrast ratio. The second factor for this

increase is the slightly higher loss in the decoder pulse shaper for 63 element M-sequence coding than for 31 element M-sequence coding. This would cause the decoder output to have different average powers depending on the specifics of the encoding-decoding process. The contribution due to this effect is expected to be small as measurements at the EDFA output for the two cases (i.e. length 31-length 31 and length 31-length 63 M-sequence improper decoding) have shown only 5% difference in average powers. The contrast ratio for 63 element M-sequence encoding-decoding is likewise higher than that for 63 element coding-31element decoding. This also appears to be related to the temporal and intensity characteristics of the improperly decoded pulses. Note that for a given M-sequence, translating the bit pattern by one-bit results in a new M-sequence that is orthogonal to every other M-sequence obtained by such bit translations. Hence a length 63 M-sequence can accommodate 63 possible users. A combination of length 63 and length 31 M-sequences thus increases the number of addresses that can be assigned to users, and also shows the robustness of the optimal CDMA system when the interfering users have different types of codes.

For two-user operation, the 2.5km fiber link was disconnected and the two pulse shapers were connected in parallel simulating two simultaneous users (see Fig. 4.14). Since we have already demonstrated nearly dispersion free propagation of femtosecond pulses through the link; here we disconnected the link to isolate effects due to encoding, decoding, and thresholding process. One pulse-shaper (PS1) represented the intended user and had all its LCM pixels programmed to a constant phase resulting in an uncoded ~ 500 fs pulse. In a full system consisting of two transmitters and two receivers, this would represent a properly decoded pulse. Note that this assumption is valid as we have already shown that the properly decoded pulse indeed closely matches an uncoded pulse in shape. The other pulse-shaper (PS2) represented the interfering user and had its LCM pixels programmed with a 63-element M-sequence. Fig. 4.15(a) shows the spectrum at the output of the thresholder fiber with both pulse-shapers connected representing (for a full system) one intended and one interfering user, and Fig. 4.15(b) shows the output of the thresholder fiber with only PS2 connected, representing multi-access interference. The frequency shifts due to the nonlinear effects in the thresholder fiber are clearly seen

in Fig. 4.15 (a). The contrast ratio between uncoded and coded signals as measured by a photodetector for a spectral filter cut-off wavelength > 1573 nm is shown in Fig.4.15 (c). A ~ 25 dB contrast ratio is obtained for ~ 2 mW total average power in the thresholder fiber. Such high contrast clearly indicates the interference suppression capabilities of this CDMA system and lays the groundwork for future experiments involving multiple-users.

Stretched-pulse Mode-locked Fiber Ring Laser

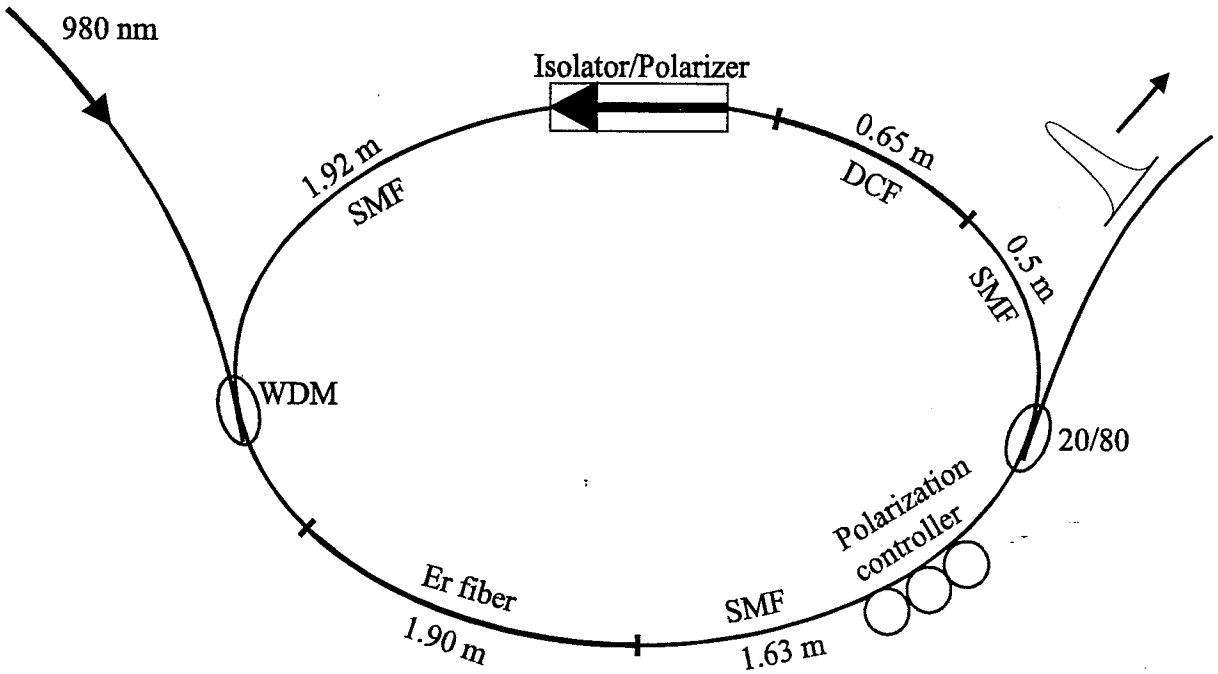

Fig. 4.1. Stretched pulse fiber ring laser.

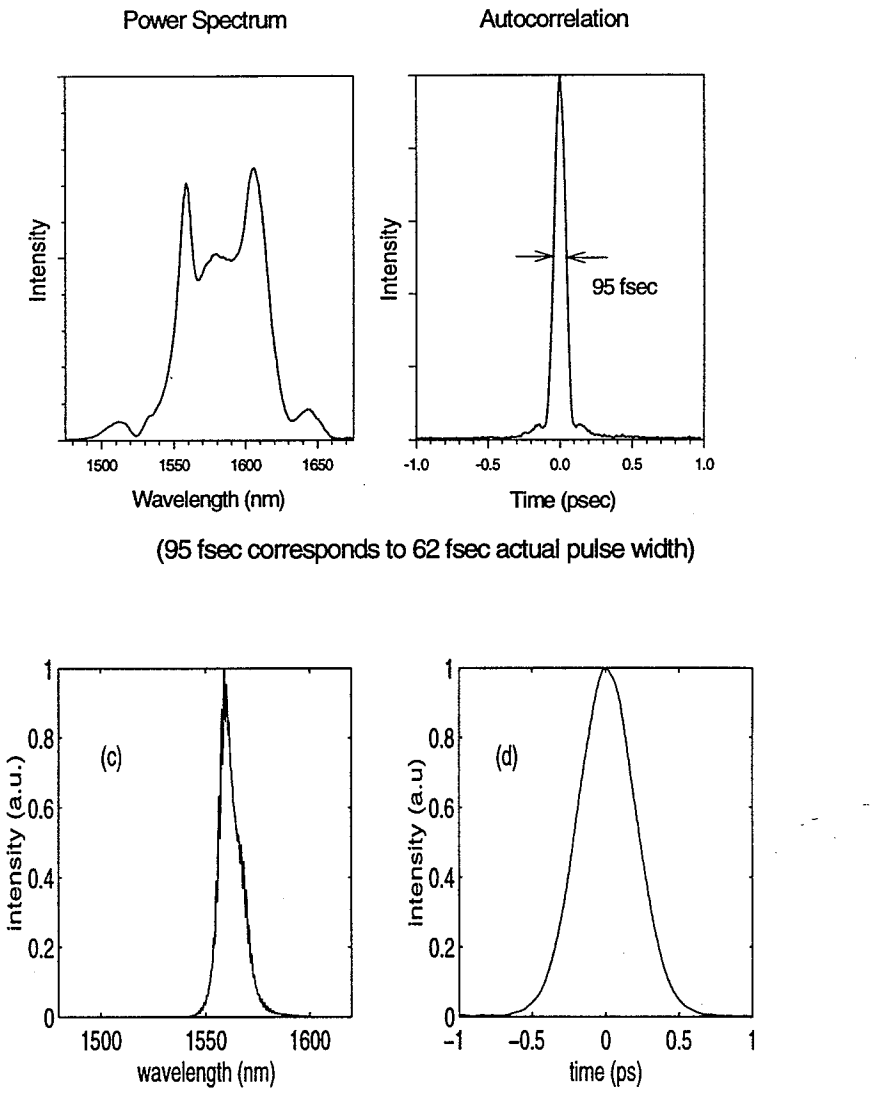

Fig. 4.2. Intensity autocorrelation and power spectra at the output of the laser (figures (a), (b)), and after bandpass filter (figures (c), (d)).

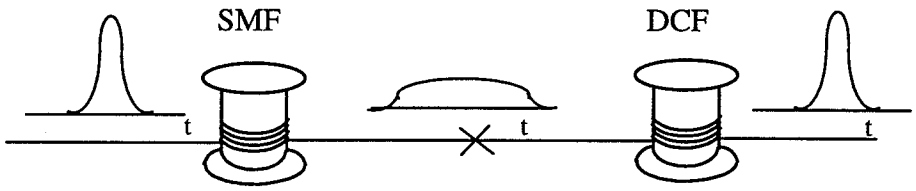

Fig. 4.3. Schematic of dispersion compensation scheme.

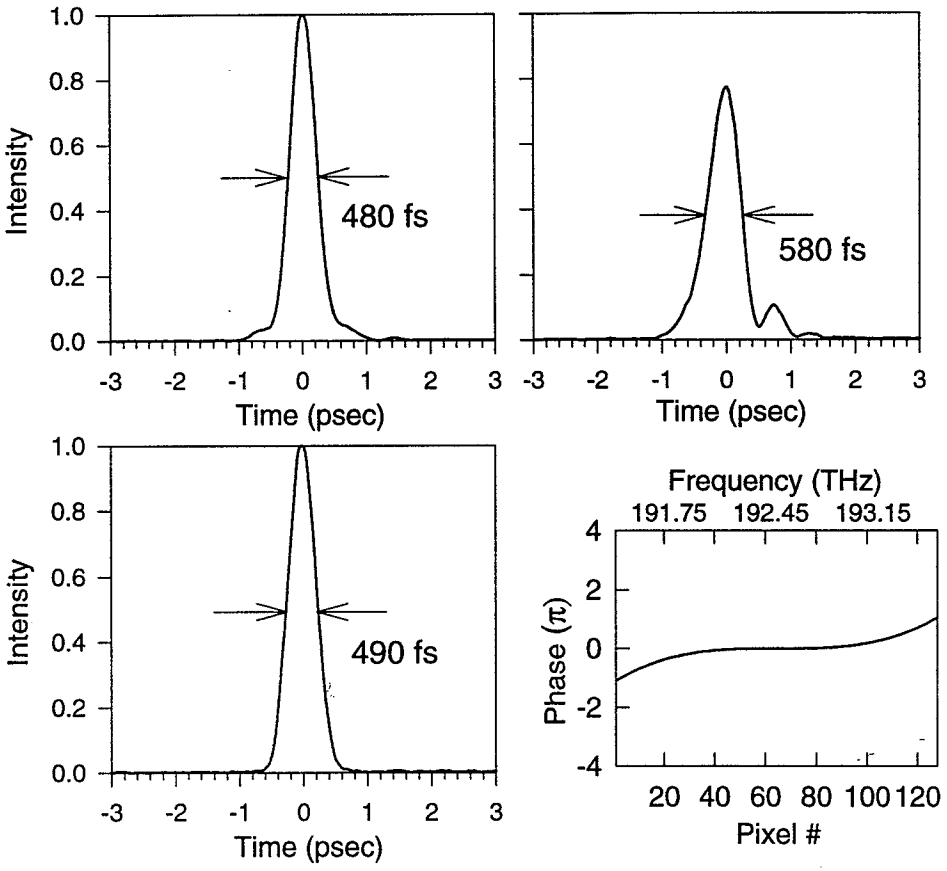

Fig. 4.4. Cross-correlation data for pulses at the input and output of the 2.5km link. (a) Input pulse, (b) output pulse after the 2.5km link, (c) output pulse after 2.5km link with third order dispersion compensation, (d) phase pattern applied to the LCM in the encoder.

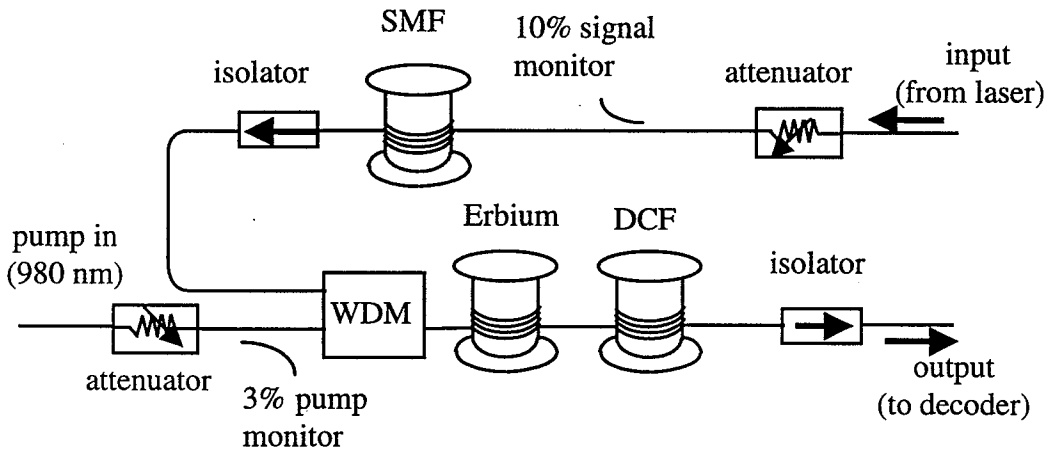

Fig. 4.5. Schematic of the chirped pulse amplification erbium doped fiber amplifier (CPA-EDFA).

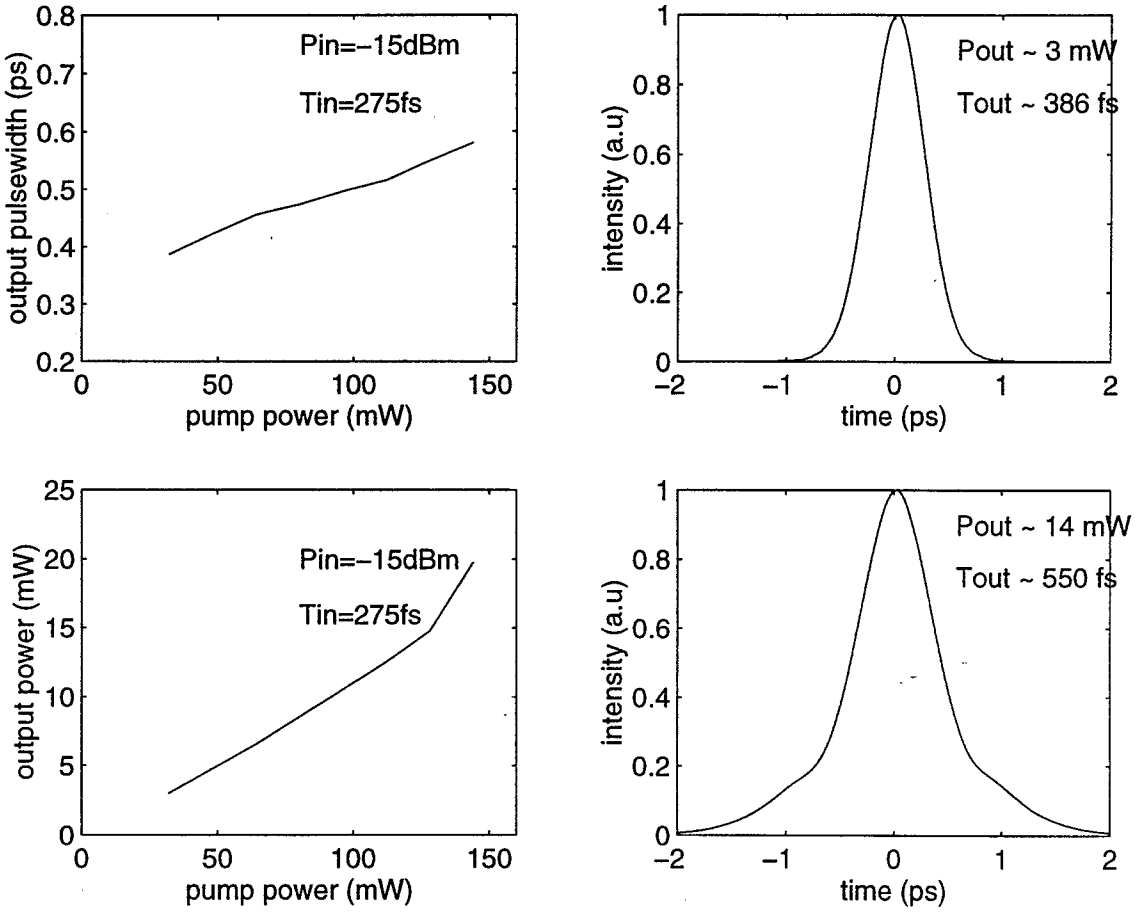

Fig. 4.6. Output characteristics of the CPA-EDFA. (a) variation of output pulsewidth with pump power, (b) variation of output signal power with pump power, (c) output temporal shape at low power, (d) output temporal shape at high power.

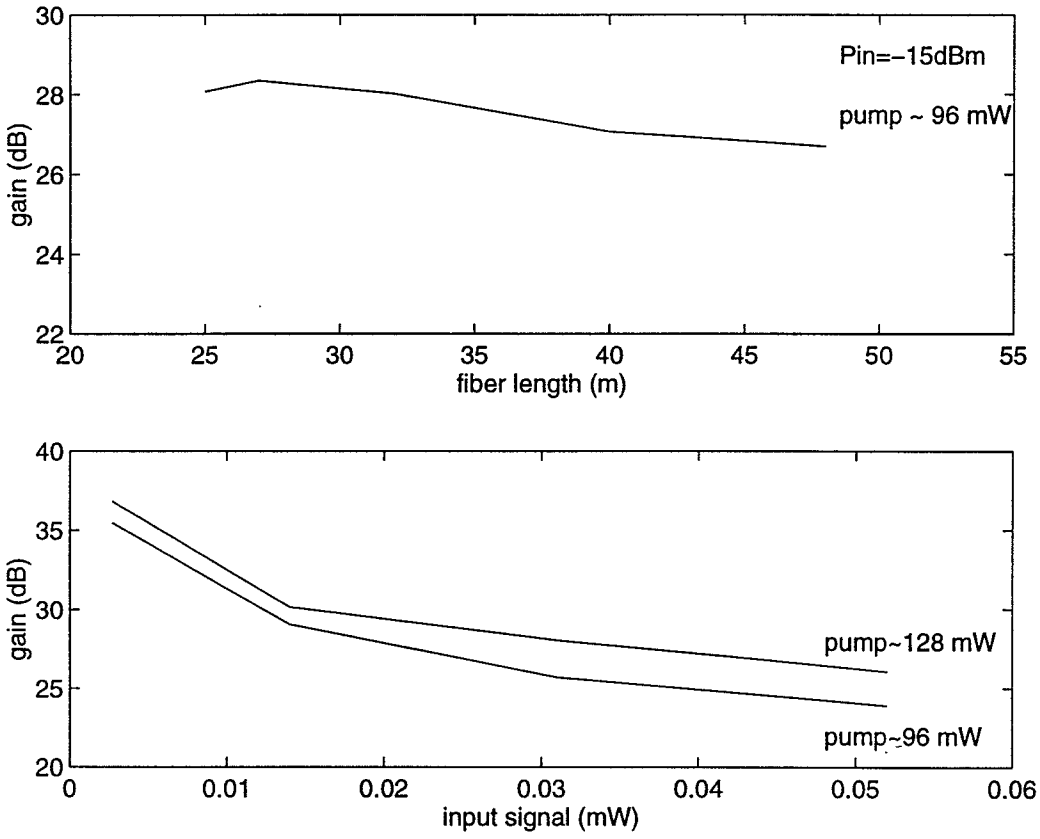

Fig. 4.7. Output characteristics of the CPA-EDFA. Top figure shows the variation of amplifier gain with length of erbium doped fiber, and bottom figure shows gain saturation effects for different pump power levels as a function of the input signal to the amplifier

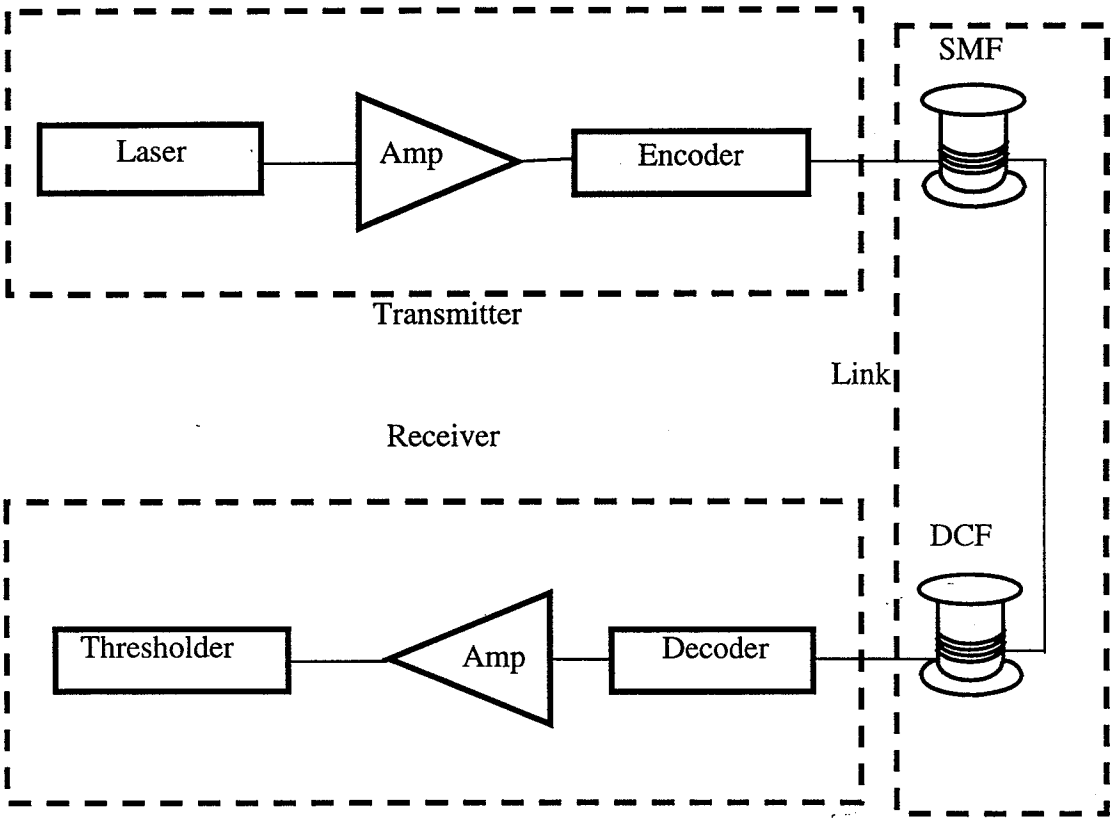

Fig. 4.8. Femtosecond CDMA test-bed.

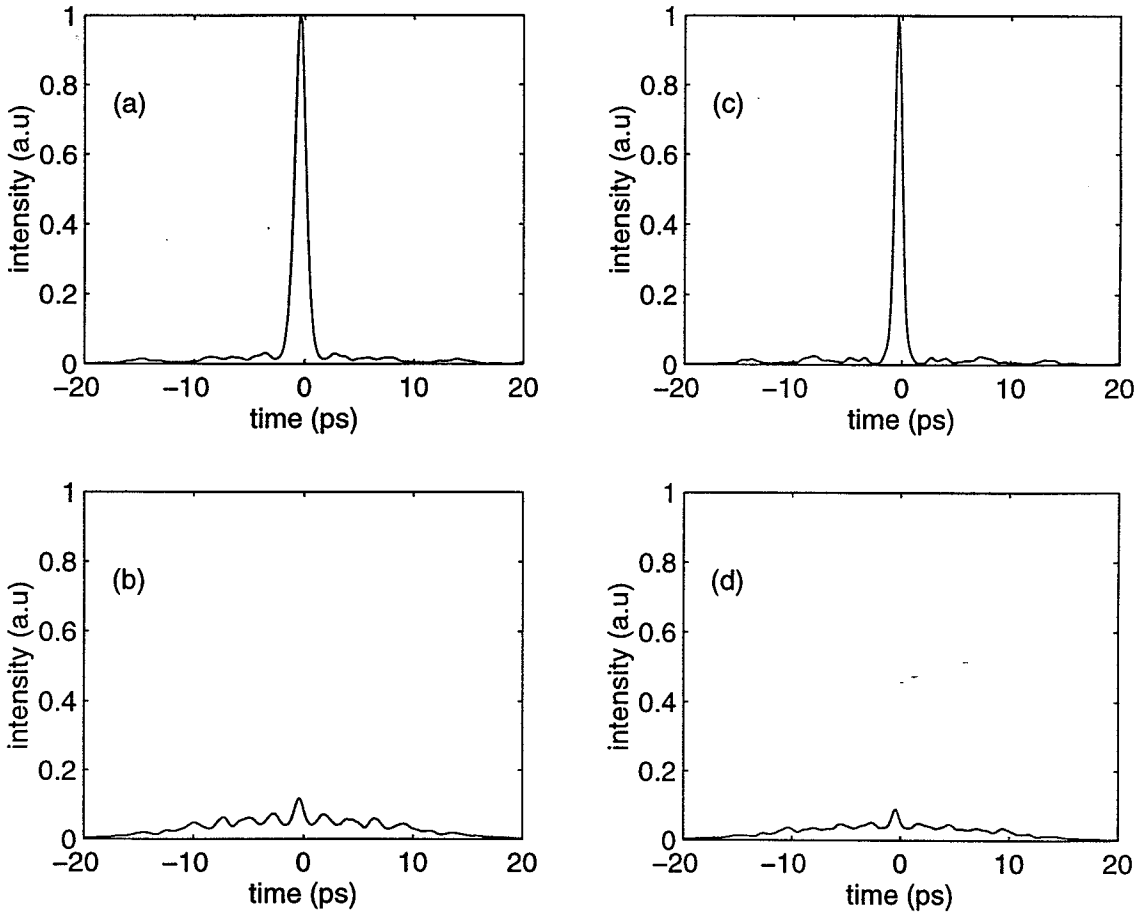

Fig. 4.9. Encoding-decoding operation for 2.5km fiber propagation. (a) Properly decoded signal after decoder, (b) improperly decoded signal after decoder, (c) properly decoded signal after decoder with third order dispersion correction, (d) improperly decoded signal after decoder with third order dispersion correction.

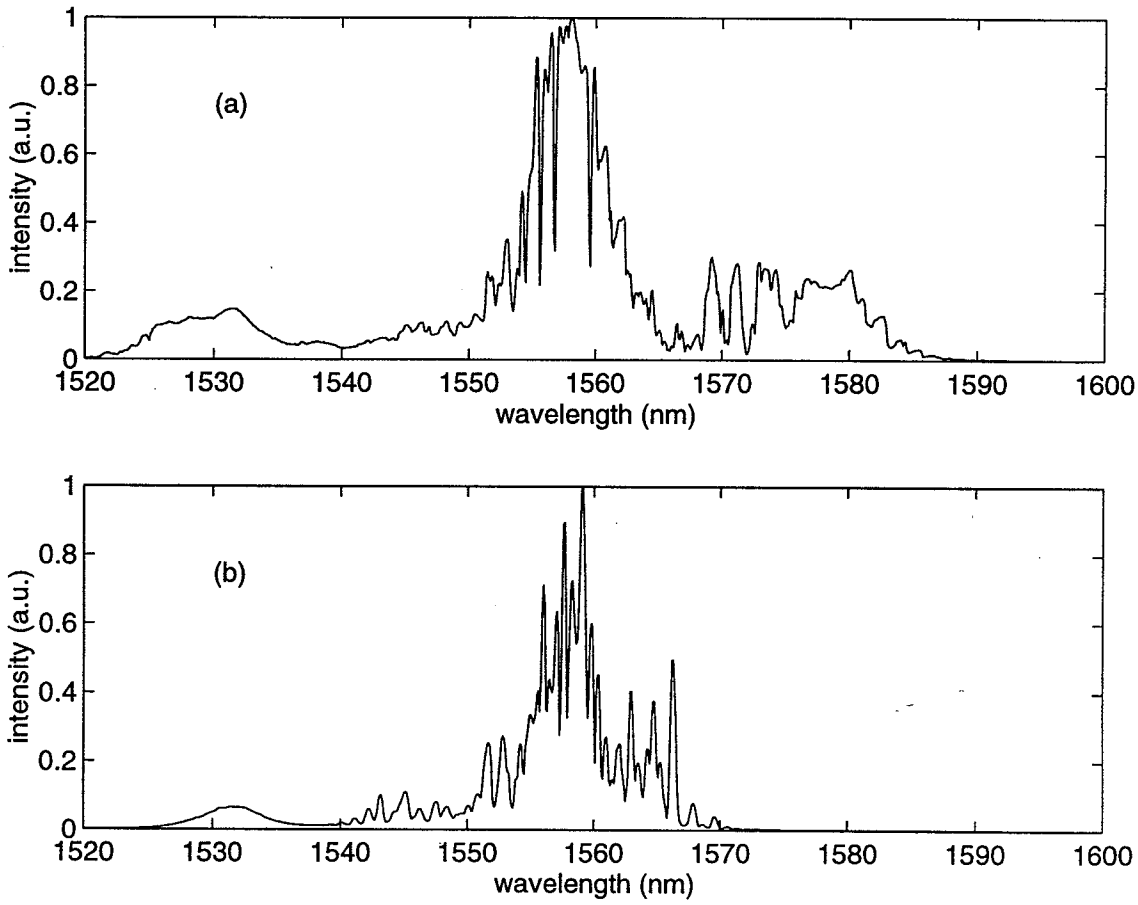

Fig. 4.10. Power spectral data at the output of the thresholder fiber for properly (top figure) and improperly (bottom figure) decoded pulse for length 31 M-sequence coding. The thresholding mechanism was nonlinear self-phase modulation.

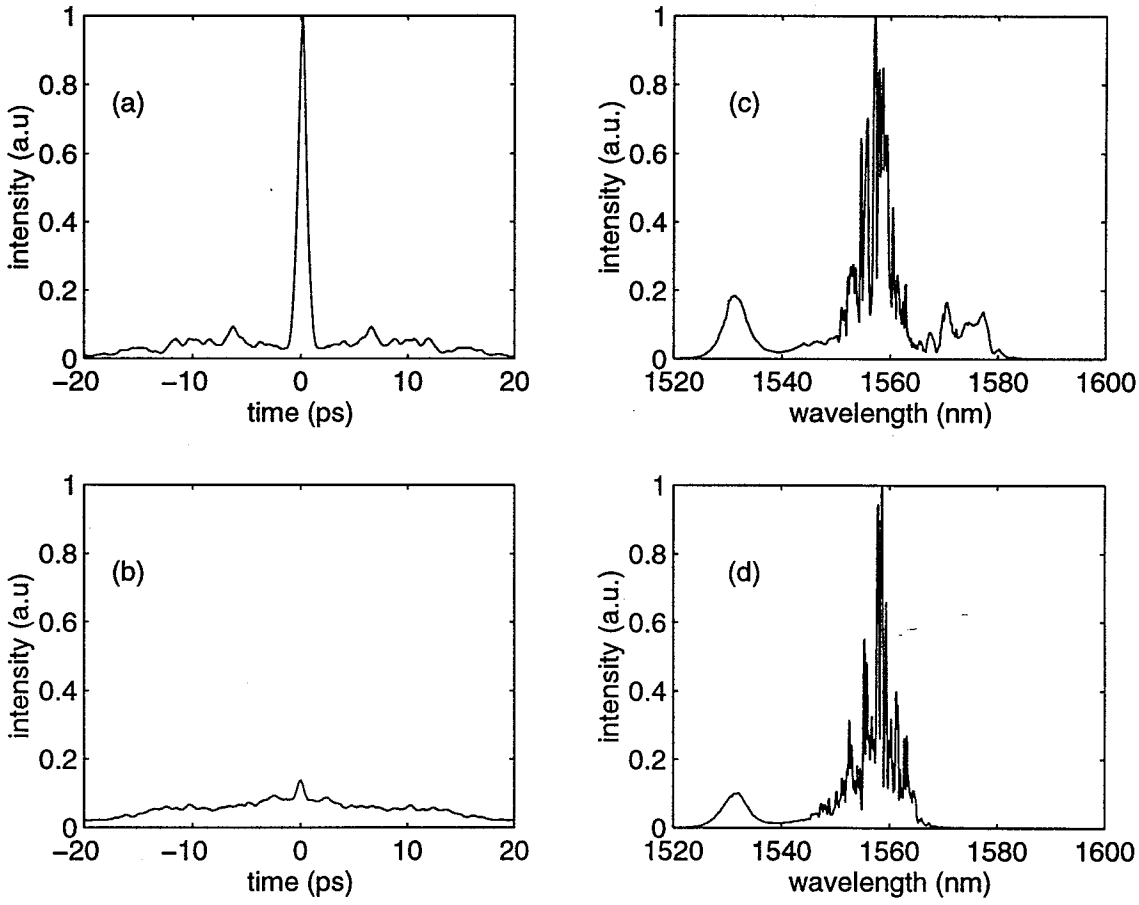

Fig. 4.11. Encoding-decoding autocorrelation data and corresponding thresholder power spectral data for length 63 M-sequence coding. The thresholding mechanism was nonlinear self-phase modulation.

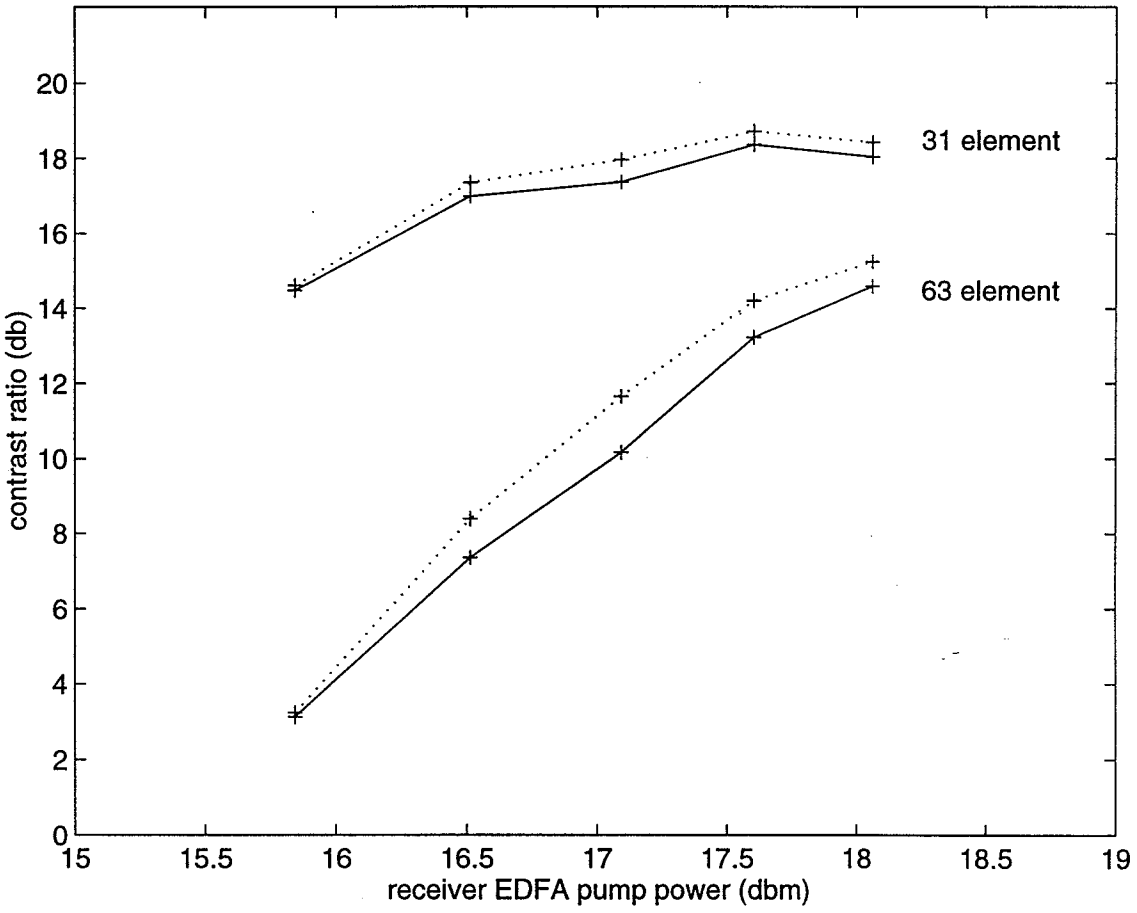

Fig. 4.12. Contrast ratio after the nonlinear thresholder for length 31 and length 63 M-sequence coding for output long wavelength pass filter cutoff wavelength of ~ 1573nm. The thresholding mechanism was nonlinear self-phase modulation. The dotted line shows the contrast ratio variation with third-order dispersion correction applied to the LCM of the encoder.

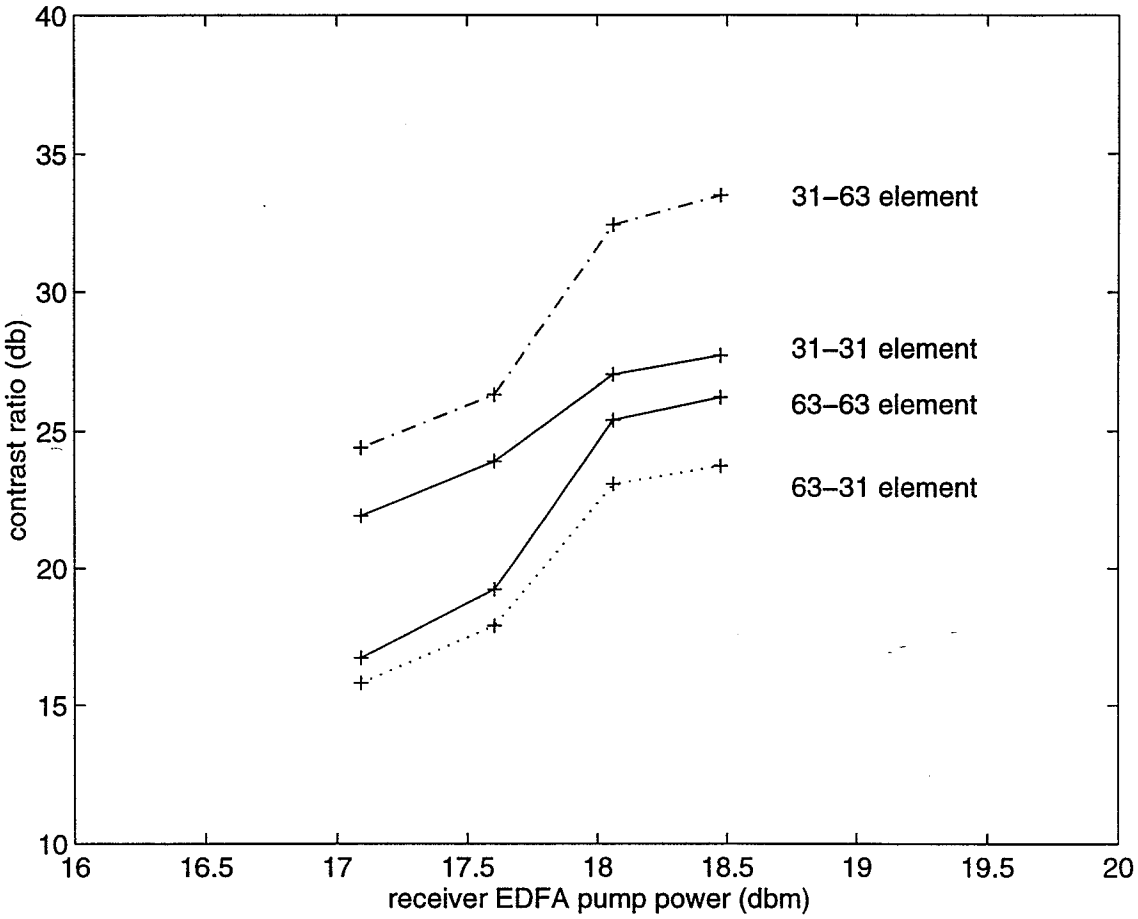

Fig. 4.13. Contrast ratio after the nonlinear thresholder for length 31 and length 63 M-sequence coding for output long wavelength pass filter cutoff wavelength of >1573nm. The dotted and dash-dot lines are for an interfering having a different length of M-sequence. The thresholding mechanism was nonlinear self-phase modulation.

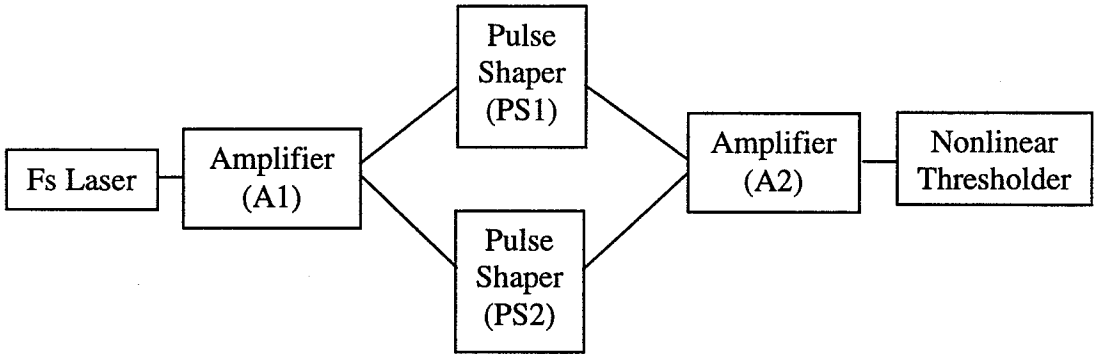

Fig. 4.15. Block diagram of the CDMA test-bed configured to simulate two-user operation.

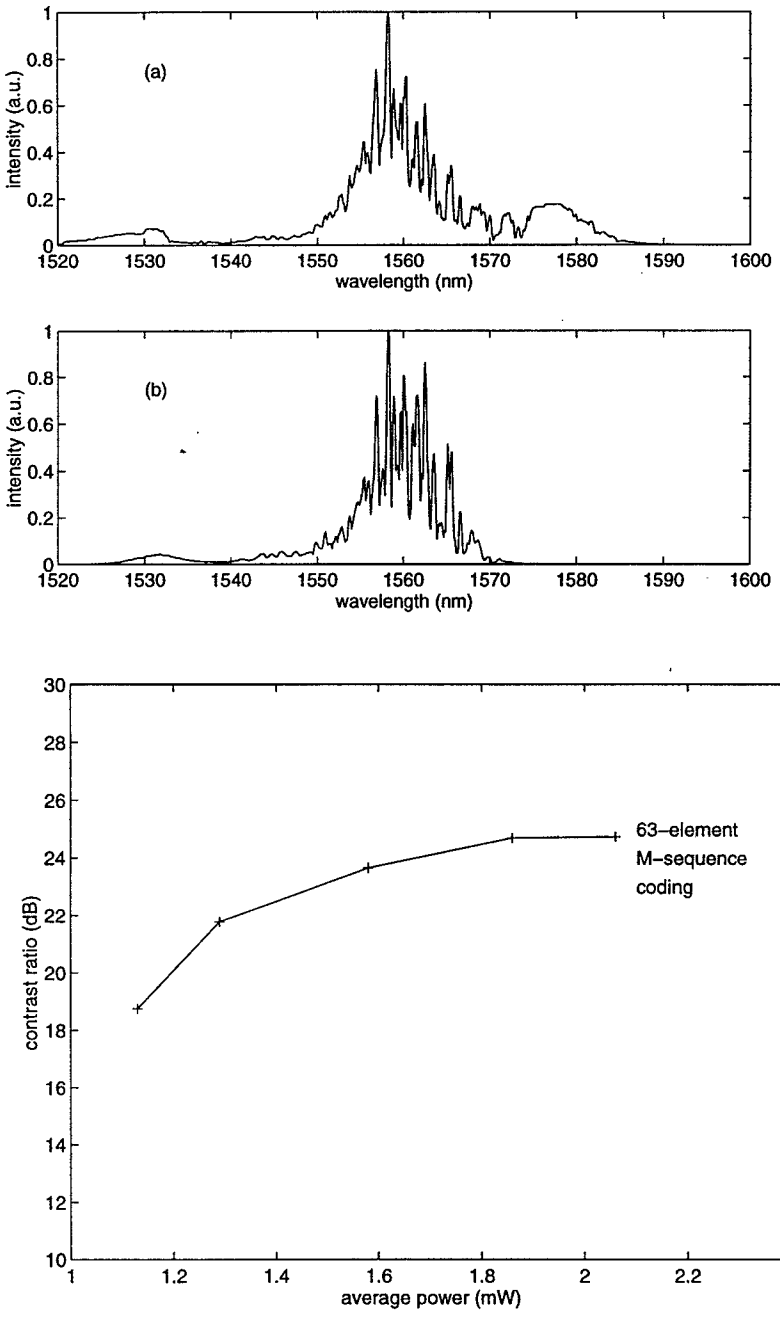

Figure 4.14: (a) Power spectrum at the output of the thresholder with one intended and one interfering user, (b) with only the interfering user, (c) contrast ratio at the output of the thresholder for output long wavelength pass filter cutoff wavelength of >1573nm. The thresholding mechanism was nonlinear self-phase modulation.

5. CONCLUSIONS

5.1. Summary

In this thesis I have presented a detailed description of femtosecond encoder-decoders, ultrafast nonlinear thresholders, and their integration in a femtosecond optical CDMA scheme. On the sub-system level the two component technologies developed in this thesis, namely, femtosecond encoding-decoding and ultrafast nonlinear thresholding have shown good performance results. The high fidelity femtosecond encoding-decoding obtained for length 63 and length 31 M-sequences shows potential for true multi-user operation. The high contrast thresholding obtained at relatively low average powers also shows potential for receiver operation with multiple users. The numerical model developed for the femtosecond encoder-decoders showed good qualitative and quantitative agreement with experimental results. In the future this could be a useful tool to determine the performance of the encoding-decoding operation for arbitrary length M-sequences. The numerical model developed for the ultrafast nonlinear thresholders showed only a qualitative agreement with experimental results. Nevertheless, based on the qualitative similarities this numerical solver could be used to develop other novel fiber-optic thresholding designs. It could be also used to analyze a host of other effects related to ultrashort pulse propagation in optical fibers like the effects of channel nonlinearity on coded-pulse propagation.

In addition to the two component technologies discussed here, the development of femtosecond lasers and femtosecond dispersion compensation that was carried out in parallel by a colleague also showed good performance results [84]. Femtosecond dispersion compensation, especially with residual third-order dispersion correction should extend the propagation distance to over 10km. This success of the four

component technologies made it possible to integrate them to form a femtosecond CDMA test-bed. On the system level, the ability to propagate a coded pulse and decode it with a 27.5dB contrast against interference demonstrates the potential of this CDMA scheme for multi-user operation. The high contrast ratios obtained for different length M-sequence coding shows potential to add more users without having to go to longer length M-sequences. The preliminary results simulating two-user operation demonstrate the interference suppression capabilities of femtosecond CDMA and lay the groundwork for future experiments involving multiple-users. In the future, the component technologies and CDMA test-bed developed here could be used in experiments demonstrating data transmission in local area network applications.

5.2 Conclusions And Future Work

In conclusion, this thesis contains the first experimental demonstration of femtosecond encoding-decoding operation using two separate low loss fiber pigtailed pulse shapers. It also demonstrates for the first time ultrafast fiber-optic thresholder operation with high contrast ratios, and the first successful demonstration of femtosecond optical code-division multiple-access over 2.5km of optical fiber.

Future work can be concentrated either at the sub-system level or at the system level. Some suggestions for improvement and further research will be made here. At the sub-system level efforts can be directed to understand the polarization effects in the pulse-shapers, as well as in modeling ultrafast nonlinear thresholders. Some effort could also be directed in determining other novel technologies for the encoding-decoding operation that would be more compact and lend more easily to integration. Although the thresholders developed here exhibited high contrast ratios, efforts could be directed to achieving such high contrast thresholding at less than a tenth of a milliwatt average power. This would be particularly useful when designing the receivers for multi-user CDMA, as most EDFA's are currently limited in saturation power to only several tens of milliwatts.

On a system level as more users are added to the CDMA test-bed the nonlinear effects in the transmission channel may become important. Some effort could be directed in understanding and predicting the effects of channel nonlinearity on CDMA operation. The effect of multi-access interference, both in the channel and in the receiver could also be an area of further study. Finally, if this CDMA scheme has to become a practical reality, some synergetic research has to be undertaken that combines the architectural and economic aspects of femtosecond CDMA with the component and systems technologies developed here.

REFERENCES

[1] G. Keiser, "Optical Fiber Communications," second edition, McGraw-Hill, 1991.

[2] P. E. Green, Jr., "Optical Networking Update," IEEE J. Selec. Areas Comm., vol. 14, pp. 764-779, 1996.

[3] H. Onaka et al., "1.1 Tb/s WDM transmission over 150 km 1.3 mm zero-dispersion single-mode fiber," in Conf. Optic. Fiber Commun. (OFC'96), postdeadline paper pd19, San Jose, CA, 1996.

[4] A. H. Gnauck et al., "One Terabit/s Transmission Experiment," in Conf. Optic. Fiber Commun. (OFC'96), postdeadline paper pd20, San Jose, CA, 1996.

[5] T. Morioka et al. "100 Gb/s x 10 channel OTDM/WDM transmission using a single supercontinuum source," in Conf. Optic. Fiber Commun. (OFC'96), postdeadline paper pd21, San Jose, CA, 1996.

[6] N. S. Bergano et al., "100 Gb/s error free transmission over 9100 km using twenty 5 Gb/s WDM data channels," in Conf. Optic. Fiber Commun. (OFC'96), postdeadline paper pd23, San Jose, CA, 1996.

[7] T. Naito et al. "128-Gbit/s WDM transmission of 24 5.3-Gbit/s RZ signals over 7828 km using gain equalization to compensate for asymmetry of EDFA gain characteristics," in technical digest, Conf. Optic. Fiber. Commun. (OFC' 97), paper TuJ2, pp. 45-46, 1997.

[8] S. Kawanishi et. al., "400 Gbit/s TDM transmission of 0.98 ps pulses over 40km employing dispersion slope compensation," in Conf. Optic. Fiber Commun. (OFC'96), postdeadline paper pd24, San Jose, CA, 1996.

[9] S. J. B. Yoo, "Wavelength Conversion Technologies for WDM Network Applications," J. Lightwave Technol., vol. 14, pp. 955-966, 1996.

[10] J. A. Salehi, "Code Division Multiple Access Techniques in Optical Fiber Networks," IEEE Trans. Commun., vol. 37, pp. 824-833, 1989.

[11] J. A. Salehi, A. M. Weiner, and J. P. Heritage, "Coherent Ultrashort Light Pulse Code-Division Multiple Access Communication Systems," J. Lightwave Technol., vol. 8, pp. 478-491, 1990.

[12] P. R. Prucnal, M. A. Santoro, and T. R. Fan, "Spread Spectrum Fiber-Optic Local Area Network Using Optical Processing," J. Lightwave Technol., vol. 4, pp. 547-554, 1986.

[13] S. Tamura, S. Nakano, and K. Okazaki, "Optical Code-Multiplex Transmission by Gold Sequences," J. Lightwave Technol., vol. 3, pp. 121-127, 1985.

[14] R. A. Griffin, D. D. Sampson, and D. A. Jackson, "Coherence coding for photonic code-division multiple access networks," J. Lightwave Technol., vol. 13, pp. 1826-1837, 1995.

[15] A. S. Holmes and R. R. A. Syms, "All-Optical CDMA using Quasi-Prime Codes," J. Lightwave Technol., vol. 10, pp. 279-286, 1992.

[16] J. Y. Hui, "Pattern Code Modulation and Optical Decoding-A Novel Code-Divison Multiplexing Technique for Multifiber Networks," IEEE J. Selec. Areas Commun., vol. 3, pp. 916-927, 1985.

[17] M. E. Marhic and Y. L. Chang, "Pulse coding and coherent decoding in fibre-optic ladder networks," Elect. Lett., vol. 95, 1535-1536, 1989.

[18] D. Zaccarin and M. Kavehrad, "An Optical CDMA System Based on Spectral Encoding of LED," IEEE Photon. Tech. Lett., vol. 4, pp. 479-482, 1993.

[19] I. N. Duling, "Subpicosecond All-Fiber Erbium Laser, Electron. Lett., vol. 27, pp. 543-544, 1991.

[20] M. Nakazawa, E. Yoshida, and Y. Kimura, "Generation of 98 fs Optical Pulses Directly from an Erbium-Doped Fiber Ring Laser at 1.57mm," Electron. Lett., vol. 29, pp. 62-63, 1993.

[21] K. Tamura, E. P. Ippen, H. A. Haus, and L. E. Nelson, "77-fs pulse generation from a stretched-pulse modelocked all-fiber ring laser," Opt. Lett., vol. 18, pp. 1080-1082, 1993.

[22] M. E. Fermann, V. da Silva, D. A. Smith, Y. Silberberg, and A. M. Weiner, "Shaping of ultrashort optical pulses by using an integrated acousto-optic tunable filter," Opt. Lett. vol. 18, pp. 1505-1507, 1993.

[23] C. Froehly, B. Colombeau, and M. Vampouille, "Shaping and analysis of picosecond light pulses," Progress in Opt. XX, pp. 64-153, 1983.

[24] A. M. Weiner, D. E. Leaird, J. S. Patel, and J. R. Wullert, "Programmable shaping of femtosecond optical pulses by use of a 128-element liquid crystal phase modulator," IEEE J. Quantum Electron., vol. 28, pp. 908-920, 1992.

[25] J. P. Heritage, A. M. Weiner, and R. N. Thurston, "Picosecond pulse shaping by spectra phase and amplitude manipulation," Opt. Lett., vol. 10, pp. 609-611, 1985.

[26] A. M. Weiner, J. P. Heritage and J. A. Salehi, "Encoding and decoding of femtosecond pulses," Opt. Lett., vol. 13, pp. 300-302, 1988.

[27] R. Kashyap, S. V. Chernikov, P. F. McKee, and J. R. Taylor, "30 ps chromatic dispersion compensation of 400 fs pulses at 100 Gbit/s in optical fibers using an all fiber photoinduced chirped reflection grating," Electron. Lett., vol. 30, pp. 1078-1080, 1994.

[28] M. Stern, J. P. Heritage, and E. W. Chase, "Grating compensation of third order fiber dispersion," IEEE J. Quantum Electron., vol. 28, pp. 2742-2748, 1992.

[29] S. Watanabe, T. Naito, and T. Chikama, "Compensation of chromatic dispersion in a single mode fiber by optical phase conjugaton," IEEE Photon. Technol. Lett., vol. 5, pp. 92-95, 1993.

[30] A. M. Vengsarkar, A. E. Miller, M. Haner, A. H. Gnauck, W. A. Reed, and K. L. Walker, "Fundamental-mode dispersion compensating fibers: Design considerations and experiments," in technical digest, Conf. Optic. Fiber. Commun. (OFC' 94), paper Thk2, pp. 225-227, 1994.

[31] C.-C. Chang, A, M. Weiner, A. M. Vengsarkar and D. W. Peckham, "Broadband dispersion compensation for sub-100 fs pulses with a compression ratio of 300," Opt. Lett., vol. 21, pp. 1141-1143, 1996.

[32] C.-C. Chang and A. M. Weiner, "Fiber transmission of sub-500-fs pulses using a dispersion-compensating fiber," in press, IEEE J. Quantum Elect., 1997.

[33] P. Meystre and M. Sargent III, Elements of Quantum Optics, Berlin: Springer-Verlag, 1990.

[34] A. Yariv, Quantum Electronics, 3rd ed. New York, NY: John Wiley & Sons, 1989.

[35] G. P. Agrawal, Nonlinear Fiber Optics 2nd ed. San Diego, CA: Academic Press, 1995.

[36] S. R. Friberg, A. M. Weiner, Y. Silberberg, B. G. Sfez, and P. W. Smith, "Femtosecond switching in dual-core-fiber nonlinear coupler," Opt. Lett., vol. 13, pp. 904-906, 1988.

[37] R. H. Stolen, J. Botineau, and A. Ashkin, "Intensity Discrimination of optical pulses with birefringent fibers," Opt. Lett., vol. 7, pp. 512-513, 1992.

[38] B.-E. Olsson and P. A. Andrekson, "Extinction ratio improvement using the nonlinear optical loop mirror," IEEE Photon Tech. Lett., vol. 7, pp. 120-122, 1995.

[39] H. P. Sardesai and A. M. Weiner, "Nonlinear fibre-optic receiver for ultrashort pulse code division multiple access communications," Elect. Lett., vol. 33, pp. 610-611, 1997.

[40] H. P. Sardesai and A. M. Weiner, "A Nonlinear Fiber-Optic Receiver for Spectrally coded Ultrashort Pulses Using the Soliton Self Frequency Shift," in press, IEEE Photon. Tech. Lett., 1997.

[41] M. Stern, J. P. Heritage, W. T. Anderson, and J. Kilmer, "Soliton technique to characterize single-mode fibre dispersion," J. Lightwave Technol., vol. 10, pp. 1777-1779, 1992.

[42] G. P. Agrawal and M. J. Potasek, "Nonlinear pulse distortion in single-mode optical fibers at zero-dispersion wavelength," Phys. Rev. A., vol. 33, pp. 1765-1776, 1986.

[43] J. P. Gordon, "Theory of the soliton-self-frequency shift," Opt. Lett. vol. 11, pp. 662-664, 1986.

[44] J. K. Lucek and K. J. Blow, "Soliton self-frequency shift in telecommunication fibers," Phys. Rev. A., vol. 45, pp. 349-354, 1986.

[45] B. L. Heffner, D. A. Smith, J. E. Baran, A. Y. Yan, and K. W. Cheung, "Integrated-optic acoustically tunable infra-red optical filter," Elect. Lett., vol. 24, pp. 1562-1563, 1988.

[46] A. Bruce Carlson, *Communication Systems*, 3rd ed., McGraw-Hill, 1986.

[47] A. M. Weiner, J. P. Heritage, and E. M. Kirschner, "High-Resolution femtosecond pulse shaping," J. Opt. Soc. Am. B, vol. 5, pp. 1563-1572, 1988.

[48] A. M. Weiner, D. E. Leaird, D. H. Reitze, and E. G. Paek, "Spectral Holography of shaped femtosecond pulses," Opt. Lett., vol. 17, pp. 224-226, 1992.

[49] C. W. Hillegas, J. X. Tull, D. Goswami, D. Strickland, and W. S. Warren, "Femtosecond laser pulse shaping by use of microsecond radio-frequency pulses," Opt. Lett., vol. 19, pp. 737-739, 1994.

[50] A. M. Weiner, "Femtosecond optical pulse shaping and processing," Progress in Quantum Electronics, vol. 3, pp. 161-233, 1995.

[51] R. N. Thurston, J. P. Heritage, A. M. Weiner, and W. J. Tomlinson, "Analysis of picosecond pulse shape synthesis by spectral masking in a grating pulse compressor," IEEE J. Quantum Elect., vol. 22, pp. 682-696, 1986.

[52] A. Efimov, C. Schaffer, and D. H. Reitze, "Programmable shaping of ultrabroad-bandwidth pulses from a Ti-Sapphire laser," J. Opt. Soc. Am. B., vol. 12, pp. 1968-1980, 1995.

[53] J. K. Lucek and K. J. Blow, "Optical intensity-dependent switching using the soliton self-frequency shift," Elect. Lett., vol. 27, pp. 882-884, 1991.

[54] T. Morioka, M. Saruwatari, and A. Takada, "Ultrafast optical multi/demultiplexing utilizing optical Kerr effect in polarization-maintaining single-mode fibers," Elect. Lett., vol. 23, pp. 453-454, 1987.

[55] P. A. Andrekson, N. A. Olsson, J. R. Simpson, T. Tanbun-Ek, R. A. Logan, and M. Haner, "16 Gib/s all-optical demultiplexing using four-wave mixing," Elect. Lett., vol. 27, pp. 922-924, 1991.

[56] S. M. Jensen, "The nonlinear coherent coupler," IEEE J. Quantum Elect., vol. 18, pp. 1580-1584, 1982.

[57] G. I. Stegemen, E. M. Wright, N. Finlayson, R. Zanoni, and C. T. Saeaton, "Third-order nonlinear intergrated optics," J. Lightwave Technol., vol. 6, pp. 953-970, 1988.

[58] M. N. Islam, C. E. Soccolich, J. P. Gordon, and U. C. Paek, "Soliton intensity-dependent polarization rotation," Opt. Lett., vol. 15, pp. 21-23, 1990.

[59] N. J. Doran and D. Wood, "Nonlinear-optical loop mirror," Opt. Lett., vol. 13, pp. 56-58, 1988.

[60] K. J. Blow, N. J. Doran, and B. K. Nayar, "Experimental demonstration of optical soliton switching in an all-fiber nonlinear Sagnac interferometer," Opt. Lett., vol. 14, 1989.

[61] K. J. Blow, N. J. Doran, and B. P. Nelson, "Demonstration of the nonlinear fiber loop mirror as an ultrafast all-optical demultiplexer," Elect. Lett., vol. 26, pp. 962-964, 1990.

[62] Z. Zheng, A. M. Weiner, J. H. Marsh, and M. M. Karkhanehchi, "Ultrafast optical thresholding based on two-photon absorption GaAs waveguide photodetectors," IEEE Photon. Tech. Lett., vol. 9, pp. 493-495, 1997.

[63] Y. R. Shen and N. Bloembergen, "Theory of Brillouin and Raman Scattering," Phys. Rev., vol. 137, pp. A1787-A1805, 1965.

[64] F. M. Mitschke and L. F. Mollenauer, "Discovery of the soltion self-frequency shift," Opt. Lett., vol. 11, pp. 659-661, 1986.

[65] W. Hodel and H. P. Weber, "Decay of femtosecond higher-order solitons in an optical fiber induced by Raman self-pumping," Opt Lett., vol. 12, pp. 924-926, 1987.

[66] K. J. Blow and D. Wood, "The evolution of solitons from non-transform limited pulse," Opt. Commun., vol. 58, pp. 349-354, 1986.

[67] C. Desem and P. L. Chu, "Effect of chirping on soliton propagation in single-mode optical fibers," Opt. Lett., vol. 11, pp. 248-250, 1986.

[68] R. H. Stolen, C. Lee, R. K. Jain, "Development of the stimulated Raman Spectrum in single-mode silica fibers," J. Opt. Soc. Am. B., vol. 1, pp. 652-657, 1984.

[69] R. H. Stolen, J. P. Gordon, W. J. Tomlinson, and H. A. Haus, "Raman response function of silica-core fibers," J. Opt. Soc. Am. B., vol. 6, pp. 1159-1166, 1989.

[70] R. H. Stolen, and W. J. Tomlinson, "Effect of the Raman part of the nonlinear refractive index on propagation of ultrashort pulses n fibers," J. Opt. Soc. Am. B., vol. 9, pp. 565-573, 1992.

[71] K. J. Blow and D. Wood, "Theoretical description of transient stimulated Raman scattering in optical fibers," IEEE J. Quantum Elect., vol. 25, pp. 2665-2673, 1989.

[72] W. Zhao and E. Bourkoff, "Femtosecond pulse propagation in optical fibers: higher order effects," IEEE J. Quantum Elect., vol. 24, pp. 2665-2673, 1988.

[73] E. Bourkoff, W. Zhao, R. I. Joseph, and D. N. Christodoulides, "Evolution of femtosecond pulses in single-mode optical fibers having higher order non-linearities and dispersion," Opt. Lett., vol. 12, pp. 272-274, 1987.

[74] E. P. Ippen, H. A. Haus, and L. Y. Liu, "Additive pulse mode-locking," J. Opt. Soc. Am. B, vol. 6, pp. 1736-1744, 1989.

[75] H. A. Haus, J. G. Fujimoto, and E. P. Ippen, "Structures for additive pulse mode locking," J. Opt. Soc. Am. B, vol. 8, pp. 2068-2076, 1991.

[76] M. Hofer, M. H. Ober, F. Haberl, and M. E. Fermann, "Characterization of ultrashort pulse formation in passively mode-locked fiber lasers," IEEE J. Quantum Elect., vol. 28, pp. 720-728, 1992.

[77] C.-C. Chang, H. P. Sardesai, and A. M. Weiner, "Dispersion-free fiber transmission for femtosecond pulses using a dispersion-compensating fiber and a programmable pulse shaper," submitted to Opt. Lett., 1997.

[78] P. Maine, D. Strickland, P. Bado, M. Pessot, and G. Mourou, "Generation of ultrahigh peak power pulses by chirped pulse amplification," IEEE J. Quantum Elect., vol. 24, pp. 398-403, 1988.

[79] A. Galvanauskas, M. E. Fermann, and D. Harter, "High-power amplification of femtosecond optical pulses in a diode-pumped fiber system," Opt. Lett., vol.19, pp. 1201-1203, 1994.

[80] M. L. Stock, A. Galvanauskas, M. E. Fermann, G. Mourou, and D. J. Harter, "Generation of high-power femtosecond optical pulses by chirped pulse amplification in erbium doped fibers," in Technical Digest of Nonlinear Guided-Wave Phenomena Topical Meeting, Optical Society of America, 1993.

[81] M. Nakazawa, K. Kurokawa, H. Kubota, K. Suzuki, and Y. Kimura, "Femtosecond erbium-doped optical fiber amplifier," Appl. Phys. Lett., vol. 57, pp. 653-655, 1990.

[82] I. Yu. Khrushchev, A. B. Grudinin, E. M. Dianov, D. V. Korobkin Jun, V. A. Semenov, A. M. Prokhorov, "Amplification of femtosecond pulses in Er+3 doped single-mode optical fibers," Elect. Lett., vol. 26, pp. 456-458, 1990.

[83] H. P. Sardesai, C.-C. Chang, and A. M. Weiner, "Encoding-decoding of femtosecond pulses using a pair of fiber pigtailed pulse-shapers," submitted to IEEE Photon. Tech. Lett., 1997.

[84] C.-C. Chang, Ph.D dissertation (in preparation), Purdue University, 1997.

VITA

Harshad P. Sardesai was born in Bombay, India on July 6, 1967. He received the B.S. degree in Electrical Engineering from Victoria Jubilee Technical Institute, University of Bombay in 1988, the M.S. degree in Electrical Engineering from The University of Texas at Arlington in 1991, and the Ph.D. degree in Electrical Engineering from Purdue University in 1997. His research interests are in ultrafast optics and fiber communications. He has published over 20 articles in conferences and journals and is a member of Eta Kappa Nu, OSA and IEEE.